Vehicle Safety Institute

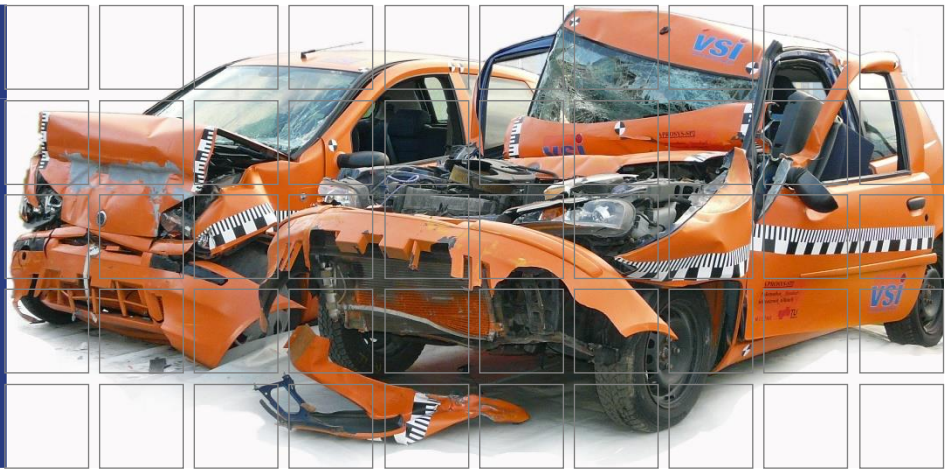

Alexander Schubert, BSc

Development of a 50th percentile female femur model

MASTER'S THESIS to achieve the university degree of

Master of Science

Master's Degree Program: Mechanical Engineering

Submitted to

Graz University of Technology

Supervisor: Ass.Prof. Dipl.-Ing. Dr.techn. Klug Corina

Vehicle Safety Institute

Graz, March 2021

AFFIDATIV

I declare that I have authored this thesis independently, that I have not used other than the declared sources/resources, and that I have explicitly marked all material which has been quoted either literally or by content from the used sources. The text document uploaded to TUGRAZonline is identical to the present master‘s thesis.

Graz, _____ _____

Signature

ABSTRACT

Within this thesis, a generic femur model representative for a 50th percentile female in terms of geometry, material data, and injury risk curve was developed. Because proximal femur fractures were found to be a relevant injury for female pedestrians and cyclists, this study specifically focused on that area.

The outer shape and cortical thickness of the femur shaft were adjusted to meet a regression model reported in a previous study for an average 50-year-old female. To derive the cortical thickness of the proximal femur, five scans from female specimens were morphed to the target geometry and the mean nodal cortical thickness was calculated. Material parameters for the cortical bone were taken from experimental data of female femur shaft specimens for tension and compression and scaled for the application in the neck and head area.

The femur mid-shaft was validated in a conventional three-point bending setup. To validate the proximal model, 20 dynamic tests of female cadavers were reproduced in simulation by prescribing the experimental displacements of the greater trochanter or head to a rigid loading plate. Only small deviations between simulated and measured forces were observed, namely the maximum forces were slightly higher in the simulations. This was especially true for specimen where low bone density was reported in the experiments. The obtained simulated maximum forces are generally within the range of fracture forces reported in literature. Maximum principal strains in the cortical bone at the time of fracture were evaluated to derive a model specific injury risk curve based on the tests.

A femur model consisting out of 14 520 hexahedral elements was developed, calibrated, validated and a model specific injury risk curve derived. The model and the related post-processing scripts are openly available and can be used to study sex-specific differences in injury patterns of the femur. By applying additional datasets, the risk curve could be further refined in future studies.

KURZFASSUNG

Diese Studie veranschaulicht die Entwicklung eines generischen Femur-Modells, das in Bezug auf Geometrie, Materialdaten und Verletzungsrisikokurve repräsentativ für eine 50-percentil Frau ist. Da sich herausstellte, dass proximale Femur-Frakturen eine relevante Verletzung für Fußgängerinnen und Radfahrerinnen sind, konzentrierte sich diese Studie speziell auf diesen Bereich.

Die äußere Form und die kortikale Dicke des Femur-Schafts wurden so angepasst, dass sie einem Regressionsmodell entsprachen, das in einer früheren Studie für eine durchschnittliche 50-jährige Frau berichtet wurde. Für den proximalen Femur-Knochen wurden fünf CT-Scans von weiblichen Probanden auf die Zielgeometrie gemorpht und die mittlere kortikale Dicke berechnet. Die Materialparameter für den kortikalen Knochen wurden aus experimentellen Daten von weiblichen Proben aus dem Femur-Schaft für Zug und Druck entnommen und für die Anwendung im Hals und Kopf skaliert.

Der Femur-Schaft wurde in einem konventionellen Drei-Punkt-Biegeversuch validiert. Zur Validierung des proximalen Bereichs wurden 20 dynamische Tests an weiblichen Kadavern in der Simulation nachgebildet, indem die experimentellen Verschiebungen des Trochanter major oder des Femur-Kopfes einer Belastungsplatte vorgegeben wurden. Es wurde eine gute Korrelation zwischen Simulationen und Experimenten erreicht, bevor ein Bruch auftritt. Das entwickelte Modell überschätzt die Maximalkraft zum Zeitpunkt des Bruchs, insbesondere für Proben, bei denen in den Experimenten eine geringe Knochendichte festgestellt wurde. Die simulierte Maximalkraft steht jedoch im Einklang mit den in der Literatur berichteten durchschnittlichen Bruchkräften in ähnlichen Versuchen. Die maximale Hauptdehnung im kortikalen Knochen zum Zeitpunkt der Fraktur im Test wurde ausgewertet, um auf deren Grundlage Verletzungsrisikokurven abzuleiten.

Ein Femur-Modell, bestehend aus 14 520 hexaedrischen Elementen, wurde entwickelt, kalibriert, validiert und mit einer modell-spezifischen Verletzungsrisikokurve versehen. Das Modell und die zugehörigen Post-Processing-Skripte sind frei verfügbar und können verwendet werden, um geschlechtsspezifische Unterschiede in Verletzungsmustern des Oberschenkels zu untersuchen. Durch die Verwendung zusätzlicher Datensätze könnte die Risikokurve in zukünftigen Studien weiter verbessert werden.

PREAMBLE

I would like to take this opportunity to thank everyone who assisted me in the preparation of this thesis and throughout my studies.
This master thesis was scientifically supervised at the Institute for Vehicle Safety of the Graz University of Technology. A big thank you goes to my supervisors, Ass.Prof. Dipl.-Ing. Dr.techn. Corina Klug and Dipl.-Ing. Christoph Leo, for their professional support and interesting discussions. Even in the current special state of things, their (virtual) door was always open and I was never able to ask a stupid enough question that threw them off track.

I would especially like to thank my family. Although it took me a little longer to complete my studies, they were never impatient and stood by me with advice and support. This kind of unconditional support was decisive for the completion of my studies and I will be always grateful to them for it.
Additionally, I would like to thank my friends, who have accompanied me in my life during the last years. My flatmates (Ali, Maxl and Wolfi) hold a special place in my heart, as they made some difficult times a lot easier and often forced me out of the mechanical engineering bubble.
Finally, I would like to thank my loving girlfriend Verena, who supports me in every situation and always stands behind me; thank you for being here!

Graz, Spring of 2021

TABLE OF CONTENTS

LIST OF FIGURES

LIST OF TABLES

1 INTRODUCTION

1.1 Motivation

While the global death rate per 100.000 cars has been steadily decreasing in recent years, traffic death is still at an eight place in the ranking of causes of deaths across all age groups and even the leader among 5-29-year-olds. (World Health Organization, 2018)

Car manufacturers have developed new safety systems or enhanced existing ones for decades. Traditionally, this process has involved the use of anthropometric test devices (ATDs), known colloquially as crash-test dummies. These dummies are usually designed for a specific load case (front crash, side crash...), for some of these partial impactors alone are used. As a consequence, there is a large number of different dummies on the market today, but testing is still limited to those configurations for which a suitable ATD is available. Additionally, due to the high loads involved in car crashes, these ATDs have to be built very robust which limits their biofidelity.

Some studies show that risk of injury and death is not equally distributed between females and males. Comparing the fatality risk, recent research found a 20-25 % higher chance for female vehicle occupants to die in a fatal crash (Abrams & Bass, 2020). This trend also continues with non-fatal crashes; even though male drivers hold a bigger share in the accident statistic, female drivers in the US were 47 % more likely to sustain serious injuries than their male counterparts in a comparable car crash (Bose et al., 2011; Kahane, 2013). A similar imbalance in the effectiveness for restraint systems for males and females was found by Kullgren et al. (2013), who investigated whiplash-injuries and found significantly more women affected than men. This cannot be explained by a greater number of women on the road; in 2018, there were only a few thousand more female than male license holders in the United States as published by the Insurance Institute for Highway Safety (2021).

The primary use of ATDs is part of the explanation why the gender-gap in safety is so staggering; most adult safety system assessments are targeting 50^{th} percentile males (Linder & Svensson, 2019). While representative female dummies have been developed by scaling existing 50^{th} percentile male ATDs to the appropriate female anthropometry (Carlsson et al., 2012), they were not employed for the use in any assessment program.

In the last decades, traditional physical testing has been slowly but surely augmented by new virtual opportunities. Where previously lengthy, and costly, development processes with physical prototypes and countless trials were necessary, today digital tools are increasingly being used.

One immanent advantage of virtual testing is the chance to perform assessments with a higher degree of variability and therefore make these evaluations more robust. Virtual testing, however, holds a

whole other opportunity; to finally close the gender-gap in vehicle safety by including female anthropometries early in the development and assessment process.

In the virtual testing environment, humans can be represented by Human Body Models (HBMs). These are numerical and highly detailed representations of the human body with several key advantages over traditional ATDs (Lanner et al., 2010; Park et al., 2014). One of the benefits is the possibility to morph HBMs, which means that characteristics like height, weight, body mass index (BMI), age and gender can be altered with limited effort (Larsson et al., 2019). Unfortunately, the vast majority of currently available HBMs is still based on CT scans of individuals with the appropriate target anthropometry, most of the time a 50th percentile male (Linder & Svensson, 2019; Schoell et al., 2015). While these base models have been morphed into other anthropometries to cover a bigger range of occupant heights and weights, female HBMs are still scarce. Efforts have been made by Sato et al. (2017) and Östh et al. (2017) to develop average female body models, the first one being a modified version of an existing model (Total Human Model for Safety (THUMS) 5th percentile female) and the latter being a new development based on a 31 year old female subject close to the 50th percentile anthropometry (original VIVA model). Both studies focused on the assessment of whiplash associated disorders and therefore turned their attention specifically to the modeling and validation of the cervical spine and rear impact load cases. The extremities of the original VIVA model were modelled as rigid bodies, as they were not relevant for the purpose of the study (Östh et al., 2017).

Vulnerable Road Users (VRUs) are at disproportionately high risk of injury and death, with pedestrians, cyclists and drivers of motorized two- and three-wheeled vehicles together accounting for 54 % of all global traffic fatalities (World Health Organization, 2018). These road users affected more severely because they are usually not protected by any crumple zone or restraint systems. Although many car manufacturers have been trying to address this issue for several years and develop special safety systems for pedestrians and cyclists (e.g. active bonnet, airbags), the reliable evaluation of these systems is difficult. Since conventional ATDs often cannot represent the actual kinematics of living humans, the use of digital human models is also promoted here and has already been adapted successfully. The first Euro NCAP protocol to approve the use of HBMs was recently formulated for the assessment of deployable systems (Klug et al., 2019).

A project aiming to change these limitations, especially concerning underrepresentation of the average female anthropometry is the Horizon 2020 "*Project Virtual*". Within the project, open source female human body models (called VIVA+, Klug et al. (2020)) are developed, which can be used to study sex-specific differences and perform safety assessments for a wider range of road users (VRUs, public transport users etc.) in which females and males are equally considered.

1.2 Objectives

The aim of the present thesis was to develop and validate a femur model for the VIVA+ 50th percentile female (VIVA+ 50F) model applicable for virtual testing procedures. To be aligned with the rest of the VIVA+ 50F model, the femur should be representative for a 50 years old women with a stature of 168 cm and weight of 62 kg in terms of geometry and mechanical properties. To make the model applicable for virtual testing procedures it has to be accompanied by assessment criteria and a related injury risk curve.

Within this thesis, it is investigated if a representative female femur model can be developed and validated with a focus on the proximal region and used to predict injuries in this area based on publicly available data.

2 BACKGROUND

2.1 Femur geometry

The human body can be divided into four major regions; the head, torso, upper and lower extremities. The literal backbone of the human, the spine, is connected to the lower extremities via the pelvis. Since the pelvis is mechanically the only load path to transfer the upper body's weight to the ground, it is quite large. The hip bones distribute this weight to the two toughest and longest bones in the human skeleton, the femora. Like most long bones, the femur consists of a diaphysis (shaft) and two epiphyses (end pieces). The femur head on the proximal (= closer to the heart) epiphysis sits in the hips acetabulum, which allows movement of the hip joint. On the distal (= further away from the heart) epiphysis of the femur, the knee joint connects the only bone of the upper leg with the tibia, one of the two bones of the lower leg. Like in most other bones, the femoral bone structure can be divided in cortical (compact) and trabecular (cancellous, spongy) bone. The cortical bone is the hard outer layer of the femur, while the trabecular bone provides the internal tissue. (Schmitt et al., 2014)
In the case of the femur, trabecular bone is only found in the epiphyses. For reference, a cross-section of the developed femur model is shown in Figure 2-1, where the orange area indicates the trabecular and the grey area the cortical bone.

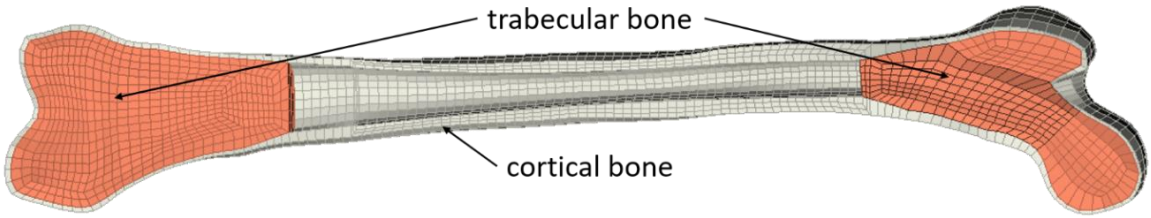

Figure 2-1: cross-section of VIVA+ femur model with cortical and trabecular bone

In the following sections and Figure 2-2 the anatomy of the femur is described in more detail.

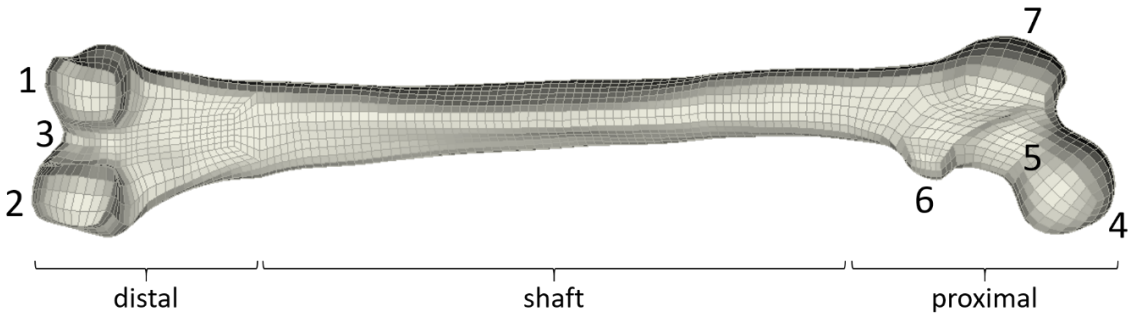

Figure 2-2: femur taken from VIVA+ model

2.1.1 Distal Femur

The distal end of the femur is the largest part of the bone and dominated by two, almost parallel protuberances called condyles, as shown in Figure 2-2, (medial condyle (2), lateral condyle (1)). These surfaces form the knee joint and leave enough space between them for the ligaments (intercondylar fossa (3)). The numbers refer to the regions marked in Figure 2-2. The cavity formed by the distal cortical shell is filled with highly heterogeneous trabecular bone.

2.1.2 Shaft of femur

The body of the femur can be described as a long tube with slightly varying cross-sections. The shaft is somewhat flattened towards the distal end, narrows in the middle, and finally broadens again at the proximal end. The shaft is noticeably convex in the front (average curvature radius = 120 cm (Karakaş & Harma, 2008)) and traversed by three rougher ridges that serve as attachments for the adductors. Average female bone cross-section areas in the shaft range from about 600 mm² (distal and proximal end) to about 500 mm² in the mid-shaft (Klein et al., 2015). The femur shaft is not filled with trabecular bone, but rather with bone marrow, the tissue responsible for the production of new blood cells.

2.1.3 Proximal Femur

The proximal femur is commonly divided into four distinct regions (see Figure 2-2): head (4), neck (5), intertrochanteric and subtrochanteric (from lesser trochanter towards the shaft) region. The intertrochanteric area is framed by the greater (7) and lesser trochanter (6), small elevations which serve as anchor points for the hip muscles (Clauss & Clauss, 2018). The angle between neck and shaft varies between individuals and with age, but a value of approximate 128° can be estimated for adults (Chandran et al., 2019; Konda, 2018). The femur neck is considered as the weakest part of the bone (Vulović & Filipovic, 2020). The proximal femur is again filled with trabecular bone with heterogeneous density. Cortical thickness in the femoral head is slim, with mean values of about 1.2 mm, and increases towards the subtrochanteric region, where the it reaches thicknesses of up to 5 mm based on our own calculations (see section 4.1).

2.2 Mechanical bone properties

The properties of the different bone structures (trabecular and cortical) are divergent. The two types of bone are usually most easily distinguished by their different density and porosity, but there is also a difference is in the microstructure. The microstructure of cancellous bone is comprised by irregular sinuous convolutions of lamellae, in contrast, in the cortical bone these lamellae are packed into so

called osteons and cylindrical and regular of nature. (Rho et al., 1998) A generic cross-section of bone is depicted in Figure 2-3, showing cancellous bone (2) in the center surrounded by cortical structure (1) with a highlighted osteon (3).

Both the medical and engineering communities have a great interest in better understanding the material properties of bone, whether to develop better prostheses or to enable reliable predictions of fractures and thus improve prevention. The following sections should further provide further insight into the different material properties of the two bone structures.

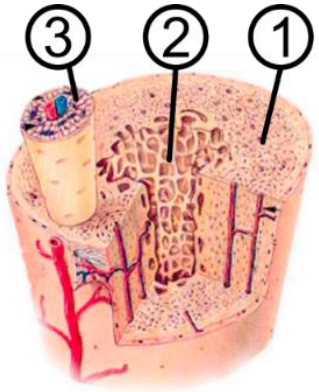

Figure 2-3: bone cross section, adapted from (National Cancer Institute, 2019)

2.2.1 Cortical bone

As described earlier, osteons, i.e. those densely packed, concentric and parallel lamellar bundles seen in Figure 2-3, form the main structural component of cortical bone. Held together by cement-like structure and covered by connective tissue, compact bone can be described as an anisotropic material. Similar to fiber-reinforced composite materials it's mechanical properties depend on the direction of loading. In the case of cortical bone, the tensile and compressive moduli and strength are greater along the longitudinal axis (osteon direction), while the properties in other directions (radial, circumferential) are similar enough to be treated as isotropic. These characteristics can be summarized with the term transversely isotropic material. Additionally, material properties are different for loading in tension and compression (Viano, 1986). Generally speaking, the fracture strain depends on the direction of loading; under tension, bone withstands about 3 % strain, whereas failure occurs at about 1.5 % strain under compressive loading (Morgan et al., 2018).

The mechanical properties of bone are also strongly related to its apparent density (ρ_a), however many different formulations of the dependencies exist in literature (Bouxsein, 2001; Keller et al., 1990). Unfortunately, no truly universal formulation of the dependency between ρ_a and, e.g., the Young's modulus has yet been found. The matter is aggravated by the fact that these coherencies are dependent on the location of the specimen collection and on the exact test procedure. The properties of cortical bone are a function of the location on the bone, e.g. Lotz, Gerhart et al. (1991) note a 24 % decrease of the elastic modulus measured at the intertrochanteric region compared to the diaphysis of the human femur. This makes comparing different studies on the subjects difficult, but even still a standardized test in this respect does not exist, although it has often and long been requested (Helgason et al., 2008; Reilly & Burstein, 1975). A complication for the realization of reliable test methods is the dependence of the material properties on the strain rate (Evans, 1973; McElhaney, 1966; Sedlin & Hirsch, 1966). Hansen et al. (2008) found out that especially the post-yield behavior is

influenced by the strain rate, but also the Young's modulus, the maximum load and the yield point show a dependence. Hoffler et al. (2005) show similar results concerning strain rate sensitivity and additionally provide evidence of significant correlation between elastic modulus and hardness measured in nanoindentation testing.

A summary of relevant material data for cortical bone from femoral specimen is provided in Table 2-1. The properties stated here are taken from macroscopic specimen. Unfortunately, yield properties are not published regularly, but are included were available. If the young's modulus is stated as a single value it is the provided mean value in the original source.

Table 2-1: cortical bone properties summary,
young's modulus in longitudinal direction, rect. = rectangular, * = includes samples from tibia

	Specimen type	Specimen location	Young's modulus [GPa]	Yield Stress [GPa]	Ultimate Stress [GPa]
Evans & Lebow, 1951	Flat – Tensile (wet)	Femur (shaft)	15.7	0.081	-
Sedlin & Hirsch, 1966	Flat – Tensile (wet)	Femur (shaft)	4.5-7.2		0.08-0.10
	Flat – Bending (wet)		10.6-19.7		0.11-0.21
McElhaney, 1966	Rect. – Comp.	Femur (shaft)	15.2-42.1		0.15-0.32
Mather, 1967	Bending	Femur	7.6-19.0		0.09-0.23
Mather, 1968	Bending	Femur	13.2		0.15
Yamada, 1970	(wet)	Femur	17.3		0.12
Evans, 1973	Tensile (wet)	Femur			0.05-0.11
Reilly et al., 1974	Rect. – Tensile (wet)	Femur (shaft)	11.4-19.3		0.11-0.15
	Rect. – Comp. (wet)		15.1-19.7		0.16-0.21
Reilly & Burstein, 1975	Round – Tensile (wet)	Femur (shaft)	15.6-17.9	0.11	0.13
Burstein et al., 1976*	Rect. – Tensile (wet)	Femur (shaft)	15.6-17.7	0.10-0.12	0.12-0.14
Saha & Hayes, 1976	Flat – Tensile	Femur (shaft)	14.5		0.13
Fung, 1993	Tensile	Femur	17.6		0.12
Keller et al., 1990	Rect. – Bending	Femur (shaft)	12.1		0.17
Lotz, Gerhart et al., 1991	Rect. – Bending	Femur (neck)	9.7		0.10
Currey et al., 1997	Rect. – Bending	Femur (shaft)	9.1-13.6		0.14-0.17
Currey, 2004	Square - Tension	Femur	16.7	0.12	
Cuppone et al., 2004	Flat – Bending	Femur (shaft)	18.6		
Bayraktar et al., 2004	Rect. – Tension (wet)	Femur (shaft)	17.8	0.11	

2.2.2 Trabecular bone

The cancellous bone is best described as a porous sponge or cellular material like polymeric foam. Only about 20 % of the volume in the trabecular compartment are made of bone tissue, the remaining space is filled with marrow and fat. This also means that trabecular bone contains less calcium and more water, so the overall, structural material properties are fundamentally different from those of cortical bone. (Ott, 2018)

In addition, cancellous bone has a significantly higher turnover (renewal of the tissue over time) than total cortical bone (17.7 % vs. 7.7 % per year respectively), although the exact turnover rate in the cortical structure is highly dependent on the radial layer (Parfitt, 2002).

Nevertheless, it is essential to differentiate between the structural and material properties of trabecular bone. The structural properties are decisive for work aiming for global analysis (such as the present one), while the material properties are relevant for small-scale processes such as bone pathologies or micro-level stress analyses. (Ashman & Rho, 1988)

Some research has therefore focused on the nanoscale testing trabecular bone, be it with the aid of nano-/microindentation or with the help of micromechanical testing performed on individual, extracted trabeculae (lamellae of bone) to really gain insight on the micromechanical properties of trabecular bone (Jirousek, 2012; Pawlikowski et al., 2017). Recent research was also able to replicate trabecular bone on a tissue level in numerical simulations, which shows to be a very reliable mean to predict failure, provided appropriate element formulations are used (Dagan et al., 2004; Niebur et al., 2000; Park et al., 2013; Verhulp et al., 2008).

An early extensive summary on the different properties of trabecular bone is offered by Goldstein (1987), who also emphasizes the dependency of mechanical properties on the anatomic position, as later confirmed by, e.g. Morgan et al. (2003). When averaged, the apparent density of trabecular bone in the femur, proximal tibia and vertebra was 0.27 g/cm³ with a reported range from 0.18 to 0.56 g/cm³. The extreme dependency of trabecular bone on the anatomical location is also underlined by Keaveny and Hayes (1993) in their literature review as they conclude: *"[…] trabecular bone is an extremely heterogeneous material—modulus can vary 100-fold even within the same metaphysis […]"* (Keaveny & Hayes, 1993, p. 534)

Similar variation is stated for the anisotropic behavior of trabecular bone. Martens et al. (1983) state that this nature is particularly apparent in the femoral neck, were elastic modulus and compressive strength in radial direction is only a fraction of the values obtained from testing in axial direction. However, the principal tensile-compressive asymmetry of the tissue is comparable to cortical bone (Bayraktar et al., 2004).

In a study on specimen extracted from the proximal tibia, Keyak et al. (1994) found strong correlations between ash density and orthogonal moduli and specimen strength and supply formulations for the

correlations between different density measurements (wet, dry, ash, QCT-based). The density dependency of elastic modulus, yield stress and ultimate stress is also described in the study by Kopperdahl and Keaveny (1998). Additionally, they found compressive yield strains to be only weakly dependent on the apparent density, with no correlation in tension. However, contradicting information on this topic exists (Ford et al., 1996; Mosekilde et al., 1987).

Gibson (1985) compares the structural failure behavior of trabecular bone to other cellular materials, describing the same 3 stages during collapse in compression: first, linear elastic behavior is apparent until the trabeculae give in, followed by a second phase of relatively constant force until finally the resistance by cells touching increases rapidly again in the third phase (densification). The same principle is applied by Helgason et al. (2014) in their work on femur FEM-models.

Table 2-2 provides an overview of some of the most prominent studies who report original structural material data of trabecular bone samples obtained from human femora. Other studies on the cancellous bone of the tibia (e.g. Ding et al. (1997), Keyak et al. (1994)) or vertebrae (e.g., Kopperdahl and Keaveny (1998)) are available, but not included in this table due to the aforementioned local variations of the material properties. Also not included are studies where micro-mechanical properties of trabecular tissue (Bini et al., 2002; Dagan et al., 2004; Pawlikowski et al., 2017) or tissue modulus (Bayraktar et al., 2004; Jirousek, 2012) was tested.

Table 2-2: trabecular bone properties summary, young's modulus is structural,
IT = intertrochanteric, * = female specimen only, [+] = along neck axis, [#] = data from Goldstein (1987)

	Specimen type	Specimen location	Young's modulus [MPa]	Yield Stress [MPa]	Ultimate Stress [MPa]
Knese, 1958	Comp.	Femur (head)	57 - 87		9.4 - 11.4
Evans, 1973	Rectangular (wet)	Femur (proximal)	206 - 380		2 - 4
Schoenfeld et al., 1974	Comp.	Femur (head)	344		0.15 - 13.5[#]
Brown & Ferguson, 1980	Cubic – Comp.	Femur (proximal)	1967-3386		120-310
Martens et al., 1983 *[+]	Cylinder – Comp. (wet)	Femur (head)	2248		16
		Femur (neck)	2024		18.7
		Femur (IT)	409		7.1
Ashman & Rho, 1988	Cylinder – Ultrasonic (wet)	Femur	959-2170		
Lotz et al., 1990	Comp.	Femur (neck)	441		6.8
Ciarelli et al., 1991	Cubic – Comp.	Femur (proximal)	424		5.6
Rho 1995	Ultrasonic (wet)		1300		
Ciarelli et al., 2000 *	Cubic – Comp. (wet)	Femur (head)	1150		15
Morgan & Keaveny, 2001	Cylinder – Comp. (wet)	Femur (neck)	3230	17.45	
		Femur (GT)	622	3.21	
	Cylinder – Tension (wet)	Femur (neck)	2700	10.93	
		Femur (GT)	597	2.44	

2.2.3 Effects of ageing

Wall et al. (1979) found evidence for age dependency of ultimate tensile strength (UTS) and density in cortical bone combining data from their own study with literature like Burstein et al. (1976), Yamada (1970) and Lindahl and Lindgren (1967). They note an UTS-decrease of about 20 % while the density only declined by 2.6 % when comparing age groups 30-39 and 70-79 year olds. Similarly, mechanical tests performed by Wang et al. (2002) indicate age-related deterioration of the collagen network in femoral bone, which is reflected by a decrease of failure strength (35 %), elastic modulus (~30 %) and work to fracture (50 %) comparing 19-49 year olds to specimen from over 70 year olds.

Ding (2000) noted a rapid decrease of Young's modulus and ultimate stress in trabecular bone after 60 years of age, suggesting less elastic behavior. This is supported by Milovanovic et al. (2012) in their nanoindentation study on trabecular tissue, who additionally attested increased hardness with age. Although their sample size is not huge in this study (five young: aged 32±5 years, and three elderly: aged 88±6 years) the result is also in line with their earlier findings of increased mineral grain sizes (causing decreased material strength) in bone from elderly specimen (Milovanovic et al., 2011). A

different study concurs that even though the outer diameter of long bones increases slightly with age, overall a decreasing strength can be noted: *"With aging or disease, the cortex becomes more porous, thus gaining surface area but losing strength."* (Ott, 2018, p. 373)

On the other hand, Wolfram et al. (2010) could not find a correspondence of elastic modulus and age in trabecular bone, and even though evidence can be found for an effect of osteoarthritis on the hardness of trabecular tissue, no direct influence of age could be noted by Dall'Ara et al. (2011). Pawlikowski et al. (2017) recite that bone hardness reaches a plateau after the age of 30 years and remains constant from there on and support this statement with a nanoindentation study on 25 human trabecular harvested from patients suffering from osteoarthritis.

There are also opposing views on the age-dependent behavior of the cortical bone, Mirzaali et al. (2016) state that no discernable effect can be ascertained from microindentation-testing, although they also note that their lack of donors younger than 60 years might be a limitation. However, Hoffler et al. (2000) could not find a correspondence of elastic modulus and age in their data on lamellar-level behavior of cortical bone and trabecular tissue.

What most studies agree on, is a decline in bone mineral density (BMD) with age, e.g. Riggs et al. (1982) showing a 58% decrease in the femoral neck during life, and more recently Li et al. (2020) were also able to define a negative correlation between subject age and volumetric BMD (vBMD) measurements. This effect can be observed until the end of most people's lifetime: "*A significant decrease in global trabecular bone mineral density (38.1 %) and cortical thickness (13.0 %) was seen from the 9th to the 10th decade of life."* (Whitmarsh et al., 2018, p. 1)

However, Rezaei and Dragomir-Daescu (2015) point out, that the overall strength decrease of their femoral samples with increasing age could not be explained by the loss of BMD, since the later decreased about 40 % slower than the affected strength testing in a configuration used to simulate a side-ways fall. This decrease of overall fracture force with age has also been attested since Courtney et al. (1994)'s famous experiments on the effects of loading rate on the strength of the proximal femur. The decline of bone strength is also documented for the case of bending the femur mid-shaft (Forman et al., 2012). Nevertheless, Wang and Puram (2004) summarize an extensive literature research (>150 studies included) by not questioning the decrease in bone strength with age due to various reasons (porosity increase, microdamage accumulation, collagen changes etc.), but pointing out that the exact causes and mechanisms of these processes are not yet sufficiently understood.

2.2.4 Effects of gender

The influence of biological sex on the mechanical properties of bone is still a subject of debate. Once again, it is important to distinct between macro and microscopic mechanical properties. As for the age, Pawlikowski et al. (2017) and Wolfram et al. (2010) also state that elastic modulus of trabecular bone

is independent of gender, based on results from microscopic indentation testing. In their analysis on bone lamellae extracted from cortical and trabecular tissue, Hoffler et al. (2000) also found no correlation with gender and elastic modulus or hardness. Li et al. (2020) found no significant relation of vBMD with gender.

Still, Keyak et al. (1994) formulated different relationships of dry to ash density for men and women, implying a diverging behavior. Bouxsein et al. (1999) note that even though the age of female and male donors were comparable in their tested cohort, male donors hat 40 - 70 % higher BMD values, which would correlate to higher material strength. Similar findings were reported earlier by Riggs et al. (1982) who found the declining rate of BMD for males to be about two-thirds of the same measurement for female patients.

A similar conclusion can be drawn when looking at results from macroscopic or whole-bone testing. In the literature review conducted by Nasiri Sarvi and Luo (2017) on 32 sideways fall experiments it was observed that the average femoral strength of 2771 ± 1136 N of female specimen was significantly lower than that of their male counterparts, which was at 4027 ± 1464 N in comparable experiments. In the light of the previous chapter 2.2.3 it is worth mentioning that the mean age of all specimen included in this study is 73 years. Nevertheless, Patton et al. (2019) were able to make similar findings in their study on younger proximal femur specimen (mean age 58) with 58 % lower strengths reported from females. Rezaei and Dragomir-Daescu (2015) performed a study on 100 cadaveric femora which shows coinciding results, with female femurs being about 1750 N weaker when compared to males of the same age. They also indicate that the rate of decline with age is greater with women than men. Significantly lower female femur strength is also attested by Cheng et al. (1997).

Additionally, Frysz et al. (2020) found differences in geometric measurements in their study on adolescents as they noted a smaller lesser trochanter and femoral neck width in females at age 18.

Analyzing 128 cadaveric tibiae Hunter et al. (2019) found statistically significant larger morphometrics (total area, cortical area, cortical thickness etc.) in men than women, with the exception of vBMD. However, Marques et al. (2018) conclude from their case cohort study on 334 incident hip fracture cases (234 female) including a noncase sub-cohort of 1047 participants (562 female) from the population-based AGES-Reykjavik study (mean age of 77 years), that, while overall bone quality in male patients was better, female fracture cases showed higher vBMD in the proximal femur.

There’s also evidence for gender-dependent age-related bone remodeling behavior; in their study on lower limb bones from US white adults in age groups from 20 to 99 years, Ruff and Hayes (1988) state that while the cortical area is somewhat constant and the second moments of area increase slightly in males, both measurements decreased with age in female specimen.

2.3 Femur fractures

Generally, injuries occur when the body's reaction to a load exceeds certain tolerance levels. The process following this violation of the threshold until injury occurs is the so-called injury mechanism. This thesis focuses on femur bone fractures. Generally speaking, the relevant loading types for fracture are bending, torsion, shearing and compression including all possible combinations. Less common, but not impossible is fracture due to simple traction, which is often averted by the surrounding muscles. Shaft fractures of long bones under pure compression are also rare, under these circumstances the cancellous structure of the epiphyses fails before the diaphysis yields in practice. More customary are fractures due to excessive bending or bending under additional axial compression. This combined load case is also common in subjects involved in traffic accidents. (Alms, 1961) With diaphysis fractures, the mechanism is typically a direct hit (e.g. automotive side impact) and/or indirect force applied through the knee (e.g. frontal crash). (Denisiuk & Afsari, 2021)

A group were factures of the proximal femur are very common is elderly people. A majority (63-69 %) of fractures related to falls in elderly patients is caused by a fall to the side (Greenspan et al., 1998; Kannus et al., 2006). Like traffic injuries, these fractures are manifold more common with women than men (Zuckerman, 1996). This has become a worldwide health problem as it causes reduced quality of live, disability and mortality (Boonen et al., 2004). Additionally, these types of fractures emerge as an issue in another context; a study on the Swedish accident database STRADA found that fractures of the proximal femur account for a large proportion (20 %) of serious (AIS3+) injuries suffered by over 60 year olds involved in car-to-pedestrian accidents (Leo et al., 2019).

Therefore, the present work focuses on the proximal femur. Although impact velocities in a fall from standing height are typically much slower than pedestrian accident velocities (2.75 m/s vs. 14.5 m/s), many of the medical experiments described in the following chapters were chosen as important bases of comparison, since the principal injury mechanisms are similar (Huang et al., 2007; van den Kroonenberg et al., 1996).

2.4 Femur injury risk assessment

Since femur fractures are a common injury in elderly patients, extensive medical research focused on enabling reliable prediction of fracture loads by measuring BMD in various regions (e.g. Cummings et al. (1993), Bouxsein et al. (1999), Pinilla et al. (1996), Cheng et al. (1997), Lang et al. (1997), Manske et al. (2006) and Pulkkinen et al. (2008)) or even evaluating trabecular bone texture (e.g. Boehm et al. (2008), Baum et al. (2010), Kolta et al. (2012), Hansen et al. (2011) and Le Corroller et al. (2012)). However, these techniques are subject specific and not suited for universally valid assertions.

A different approach has to be taken in vehicle safety, since universal statements are of great interest here and, more importantly, being able to give an estimate of the extent of possible injuries after impact is very desirable. To use a Human Body Model for safety evaluations, assessment criteria are needed, which enable the users to relate the model response with an injury risk. In contrast to traditional Anthropomorphic Test Devices, tissue-based assessment criteria can be applied for HBM simulations and are therefore the focus of this chapter.

Trauma biomechanical research pursues the goal of increasing our understanding of failure patterns and thus providing a means of estimating injury probabilities (Kent & Funk, 2004). A widely used method for doing this is the generation of so-called injury risk functions (IRFs) or curves (IRCs). These curves provide an injury probability based on a defined predictor like force, strain or acceleration etc. The functions are expressed as probability curves rather than absolute limits or thresholds because the actual probability of injury to an individual depends on the individual characteristics such as age, gender, physical condition, etc. as described in e.g. Crandall et al. (2011).

These IRCs are usually created based on testing using post-mortem human surrogates (PMHS) (or parts of PMHS) which are then subjected to the loading condition in question, relevant data is recorded and the injury outcome observed (Kerrigan et al., 2003; Petitjean et al., 2009). As Praxl (2011) notes in his review, a careful selection of the samples is advisable, since it has to be assumed that they are representative for the population the IRC is intended to be applied for.

However, defining the exact moment of injury is often a challenge even in reality, which introduces an effect called data censoring. It is often the case that a reliable statement can only be made whether an injury occurred below (“left censored”) or above (“right censored”) a certain value. This is quite common when using data from studies which were not designed for the creation of an IRC, since fracture force is often simply defined as the maximum force recorded. This might be not an accurate definition for the true onset of injury, leading to the data being left censored.

Praxl (2011) also emphasized that the effect of test severity is a common problem for the creation of reliable IRCs, since biomechanical tests are rarely carried out in the extremes (very high, very low) of the loading spectrum, because it is believed that the results are clear anyway. However, a broad range of test severities included in the creation of an IRC can improve its reliability (Praxl, 2011).

Lastly, the statistical model used in the approximation of the density function behind the IRC strongly influences the results. For example, a risk curve based on a logistic distribution will always exhibit a small risk offset, even at zero load or whatever the predictor is (Praxl, 2011). The statistical methods used for the creation of an IRC have been studied by Petitjean and Trosseille (2011) among others, who recommended a survival analysis based on a Weibull distribution when comparing it to four other statistical models (certainty method, consistent threshold estimate, logistic regression, Mertz/Weber

method). They also emphasize that exact data can provide a more accurate risk curve and even compensate for a smaller range of test severities. The good fit of a Weibull distribution is also demonstrated by Kleiven (2020) who applied this method to real-world femoral neck force data.

The injury risk predictor used in an IRC is only useful if it actually is a reliable metric for injury. For bone fractures, a stress based injury criterion was commonly implemented in the past (Keyak et al., 2001; Lotz, Cheal, & Hayes, 1991a, 1991b). It has since been shown that bone fracture is primarily driven by deformation (Nalla et al., 2003; Taylor, 2003), which suggests that a strain based metric would be a better predictor for fracture. Studies like Schileo et al. (2008) and more recently Gustafsson et al. (2021) implemented fracture criterions based on strain with good success.

However, to the knowledge of the author no model with an IRC for the proximal femur based on strain is currently available. IRCs used in current HBMs are still often carried over from corresponding ATD measurements like axial femur force. (Hu et al., 2019; Peres et al., 2016).

2.5 Experimental testing of the femur

To understand the injury mechanisms described above, researchers have been invested in experimental testing of the femur for more than a century. The following sections should provide an overview of common experimental testing procedures. These experiments are carried out with specimen from deceased subjects. The prevalent disadvantage of this method is that the (general) high age of these subjects very likely has an influence on the material behavior of the bone (see 2.2.3). This fundamental limitation is difficult to circumvent and is also evident in virtually all available studies on the subject.

2.5.1 Shaft

Simple three-point bending experiments of the femur were carried out long before the need for exact data to be used in finite element models, with one of the earliest examples being Weber (1859). The principle is rather simple, and calculations can be made with relative ease, based on the mechanics of a bending beam. One of the most cited modern sources on the subject is that of Yamada (1970), who published force-deflection curves from anterior-posterior and lateral-medial bending of the human femoral shaft from a study by Motoshima (1960). In his book, Yamada (1970) also supplies data on the ultimate bending strength and deflection grouped by specimen age. The study by Martens et al. (1986) is a bit of an outlier, as they performed four-point bending. 33 specimens (26 male, 7 female) gathered from cadavers which were 47 to 83 years old were loaded in 200 ms.

Two similar studies were carried out by Kerrigan et al. (2003) and Funk et al. (2004) who tested femurs in dynamic three-point bending tests. The epiphyses were embedded in roller pottings and displacement rate was 1.2 m/s in both studies. While testing was only performed in lateromedial

direction in Kerrigan et al. 's study, Funk et al. also included posteroanterior testing. The same team conducted additional tests leaving the soft tissue around the midshaft intact and using a slightly higher displacement rate (mean 1.5 m/s) (Kerrigan et al., 2004).

While also leaving the soft tissue unmarred, Kennedy et al. (2004) took a different approach by utilizing a drop tower with a 9.8 kg weight being dropped from 2.17 m to reach an impact speed of 5 m/s.

A comprehensive and well-documented study was eventually published by Ivarsson et al. (2009). Here, 47 specimens were tested in either conventional 3-point bending, bending combined with axial load or pure axial compression. The loading was applied in anteroposterior or posteroanterior direction and in all but three experiments the loading rate was dynamic (1.5 m/s). Raw data for displacements, forces and moments measured in the experiments are available in the biomechanics database kept by the National Highway Traffic Safety Administration (NHTSA).

To compile a reliable database on how the fracture moment of the human femur changes with age, Forman et al. (2012), augmented data from literature with their own tests on pediatric and middle aged femora with the same procedure as described in Kerrigan et al. (2004).

A summary of the mentioned studies is supplied in Table 2-3 including loading rates, number of specimen per gender and information on whether or not the results can be assigned to the genders.

Table 2-3: femur shaft testing summary, n_f = number of female samples, n_m = number of male samples, * = impact velocity, FF = fracture force, E = young's modulus, M = moment, C = Curve, S = Strain

	Loading type	Rate [m/s]	n_f	n_m	Sex clear	Results avail.
Yamada, 1970	3-point bending	Quasi-static	-	-	No	FF, E, C
Martens et al., 1986	4-point bending	Loading <200ms	7	26	No	FF, E, M
Kerrigan et al., 2003	3-point bending	1.2	6	2	Yes	FF, M
Funk et al., 2004	3-point bending	1.2	-	15	Yes	FF, M
Kerrigan et al., 2004	3-point bending	1.5	-	6	Yes	FF, M, S, C
Kennedy et al., 2004	3-point bending	5*	12	17	Yes	FF, E, M
Ivarsson et al., 2009	3-point bending	1.5	5	5	Yes	Raw data
	Axial compr.	1.5 / 0.001	5	6	Yes	Raw data
	Combined	1.5 / 0.001	11	19	Yes	Raw data
Forman et al., 2012	3-point bending	1.5	5	18	Yes	FF, M

2.5.2 Proximal femur – side-ways fall

Especially with these studies, the background is most often rather medical and not technical, since it is hoped to establish a reliable correlation of the femur strength with non-invasively measurable biological parameters (bone mineral density, cortical thickness, neck angle, etc.). This would enable patient-specific prediction of femoral strength and therefore easier prevention with relatively simple

means. Many studies therefore focus on the relation of bone mineral density, neck area, neck length, neck angle, trabecular structure pattern etc. and fracture force.

The side-ways fall setup is often attributed to Backman (1957) and Lotz and Hayes (1990), who are frequently cited as pioneers in the field of proximal femoral fracture research. The aforementioned study by Courtney et al. (1994) however is still referenced at least once in most modern studies on the subject. Thanks to their work, the setup with 10° shaft angle and 15° internal rotation of the femoral neck is considered the quasi-standard for simulating a fall to the side.

Table 2-4 provides a non-exhaustive overview of studies which make use of this side-ways fall configuration and provide sufficiently detailed data on their failure loads and boundary conditions. The loading-direction and –rate, ultimate load (F_U) and the number of specimen is stated. Where many of the mentioned studies differ, however, are the boundary conditions. On the one hand, the restraints at the distal end are often implemented differently and on the other hand, the boundary conditions are sometimes simply not sufficiently described. This is even more frustrating since Nishiyama et al. (2013) found out that their stiffness estimation was rather sensitive to varying boundary conditions, especially the internal rotation of the neck. Therefore, studies with differing angles like Dall'Ara et al. (2013) and Keyak et al. (1997) were omitted in this table. Courtney et al. (1994) is not listed, since no exact forces are supplied in the original paper.

Eckstein et al. (2004) conclude in their study that due to the large intersubject-variability of failure loads, the upper limit of the precision error for femoral strength tested in the sideways fall configuration is about 15 %.

Table 2-4: side-ways fall configuration summary, n_f = number of female samples/cadavers, n_m = number of male samples/cadavers, F_U = ultimate load, GT = greater trochanter, * = impact velocity, $^+$ = females only, § = median speed, individual rates, $^#$ = for part of results

	Load	Rate [mm/s]	F_U [N]	n_f	n_m	Sex clear	Remarks
Cheng et al., 1997	Head	14	3140$^+$	28	36	Yes	
Bouxsein et al., 1999	Head	100	2636	16	10	Yes	
Lochmüller et al., 2002	GT	6.5	3070$^+$			No	79 specimen in side impact
Eckstein et al., 2004	GT	6.6	3926	30	24	No	Referenced by Bauer et al., 2006; Baum et al., 2010; Koivumäki, Thevenot, Pulkkinen, Kuhn, Link, Eckstein, & Jämsä, 2012; Pulkkinen et al., 2006
Manske et al., 2006	Head	100	4354	13	10	No	
Boehm et al., 2008	GT	6.66	3934			No	100 specimen total
Pulkkinen et al., 2008	GT	6.6	2899$^+$	34	28	Yes$^#$	
de Bakker et al., 2009	GT	100	4032	6	6	Yes	
Roberts et al., 2010	GT	100	6075$^+$	48	25	Yes	Referenced by Johannesdottir et al., 2017
Dragomir-Daescu et al., 2011	Head	100	4034	13	5	Yes	Referenced by Rezaei et al., 2019
Op Den Buijs & Dragomir-Daescu, 2011	Head	100	4269			No	22 specimen total
Kolta et al., 2012	Head	2	2115	7	5	No	
Le Corroller et al., 2012	GT	0.166	2612	8	5	No	
Nishiyama et al., 2013	GT	2	2748$^+$	15	5	No	
Gilchrist, 2014	GT	114	2493	15	2	Yes	Referenced by Ariza et al., 2015; Enns-Bray et al., 2018
Helgason et al., 2014	GT	3500*	3760	1		Yes	
Zani et al., 2015	Head	25§	2799	8	3	Yes	
Varga et al., 2016	Head	-	3364	10	4	No	Drop-mass of 45kg at 114mm
Askarinejad et al., 2019	Head	0.06 & 4000*	3245 & 5640	3	2	Yes	
Fleps et al., 2019	GT	3100*	5448	6	5	Yes	Testing with pelvis and simulated soft tissue, different angles
Grassi, Kok et al., 2020	Head	5	3948	12	-	Yes	
Jazinizadeh et al., 2020	GT	0.017 & 3000*	3637 & 7326	4	4	No	
Palanca et al., 2020	GT	-	2984	9	1	Yes	Drop-mass of 7/20 of bodyweight, 3 samples without fracture

2.6 Finite Element Models of the femur

2.6.1 Development Process

The basic idea behind the FE method is to find solvable mathematical formulations of real problems. In order to provide the solvability in a reasonable time, idealization of the reality is often necessary. It is therefore necessary to find the balance between the required accuracy and the computational and personnel costs. (Yang, 2017a)

Once these simplifications have been made, it is of course necessary to evaluate the procedure through verification, calibration and validation. The goal of verification is to check if the intended mathematical formulation was implemented correctly, or casually stated, to answer the question: is the model built right? The process following verification is calibration, where the model output is compared to a set of target data and the implemented parameters are tuned to increase the conformity. When every aspect and building block of the model is implemented, verified and calibrated, the final step is validation. This is where the behavior of the whole model is checked against a different set of desired results, the question is answered: is this the right model, does it do what we want it to do? In the field of biomechanical research, this process is often a comparison of a certain simulation with data from similar real world experiments (see chapter 2.6.5). (Güneş, 2009)

2.6.2 Geometric Discretization

Discretization describes the process of partitioning the entire model into smaller parts, in the case of finite element analysis (FEA), the eponymous finite elements. A very short introduction to the nomenclature is provided for clarity. These elements can be defined differently according to their dimension. One-dimensional elements are called “beams”, two-dimensional ones “shells” and “solids” are the three-dimensional realization. Common element types are triangular or quadrilateral (four-cornered) shells and tetrahedral (pyramid) or hexahedral (cube/brick) solids. On the edges of each element, the so-called “nodes” are defined according to the order of the element. Linear elements have nodes at their corners, while quadratic elements employ additional nodes in the middle of each side. (Yang, 2017c)

2.6.3 Constitutive Models

The constitutive model defines the response of a material to physical forces or external influences, it provides the stress-strain correlation of the material. This is commonly called “material model” and a set of pre-defined formulations is usually supplied with the solver used, for example, LS-Dyna’s current library (version R11) provides over 280 different materials (Livermore Software Technology Corporation, 2018). The selection of the right constitutive model is however not trivial and dependent on the problems to be solved with the FE-model. For simple calculations of the elastic behavior of a structure under load, a linear-elastic material model may be sufficient, while somewhat more complex

formulations like strain-dependent viscoelastic material laws are needed to estimate the energy absorption in the case of a car crash. However, to successfully formulate a selected model, more or less extensive knowledge about various material properties like young's modulus, tangent modulus, yield point, ultimate properties, strain rate sensitivity, asymmetry etc. is needed. These variables are commonly determined through experimental testing, often using standardized setups to allow comparability. For most engineering materials, these properties are already well characterized and the necessary parameters can be obtained from existing lists. Unfortunately, this is not so easy with biological materials due to their immense multifariousness between individuals, the difficulty of obtaining fitting test specimen (ethical and practical limits) and the increased dependency on the testing conditions. (Yang, 2017b)

2.6.4 Use in medicine

Building on the experience from experimental testing (chapter 2.5), researchers began to advance their predictions of fracture risk using specimen specific FEM-models based on imaging material.

Keyak et al. (1997) were one of the first to employ this method in their study, even including the automatic generation of the model from CT-scans based on their previous work (Keyak et al., 1990). Results showed significant correlation between simulated and measured fracture loads, but the accuracy left room for improvement, which they eventually achieved a few years later, showing that maximum shear stress and distortion energy were better predictors for failure than their original, generic metric (Keyak & Rossi, 2000).

Extensive work in this field was also done by Lotz, Cheal, & Hayes, 1991a, 1991b, who were able to achieve fracture load predictions with only 1 % deviation for simulated side-ways fall experiments using nonlinear material models originally designed for concrete to represent trabecular bone.

Similar results are published by Cody et al. (1999), who created a FEM model based on data from quantitative computer tomography (QCT) and compared the prediction accuracy of dual energy X-ray absorptiometry (DXA), QCT and FEM. While the DXA method proved to be moderately reliable, the FEM-model could explain the variance in strength at least 20% better.

Even though finite element analysis (FEA) has evolved, todays continuous models are still most commonly based on CT images (Bessho et al., 2007; Dragomir-Daescu et al., 2011; Fleps et al., 2019; Grassi et al., 2012; Helgason et al., 2014; Koivumäki, Thevenot, Pulkkinen, Kuhn, Link, Eckstein, & Jämsä, 2012; Mirzaei et al., 2014; Miura et al., 2017; Nishiyama et al., 2013; Preutenborbeck, 2018; Schileo et al., 2008; Toniolo et al., 2020; Trabelsi et al., 2011; Varga et al., 2016) or MRI-data (Rajapakse et al., 2020). Within the last years, available DXA-measurements in combination with statistical shape and appearance models (SSAM) (Grassi et al., 2017; Grassi, Fleps et al., 2020; Humbert et al., 2017; Sarkalkan et al., 2014; Väänänen et al., 2012; Väänänen et al., 2015) have been implemented

successfully too. Recent subject specific CT-based models with advanced material mapping by Gustafsson et al. (2021) were predicting the fracture load with only 1% error and the location of fracture onset was predicted within a few millimeters.

Material mapping strategy and model selection proved to be an important factor for successful implementation, as demonstrated by Enns-Bray et al. (2018), Schileo et al. (2020), Grassi et al. (2016) and Helgason et al. (2016). However, this procedure requires a sufficiently high resolution (below 2mm) of the CT scans (Preutenborbeck, 2018). Another advancement for the creation of FE-models based on CT-images is the automated distinction between trabecular and cortical bone, which has been achieved as well (Väänänen et al., 2019).

Trabecular bone however seems to play a minor role in the load bearing process, since Koivumäki, Thevenot, Pulkkinen, Kuhn, Link, Eckstein, and Jämsä (2012) could estimate the failure load of the proximal femur with FEA using only cortical bone with reasonable results. Additionally, Johannesdottir et al. (2017) were able to establish that the proportions of load distribution between cortical and trabecular bone were quite flexible, with the cortical bone taking on a greater proportion of the applied force in the case of reduced trabecular bone density.

Using individual strain rate dependent materials for every single element based on CT imaging, Grassi et al., 2016 were able to achieve high accuracy in predicting principal strains compared to strain data captured by digital image correlation.

2.6.5 Use in vehicle safety

In contrast to the medical models, models for vehicle safety applications described in this section are usually part of a full Human Body Model or at least a full leg and have to be validated for a rage of more diverse loading patterns. A short overview of some of the most prolific studies focused on the development for lower limb models created primarily for the evaluation of lateral crashes is summarized in the following section. Selected finite element models developed for the use in vehicle safety are also summarized in Table A1-I (Appendix A.1). The table includes the implemented geometric discretization, constitutive models, young's modulus and yield stress for cortical and trabecular bone. It also provides the references used for the material data and validation of the femur.

One of the first properly approximated, three dimensional leg models was created by Bermond et al. (1994), who based their geometries on human leg X-rays and created 650 shell elements with a hand drawn mesh. The model also includes knee ligaments modelled as 1D linkages and was validated against PHMS tests carried out by Kajzer et al. (1993) and Kajzer et al. (1990). Two years later, Yang et al. (1996) modelled a femur using 3072 hexahedron solid elements, but left out the femur head due to limited data. The femur was not validated explicitly, but the full leg model was compared with impact tests carried out by Aldman et al. (1985) and Bunketorp, 1983.

A hybrid approach was taken by Schuster et al. (2000), who based their geometry on different sources. Cortical bone geometry was based on (Bedewi, 1998) and modelled as shells with varying thickness (2 mm in epiphyses to 5 mm in shaft) based on (Cristofolini et al., 1996; Cristofolini & Viceconti, 2000). Trabecular bone was defined using solid elements in the areas visualized in the Visible Human Project (National Library of Medicine). Both bone tissues were discretized as composite materials to reflect the assumed transversely isotropic, non-linear compressive and tensile properties and fed with data from Viano (1986), Cowin (1989), Carter and Hayes (1977), and Evans (1961). This model was validated against a myriad of sources, the femur alone was tested statically in two directions and compared to 8 sources. The full leg model was once again validated against Kajzer et al. (1990).

A study which used the same PHMS tests by Kajzer et al. (1990) and Kajzer et al. (1993) to validate their FE-model was Beillas et al. (2001). In this study, the geometry was based on CT- and MRI-scans taken from a close-to-50th percentile male subject. They indicate that the cortical thickness in their sample ranged from 2 - 7 mm and due to computational limitations, the compact bone was modelled as shell elements. Trabecular bone was defined using eight-node solid elements. Both bone tissue materials were defined with elastic-plastic behavior and regional differences were respected based on data from literature (Atkinson, 1998; Goldstein, 1987; Linde, 1994; Lotz, Gerhart et al., 1991; Mente & Lewis, 1994; Reilly & Burstein, 1975). The full leg model consisted of about 25000 elements.

Two years later, a study was published by Snedeker et al. (2003) who modified the newly developed Total Human Body Model for Safety (THUMS) (Iwamoto et al., 2002) for the use in pedestrian accident analysis. The basic THUMS used quadrilateral shell elements for the cortical bone (thickness at epiphyses = 1.6 mm, shaft = 5.5 mm) and solid brick elements for the trabecular bone. For both tissues, an isotropic elastic-plastic material formulation was used, but cortical bone was additionally modified with plastic hardening and by implementing strain-rate-dependency using Cowper-Symond's formulation. The femur shaft was again validated against the three-point bending data published by Yamada (1970) and the proximal femur was validated with the tests published by Keyak (2000). Fracture loads in stance and SWF configuration in simulation and experiments were compared.

Untaroiu et al. (2005) developed a leg-FE-model based on subject CT-scans published in the Visible Human Male Project (National Library of Medicine), scaled to represent a 50th percentile male. The cortical bone was discretized using quadrilateral shell elements in the femoral epiphyses. Hexahedral solid elements were used for the cortical bone in the shaft and the trabecular bone. The final element count per leg was 18500. The cortical material model was based on data by McElhaney (1966). An isotropic elastic-plastic material model was used for both bone tissues. The authors noted that modelling the anisotropic behavior of cortical bone would be important with combined load cases (e.g. axial compression and bending) and emphasized that a material model with explicit strain rate

dependencies and different properties in compression and tension are important for the approximation of cortical bone. The femur model was validated in quasi-static bending for anterior-posterior and lateral-medial loading referencing tests by Ehler and Lösche (1970); Mather (1968); Yamada (1970) and Strømsøe et al. (1995); Yamada (1970) respectively. It was additionally tested in the more dynamic configuration established by Funk et al. (2004), for which the corresponding force-deflection and MPS-deflection curves are provided. (Untaroiu et al., 2005)

The setup is also used for comparison in a later study by the same team, where they investigate the possibility to determine cortical material parameters for a subject specific FE-model by automatic computational optimization (Untaroiu et al., 2006). Two years later, Untaroiu et al. (2008) publish another study on this matter, this time including a combined loading setup for the femur (axial compression + bending). All of this knowledge is finally condensed into the study published in 2013, where Untaroiu et al. (2013) base their femur model on geometries gathered from CT- and MRI-scans of a subject close to the 50th percentile male by Gayzik et al. (2011) and Gayzik et al. (2012). Cortical bone in the epiphyses was again discretized using shell elements with the appropriate thickness (1 – 4 mm), the diaphysis region and trabecular bone was defined using hex-elements. Both bone tissues properties were again implemented using an isotropic elastic-plastic material model. Cortical bone material properties were scaled based on data from Brown and Vrahas (1984), Keller et al. (1990) and Lotz, Gerhart et al. (1991) to account for the regional differences in the proximal femur. The described femur model is part of the current GHBMC (Global Human Body Model Consortium) models.

Another detailed study on the development of a lower limb model was published by Dokko et al. (2009), who enhanced the model created by Kikuchi et al. (2006) to reflect the variances of bone material behavior with age. Using data from Reilly et al. (1974), Mather (1967), Hirsch and Evans (1965), Sedlin and Hirsch (1966), Wall et al. (1979) and Ko (1953), they constructed aging functions for the cortical young's modulus, ultimate stress and ultimate strain. For trabecular bone, these functions were based on data provided by Martens et al. (1983). Differing cortical thickness with age was adjusted making use of Ruff and Hayes (1988) dataset. The femur model was validated against static and dynamic three-point bending tests by Motoshima (1960) and Kerrigan et al. (2003) as well as the stance configuration proposed by Keyak et al. (1997). In one of the last sentences, the authors draw the conclusion, that for the development of female specific FE-models, it would be important to include the reduced BMD (Riggs et al., 1981) and varying cortical thickness (Ruff & Hayes, 1988), but not so much differing material properties for cortical bone. (Dokko et al., 2009)

A very similar study on the development of an age-dependent lower-limb model was later published by Huang et al. (2018). The GHBMC 50th percentile male (M50) lower extremity model was modified to reflect the properties of a 30 and 70 years old individual. For the adjustment of the shaft cross-

sections, the same dataset by Ruff and Hayes (1988) was used. Changes in material properties were based on Ding et al. (1997), Currey and Butler (1975), Reilly et al. (1974), Mather (1967) and McCalden et al. (1993) and assumed to be the same in all long bones of the lower limb based on findings by Parfitt (1984) and Bailey et al. (1999). The reference for validation were once again provided by Kerrigan et al. (2003) and Kajzer et al. (1997), for thigh and calve and the full model respectively.

An entirely different approach was taken by Klein et al. (2015), who created a statistical femur model based on CT scans from 62 male and 36 female subjects to predict femoral geometry based on age, body mass index and femur length. The 3D meshes were created with the use of a template model (femur taken from THUMS version 4) which was morphed to the surface of the target geometries using 13 manual and 46 computed landmarks. Subsequently, principal component analysis was carried out to develop linear regression models for the prediction of cortical thickness and geometry based on femur length, age and BMI. Klein et al. (2015)'s findings were used by many subsequent studies using parametric human body models based on the GHBMC M50, such as Hu et al. (2017), Zhang et al. (2017) and Hu et al. (2019).

Similarly, Park et al. (2016) created subject-specific femur FE-models by morphing the femur from the GHBMC M50 model to the respective CT-data of tested specimen. The focus of this study was on the femoral shaft, which is why the epiphyses were only taken into account with four landmarks each. The results of the shaft morphing were very promising though, simulation results based on the three point bending by Forman et al. (2012) showed a root mean square (RMS) error of 0.16kN, although only a linear-elastic material model was used. The role of the material definition is impressively described in the following paper by the group (Park et al., 2017): the aforementioned method was applied to sixteen additional subjects from Ivarsson et al. (2009) and a variant with heterogeneous, element specific, young's modulus was created in each case based on density gathered from the CT data and a power law relationship similar to the correlations published by Helgason et al. (2008). However, taking this closer approximation to reality into account brings almost no further improvement in the predicted bending forces. It is concluded that, at least for the femoral shaft, modelling geometric variability is more important than implementing heterogeneous material properties. Similarly, Varga et al. (2016) put on record, that modelling the anisotropy of bone material did not improve fracture predictions significantly. A similar conclusion is drawn by Khor et al. (2018) for failure loads, although they could demonstrate improved prediction of torsional loads, bending moments and fracture locations using an anisotropic cortical material model.

3 METHODS

3.1 Geometry update – cortical bone thickness

The outer geometry of the generic femur model was already defined in a previous step based on the regression models developed by Klein et al. (2015). Unfortunately, Klein et al. (2015) had a limited landmark count in the proximal femur, which is why an update in this region was needed. To address this shortcoming, finite element models based on CT-scans (Siemens SOMATOM Definition, 120 kVp, 100–400 mAs, 512x512 matrix, 1.0 pitch, 300–400 mm FOV, 1.0-mm slice thickness, up-sampled with Lanczos filter kernel) of five female femoral heads (average age = 24.6 years, avg. height = 168.2 cm, avg. weight = 61.5 kg) were generously supplied by Harris et al. (2011). These surface models each contained the required cortical thickness information. To transfer the individual thicknesses to the existing generic geometry, all subjects were landmarked manually with a slightly modified definition based on Väänänen et al. (2012). Since the supplied samples were cut at varying heights of their distal end, landmarks 17-20 were moved up to the same level as 4. Internal landmarks 1, 2, 3 and 5 were not used. The same landmarks were placed on the existing outer target geometry. The used landmarks can be seen in Appendix A.3.The individual specimen meshes were subsequently morphed to fit the target geometry using a Matlab script based on Radial Basis Functions (RBF) detailed in Carr et al. (1997) and used for morphing HBMs by Hu et al. (2016) for instance. Making use of the internal ANSA (Version 20.1.0, BETA CAE Systems) function "Results Mapper", each specimen's thickness information was projected onto an empty VIVA+ mesh, leaving five identical meshes with varying thickness information. Python (Version 3.8.5) helped to calculate the mean cortical thickness value at each node of the mesh and apply these values to another empty mesh of the generic femoral head used in the VIVA+ model. A schematic of the process is pictured in Figure 3-1. Using the built-in ANSA function "Voluminize", the average shell elements were converted to solids with the appropriate dimensions. Finally, the trabecular bone was re-modelled to fit the new inner geometry.

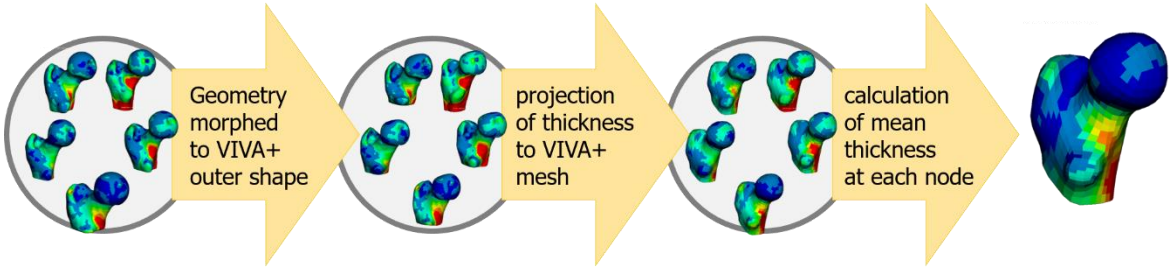

Figure 3-1: mean cortical thickness calculation process

3.2 Material data

3.2.1 Cortical bone

As described in chapter 2.2.1, cortical bone is generally characterized as a transversely isotropic material with an asymmetric behavior in tension and compression. Therefore, the LS-Dyna material model *MAT124, representing an isotropic elastic-plastic material with individual strain-stress curves for tension and compression was used. Raw data from experimental uniaxial tests with dumbbell samples originally published by Mirzaali et al. (2016) was used for this purpose. The dataset contained data from 17 tensile, 17 compression and 13 torsion tests with specimen taken from the femoral mid-diaphysis of females. Since torsion information was not needed in the following steps of this work, it is not further elaborated here. The gathered data was prepared with National Instruments DIAdem 2018 (Version 18.0.0.7097). The data consisted of signals for stroke, force, strain (directly captured in the axial channel), angle, torque and radial extension for each specimen. Since the data also covered the preloading circles, these were cut off as the first step. To do this reliably, the timestamp of the last zero-crossing of the force signal for compression and tension before loading was identified manually and all signals were cut off at this point. Since the signals were noisy and the goal was to calculate a mean curve anyways, a Savitzky-Golay filter (window size 72, polynomial order = 1) and subsequently smoothing (window size 32) was applied. The stroke signal was offset using the first-value-offset function. Next, a built-in DIAdem-function was used to identify the force peaks in every sample. The signals were cut-off again at this point, only leaving the portion from zero to the maximum force.

Subsequently, one sample in compression and two specimens in tension were excluded from the following steps, since their remaining stroke was much shorter than the one of the other samples.

To calculate a mean curve based on the individual samples, a modified script described in Klug et al. (2019) was used. With this method, all signals can be used in their original sample rate and their full length without scaling. The ordinary mean is calculated for the duration of the shortest signal, but after it ends, the algorithm switches to a different method to avoid “jumps” in the averaged curve. This method calculates the mean slope at the given point and adds a segment with this slope to the mean calculated before. In simple terms, the mean slope dictates the direction of the mean.

The force F and strain ε_{eng} signals were averaged independently as a function of time. The results are shown in Figure A.2-1 to A.2-4 in the Appendix A.2.

Engineering stress σ_{eng} was calculated as described in Equation 1, using the specimen geometry data supplied in Mirzaali et al. (2016) (cross-section radius of 1.5mm to calculated the cross section A_0).

$$\sigma_{eng} = \frac{F}{A_0} \tag{1}$$

The mean strain was then recalculated to true strain ε_{true} for the application in LS-Dyna using the formula given below (Equation 2):

$$\varepsilon_{true} = ln(1 + \varepsilon_{eng}) \tag{2}$$

Similarly, engineering stress was converted into true stress σ_{true} too, using the following formula (3):

$$\sigma_{true} = \sigma_{eng} * (1 + \varepsilon_{eng}) = \sigma_{eng} * e^{\varepsilon_{true}} \tag{3}$$

A Python script was used to identify the linear range of the given curves with the use of a rolling average window with a width of 4 % of the curve-length. The end of this linear range was defined as the yield point. Young's modulus E was calculated independently for compression and tension using the linear range identified before. The curves were then cut at the yield point and effective plastic strain $\varepsilon_{pla_{eff}}$ calculated according to Equation 4.

$$\varepsilon_{pla_{eff}} = \varepsilon_{true_{tot}} - \frac{\sigma_{true}}{E} \tag{4}$$

Although this was not clear from the documentation available, we found *MAT 124 works best if no PT and PC values are defined and the load curves are input starting at zero plastic strain but the corresponding true stress value. The material model was verified using a single element setup for compression and tension.

Based on findings from previous studies, the strain-stress curves were scaled down for the use in the greater trochanter area (factor 0.76 based on Lotz, Gerhart et al. (1991)) and the head and neck (factor 0.44 (Beillas et al., 2001; Untaroiu et al., 2013)).

3.2.2 Trabecular bone

The trabecular bone was modelled using a crush-able foam material (Fu Chang foam, LS-Dyna *MAT83) since it corresponds to the reported behavior of the tissue and Kelly and McGarry (2012) and others were able to achieve good results using similar material models. Although the real density of trabecular bone varies greatly in the proximal femur, we used the pooled value of 0.27 g/cm^3 provided by Morgan et al. (2003) for the implemented trabecular bone. To gather the needed stress-strain curves for the material model in LS-Dyna, formulas from Enns-Bray et al. (2018) and Helgason et al. (2014) were implemented in a python script and the corresponding stress-strain curves for 6 strain rates from 1E^{-6} to 10000 1/ms were calculated for tension and compression. To provide clarity, the used formulas are summarized here. In short, using the set density ρ the young's modulus E_{trab} was calculated using

Equation 5 as proposed by Morgan et al. (2003), who determined the relationship based on experimental testing of 27 femoral neck specimen.

$$E_{trab} = 6850 * \rho^{1.49} \quad (5)$$

Next, the strain rate scaling factor SRS was calculated following the routine proposed by Carter and Hayes (1977) (Equation 6), which is also used by Ariza et al. (2015) and Enns-Bray et al. (2018) among others.

$$\mathrm{SRS} = (\dot{\varepsilon}/0.005)^{0.06} \quad (6)$$

Ultimate, yield and proportional limit stresses were calculated using the formulas given in Enns-Bray et al. (2018), who refer to Carter and Hayes (1977), Helgason et al. (2008), Bayraktar et al. (2004)and Ariza et al. (2015). The formulas are based on experimental testing of small scale bone specimen and are summarized in Table 3-1 for clarity.

Table 3-1: formulas used for ultimate, yield, and proportional limit stresses and strains of the trabecular bone

	stress σ	***strain ε***
ultimate σ_u / ε_u	$49.5 * \rho_{app}^2 * SRS$	0.02
yield σ_y / ε_y	$\sigma_{ult}/1.1$	$\sigma_y/E + 0.02$
proportionality limit σ_p / ε_p	$\sigma_y * 0.8$	σ_p/E

For the tensional values, the ultimate stress and strain were multiplied by a compression/tension ratio (CTR) which was set to 0.7, based on the findings by Bayraktar et al. (2004). Yield and proportionality limits were then calculated using the same formulas stated in Table 3-1.

The trabecular bone material was defined with different post-yield behaviors for tension and compression. For tension, we used the relationship proposed by Enns-Bray et al. (2018), which describes the behavior as exponential decay as a function of strain (Equation 7).

$$\sigma_d = \sigma_u * (0.9 * e^{-25*\varepsilon_t} + 0.1) \quad (7)$$

Damage in compression follows the descriptions from Helgason et al. (2014), calculated for the selected density of 0.27 g/cm³. The described behavior was newly developed by Helgason et al. (2014) based on available data. In short, after yielding, trabecular bone exhibits a plateau (collapse of the pores) until the crushed trabeculae come into contact again, which leads to rapid hardening of the material. To avoid numerical errors when strain increases above 1 in compression, the curves were extended past the calculated maximum stress following the parable defined for the hardening process. The material model was verified using a single element setup for compression and tension.

3.3 Validation

3.3.1 Proximal femur - side-ways fall

The first setup corresponded to the widely described side-ways fall (SWF) scenario of 10° abduction and 15° internal rotation. This configuration was first mentioned by Backman (1957) and later modified by Courtney et al. (1994) and Lochmüller et al. (2002). Despite the popularity of this setup, see e.g. Boehm et al. (2008); de Bakker et al. (2009); Eckstein et al. (2004); Helgason et al. (2014); Jazinizadeh et al. (2020); Le Corroller et al. (2012); Nishiyama et al. (2013), no detailed and uniform description of all geometric boundary conditions could be found. We, therefore, based our simulation on the setup by Ariza (2014) which is also used and described in Gilchrist et al. (2013) and Gilchrist et al. (2014). The simulation setup is shown in Figure 3-2.

The distal end of the femur is potted in an aluminum cylinder using PMMA with a potting height of 182 mm (Ariza et al., 2015) . The potting was modelled using two parallel beam-elements with estimated inner and outer diameters of the PMMA-potting and the aluminum cylinder. The distal nodal rigid body used to connect the beams with the bone was additionally restricted in every movement except for a rotation in the vertical plane to mimic the boundary conditions described in Ariza et al. (2015).

PMMA-pads with a mass of about 21 g each for the head and greater trochanter (GT) were modelled to match the bone surface and meshed with similar parameters to the femur. Material properties for PMMA were taken from Villette and Phillips (2018), the pads were not modelled rigid since we didn't observe any downsides not doing it. On top of the GT-pad a rigid plate was added, which was used for the application of the desired displacements. A generic friction coefficient of 0.01 was applied in the contacts between cortical bone and PMMA-pads to mimic the low friction set in other simulations. Figure 3-2 visualizes the setup, the purple elements represent the PMMA-paddings while the rigid plate is pictured in a light blue shade. Masses of the included parts are supplied in the Appendix A.4.

Validation of the SWF-setup was carried out by applying the digitized (WebPlotDigitizer v4.4, https://automeris.io/WebPlotDigitizer) displacements from Ariza (2014) to the top rigid plate of our model. Using a central node on the GT and the contact-force between top PMMA-pad and GT force and displacement curves from the simulation were compared with the ones supplied in Ariza (2014).

For the augmentation of the injury risk curve, the same setup was tested with a constant displacement rate of 100 mm/s at the rigid pad and the distal fixture additionally allowing translation in the horizontal plane and rotation around the vertical axis based on experiments published by de Bakker et al. (2009).

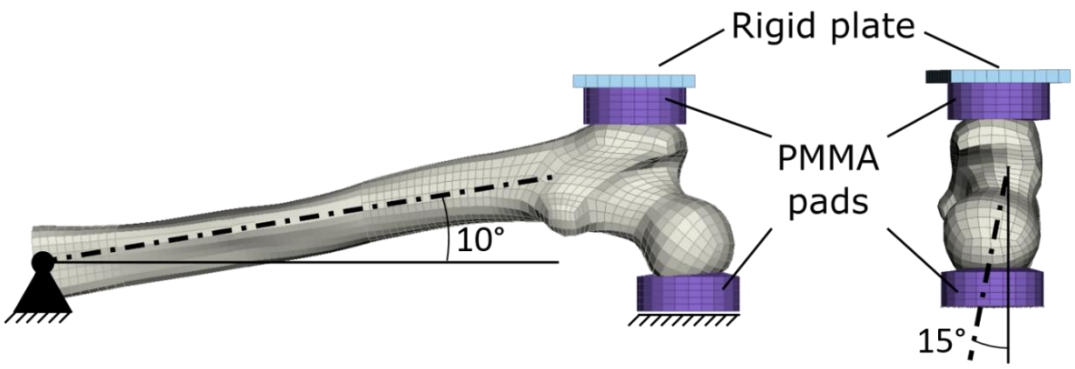

Figure 3-2: sideways fall simulation setup

This setup was also modified to allow load application with the rigid plate to the head and the trochanter pad acting as a support, since this variant of the configuration is also widely used in literature (Askarinejad et al., 2019; Bouxsein et al., 1999; Cheng et al., 1997; Dragomir-Daescu et al., 2011; Grassi, Fleps et al., 2020; Kolta et al., 2012; Manske et al., 2006; Op Den Buijs & Dragomir-Daescu, 2011; Zani et al., 2015). While different displacement rates and distal boundary conditions are frequently described in literature (Courtney et al., 1994; Grassi et al., 2012; Zani et al., 2015), we replicated the study by Dragomir-Daescu et al. (2011) where the support structure underneath the GT is fixed and the head loaded with a constant displacement of 100 mm/s.

3.3.2 Shaft - three-point bending

To specifically validate the behavior of the cortical bone, a previously built anteroposterior three-point bending scenario was adapted for use with the developed femur model. The current setup is based on the description by Funk et al. (2004) and was referred to by Yamada (1970) beforehand. The femur is embedded in rounded pottings on both the distal and proximal end, leaving only the shaft exposed. A rounded impactor subsequently strikes midshaft with an impact speed of 1.2 m/s. See Figure 3-3 for an image of the setup. The part masses of the setup used are documented in Appendix A.4.

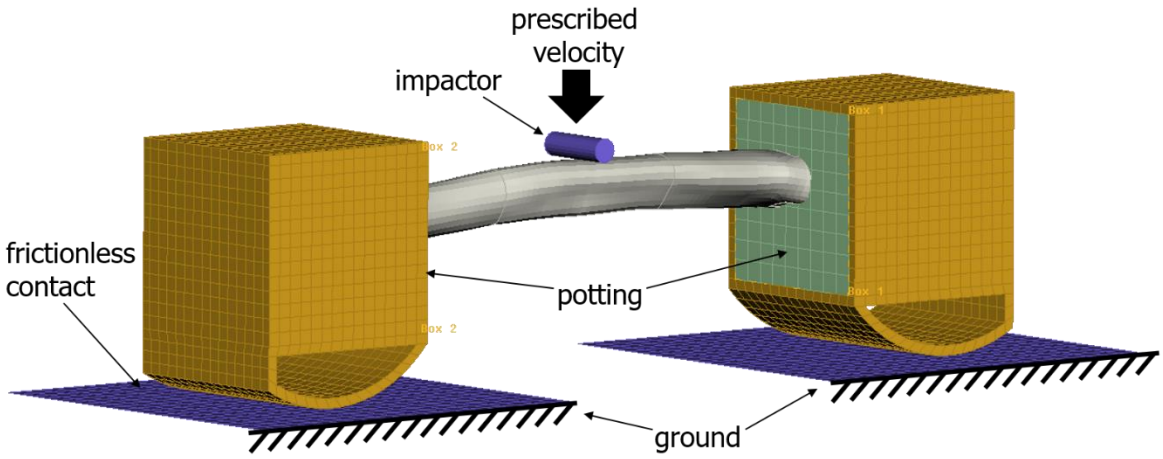

Figure 3-3: three-point bending setup

3.4 Injury Risk Curve

The IRC of the proximal female femur was created based on maximum principle strain values. For the creation, the MPS-values in the cortical bone at the time of the fracture force known from the referenced experiments were extracted from all relevant simulations using the Dynasaur (Vehicle Safety Institute - Graz University of Technology, 2021) function “stress_strain_time_history” with the settings mean integration point, “overall” for tension and compression and linear interpolation. A total of 20 simulations of female femurs tested in the side-ways fall configuration were used. Included are the 14 female specimen from Ariza et al. (2015), specimen T5, V4 and V5 (T = testing-, V = validation-cohort) from Dragomir-Daescu et al. (2011) and specimen B, K and L from de Bakker et al. (2009). The selection of the specimen from de Bakker et al. and Dragomir-Daescu et al. was restricted by the reported T-score, which had to be greater than >-1.0 to avoid osteopenic or –porotic subjects. A summary of all included subjects is given in Table 3-2.

Table 3-2: included specimen and configurations for the proximal injury risk curve

Study	***Specimen included***	***Configuration***	***Rate [mm/s]***
Ariza et al., 2015	all but H1168R; 14 in total	SWF – GT	indiv.
Dragomir-Daescu et al., 2011	T5, V4, V5	SWF – Head	100
de Bakker et al., 2009	B, K, L	SWF – GT	100

Previous studies have shown that basing the calculations on the maximum value of a single element is highly sensitive to possible numerical issues, therefore the 99 percentile MPS values were considered additionally (Peres et al., 2016). These gathered MPS-values were subsequently used for the creation of injury risk functions based on a Weibull distribution estimated with maximum likelihood estimation (MLE) in R (Version 4.0.3). Using Q-Q and P-P plots, the Weibull distribution was determined to be the best fit in comparison with gamma- and log-normal-distributions.

4 RESULTS

4.1 Cortical thickness

The average cortical thickness derived from the five CT-scans before the creation of solid elements is shown element vise in Figure 4-1 and summarized by region, which are marked in the same figure, in Also included in Table 4-1 are comparative thickness values gathered from 89 subjects (mean age 61 years) by Ramme et al. (2019). Unfortunately, for the values marked with *, the regions were defined slightly different.

Table 4-1.

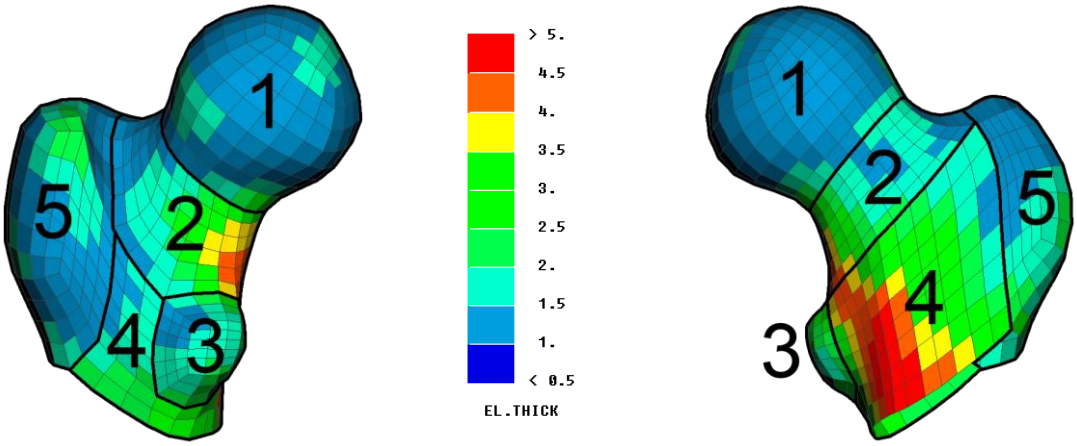

Figure 4-1: resulting average cortical thickness of the proximal femur

Also included in Table 4-1 are comparative thickness values gathered from 89 subjects (mean age 61 years) by Ramme et al. (2019). Unfortunately, for the values marked with *, the regions were defined slightly different.

Table 4-1: average cortical thickness in the proximal femur by region with comparison to Ramme et al. (2019)
* = region defined different

Region	***Average cortical thickness [mm]***	***Ramme et al., 2019***
Head (1)	1.38657	1.123
Neck (2)	2.15795	1.944
Lesser Trochanter (3)	1.90243	-
Intertrochanteric (4)	3.08508	2.114 *
Greater Trochanter (5)	1.57156	1.202 *
Total proximal femur	1.91212	1.697

4.2 Material data

4.2.1 Cortical bone

A summary of the implemented values for the Young's modulus E and yield stress σ_y calculated from Mirzaali et al. (2016) data can be found in Table 4-2. Cortical bone was set to a uniform density of 1.8 g/cm³ throughout the whole model (Carter & Hayes, 1977; Gibson, 1985).

Table 4-2: summary of calculated young's moduli and yield stresses in compression and tension

Loading	***E [GPa]***	***σ_y [GPa]***
Compression	16.479	0.08246
Tension	16.384	0.04110

The resulting mean true stress – true strain curves for tension and compression are provided in Figure 4-2 with the identified yield points marked as a black dot. The grey line is plotted using the young's modulus in compression. Figures of the scaled cortical materials used in the GT, head and neck areas are supplied in Appendix A.5.

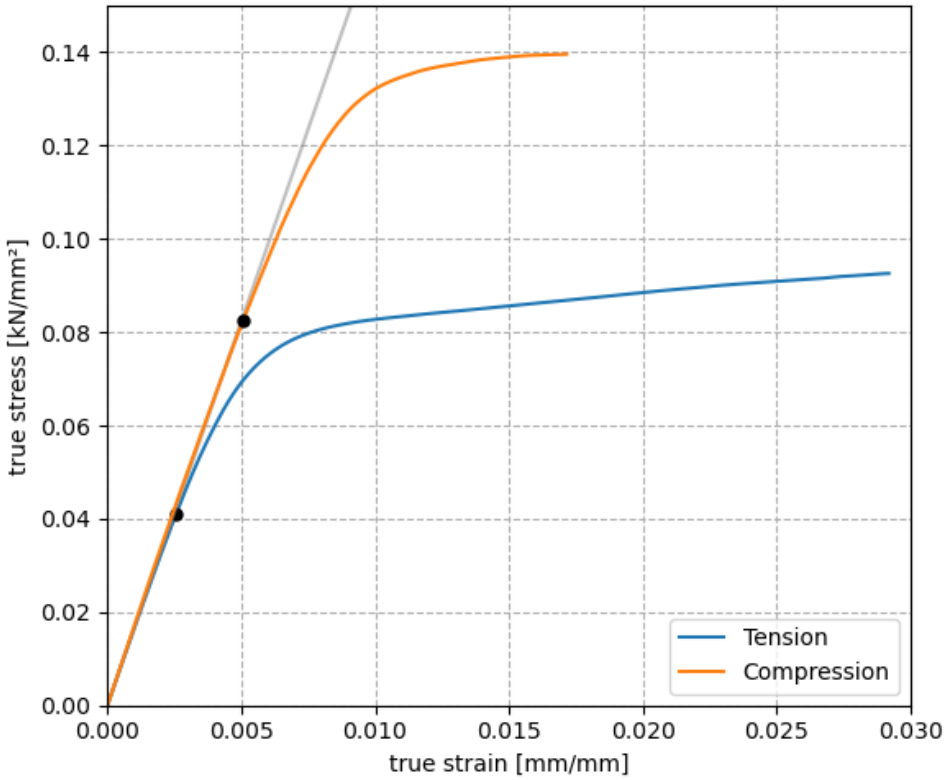

Figure 4-2: cortical true strain and stress (compression / tension)

4.2.2 Trabecular bone

The calculated strain-stress-curves are displayed in Figure 4-3, which were directly implemented in LS-Dyna's *MAT83. Therefore, the material models definitions for compression (positive strain/stress) and tension (negative stress/strain) were adopted here. As MAT83 requires uniform endpoints for all implemented curves, they were extended beyond the calculated maximum stress in compression for better numerical robustness. The smaller graph in the center shows a detail of the curves near the origin to provide a better view.

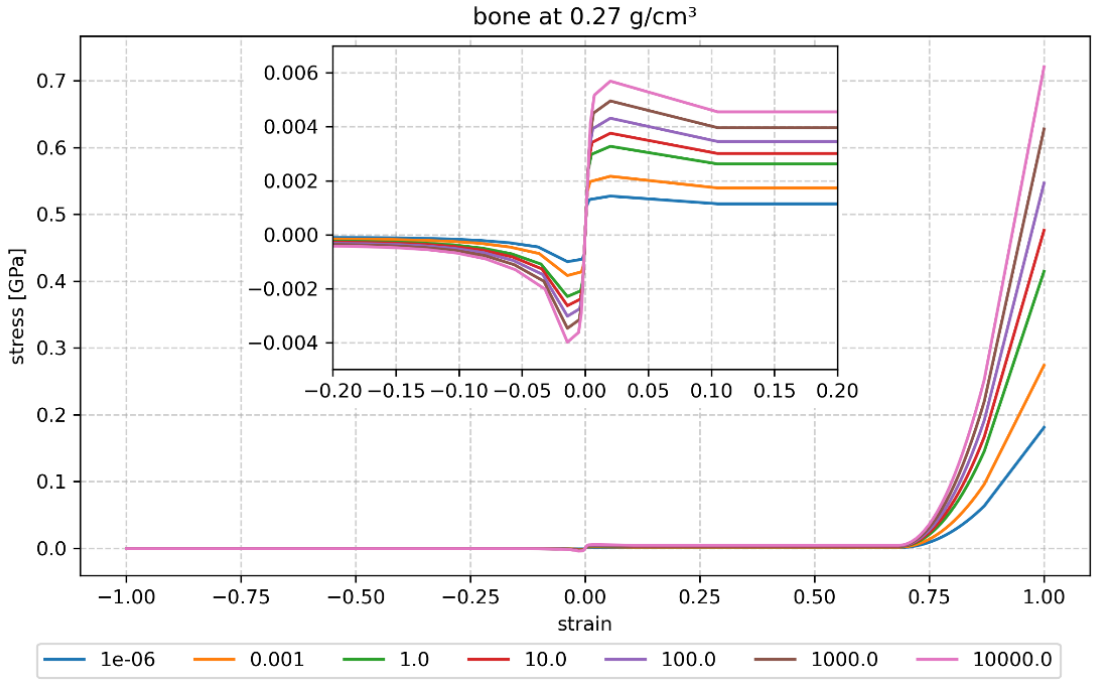

Figure 4-3: stress-strain-curves for trabecular bone, positive strain and stress is defined as compression in accordance with the material model *MAT83

4.3 Validation

4.3.1 Proximal femur - side-ways fall

A comparison of the force-time curves from our simulations (orange) and the originals (black) from Ariza et al. (2015) can be seen in Figure 4-4. The simulated force was defined as the contact force between the upper PMMA pad and the greater trochanter. Additional displacement and force-displacement curves are supplied in the Appendix A.6.

The displacement corresponds to the deflection of a node (#7171045) on the GT. In the experiments, the force was recorded with a load cell above the PMMA pad and the displacement was digitized from high-speed video. The designations in parentheses next to the specimen numbering (which is concordant to the source) reflect abbreviations of the WHO classification for the degree of osteoporosis, "N" means normal (T-score > -1), "Onic" stands for osteopenic (-1 > T-score > -2.5) and "Otic" for osteoporotic (T-score < -2.5).

The additional simulation with constant displacement of 100 mm/s at the rigid plate was primarily intended to be used as additional input for the injury risk curve. The force-time curve (using same definitions as described above) with the modified cortical material can be seen in Appendix A.6. The fracture forces of the selected samples (called B, K, L in the source) from de Bakker et al. (2009) are labeled and marked with horizontal lines.

The force-time curve of the flipped side-ways fall setup based on Dragomir-Daescu et al. (2011) is also supplied in Appendix A.6, including marks for the fracture forces of relevant specimen.

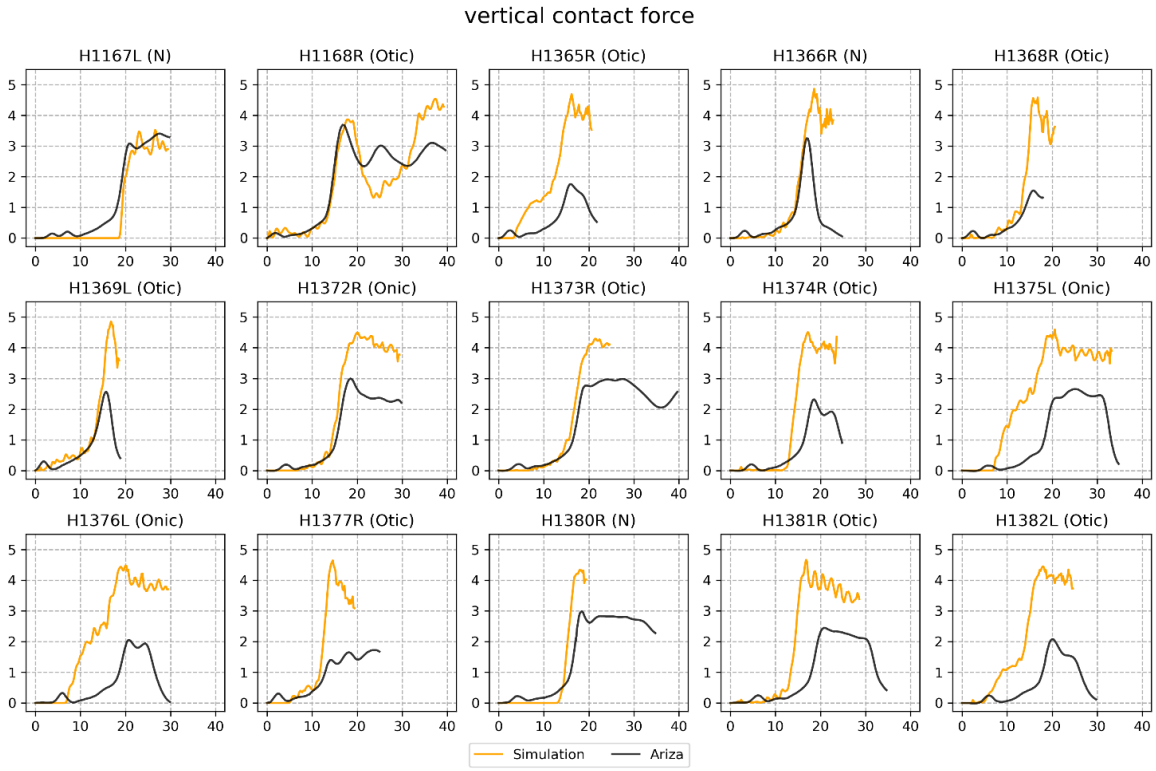

Figure 4-4: force curves from sideway falls from Ariza et al. (black) compared to our simulation with modified cortical bone (orange)

4.3.3 Shaft – three-point bending

The force-deflection curve from the simulation of the 3-point bending setup in comparison with data from Yamada (1970) is supplied in Figure 4-5. For the simulation, force was defined as the contact force between the impactor and the cortical bone of the shaft, displacement is the deflection of a node (#7203339) in the area of contact.

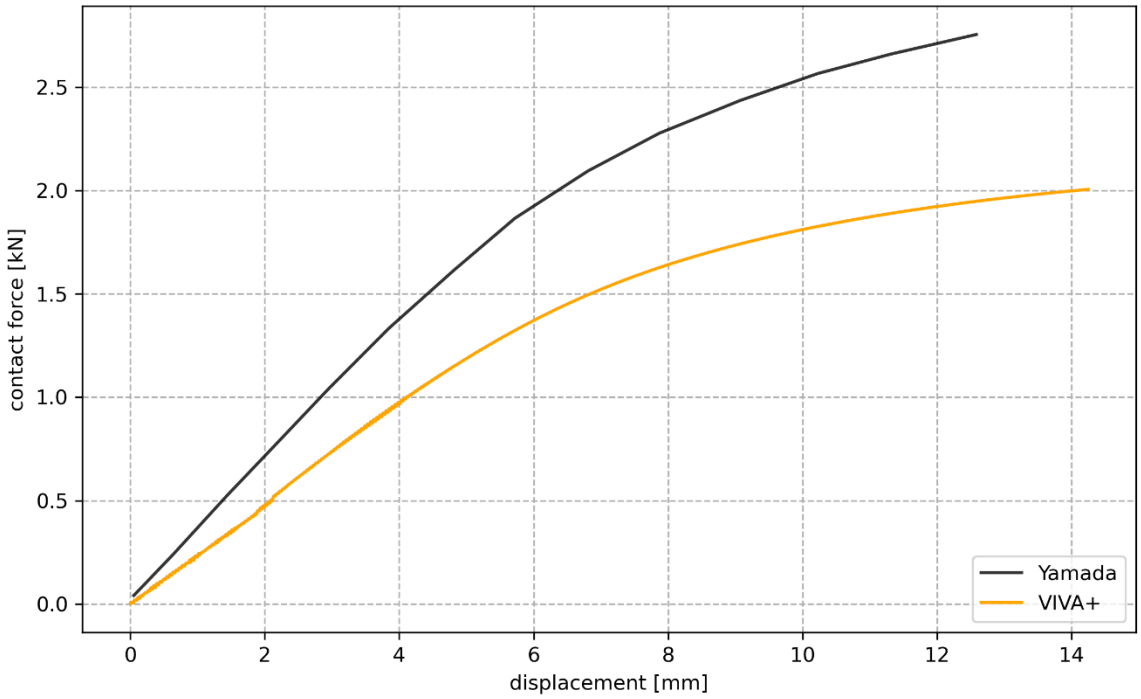

Figure 4-5: force – displacement curves from simulated three-point bending (orange) in comparison with data supplied in Yamada (1970)

4.4 Injury Risk Curve

The injury risk curves including the 95% confidence interval derived from simulations based on the side-ways fall configurations by Ariza et al. (2015), de Bakker et al. (2009) and Dragomir-Daescu et al. (2011) (n=20) is shown in Figure 4-6 (a) for the 99th percentile maximum principal strain (MPS99) and Figure 4-6 (b) for the corresponding total maximum principal strain (MPS100). The shape parameter for the underlying Weibull distribution for the MPS99 distribution was determined as 1.2289 and the scale parameter was 0.0198. The IRC based on MPS100 is defined by a shape parameter of 1.0233 and a scale parameter estimation of 0.0581. Additional figures of the IRC with the MPS99 and MPS100 values at the time of fracture included are supplied in Figure A.3-1 a and b respectively (see Appendix A.7).

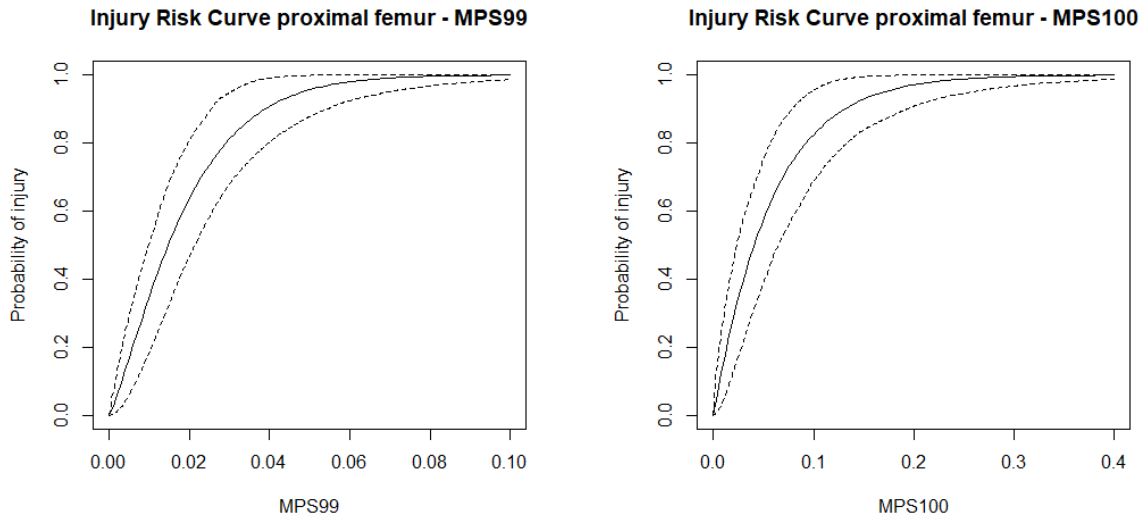

a b

Figure 4-6: injury risk curves of the proximal femur based on 99th percentile MPS (a) and the total MPS (b)

5 DISCUSSION

5.1 Cortical thickness

While the sample size for the average cortical thickness of the proximal femur defined in the first step is rather low, the resulting thickness values by region are in good correspondence with data published in literature (Du et al., 2018; Ramme et al., 2019; Snedeker et al., 2003; Treece et al., 2012). Other sources like Yang et al. (2012) state slightly lower cortical thickness for individual regions of the proximal femur, but this study was carried out on elderly people only. Since the specimen we used in this step were young and had no known bone-issues, it is safe to presume no effects of ageing affected our calculations (Harris et al., 2011). Slight deviations of the calculated average thickness and the final geometries of the solid elements were noted, especially in the region of the greater trochanter, and attributed to necessary mesh smoothing before the creation of the new trabecular solid elements. At some single nodes, these deviations are close to 10 %, which could be one attributing factor why the proximal region of the presented model is slightly stiffer than comparable examples.

Different solid element formulations ("ELFORM" in LS-Dyna) for the cortical bone were tested using the validation setup for specimen H1366R from Ariza et al. (2015). The default formulation EQ = 1 with and without hourglass definition (HIQ = 5), fully integrated elements (EQ = 2) and fully integrated elements intended for solids with poor aspect ratio (EQ = -2) were compared. The differences in stiffness were small, but the hourglass energy for ELFORM EQ = 1 was manifold greater than EQ = 2 or -2, even with applied hourglass definition. Given the lower hourglass energy and overall force, ELFORM EQ = -2 was chosen for the final model. Figures for force, force-displacement, total, internal and hourglass energy for each element formulation are supplied in Appendix A.8.

5.2 Materials modelling

Material data for cortical bone calculated from the raw data used in Mirzaali et al. (2016) is also in line with literature, the young's modulus of around 16 GPa corresponds neatly with the mentioned density-relationship by Morgan et al. (2003), assuming the density of cortical bone is 1.8 g/cm³. It is also in line with material properties published in relevant literature (Table 2-1). A boxplot comprised from mean data supplied by Evans and Lebow (1951), Sedlin and Hirsch (1966), Mather (1968), Yamada (1970), Saha and Hayes (1976), Fung (1993), Keller et al. (1990), Lotz, Gerhart et al. (1991), Currey (2004), Cuppone et al. (2004) and Bayraktar et al. (2004) is pictured in Figure 5-1. Also included is the implemented value as a blue line.

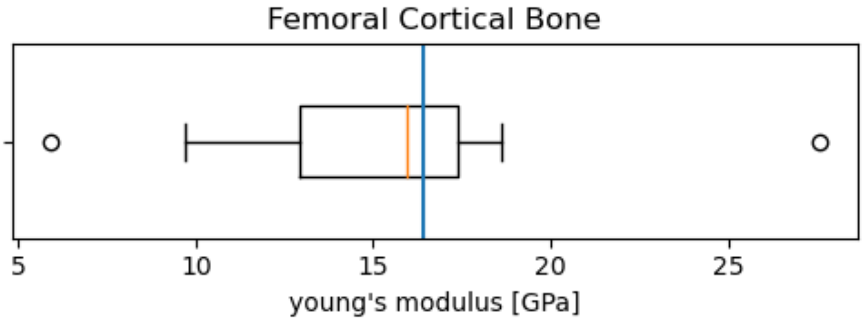

Figure 5-1: comparison of literature data with the calculated young's modulus

Other sources like Keller (1994), Lotz, Gerhart et al. (1991) and Currey et al. (1997) published lower young's moduli, but these samples were often taken from different sites of the femur and from elderly specimen. Age dependent material behavior is not implemented in the model yet, because a specific age of 50 years was targeted. However, several studies found a decreasing young's modulus with increasing age (see chapter 2.2.3), which should be considered in the future.

The current material model for the cortical bone does not consider anisotropic behavior, which constitutes a limitation, especially if the model was to be used in a torsional loading condition (Morgan et al., 2018; Shahar et al., 2007). Nevertheless, using an isotropic material model in bending configurations was shown to be sufficient. However, the presented model should not be used for detailed fracture pattern analysis. (Khor et al., 2018)

Scaling of the cortical material was initially based on findings by Lotz, Gerhart et al. (1991), who found a 24 % percent decrease in the elastic modulus measured in the femoral metaphysis compared to the diaphysis. The samples used for the macro-mechanical testing by Mirzaali et al. (2016) were extracted from mid-diaphyseal sites of the femora, indicating that the calculated properties need to be scaled down for the use in the proximal femur. This assumption is also supported by implementations such as Beillas et al. (2001) and Untaroiu et al. (2013), who scaled down the shafts young's modulus by 66 % for the neck and 85 % for the head (Untaroiu et al., 2013) or 25 % for the metaphysis and 66 % for the epiphyses (Beillas et al., 2001). Our applied reduction of 66 % for the neck and head is based on the ratios from Beillas et al. (2001), who refers to Atkinson (1998) and Mente and Lewis (1994) for the magnitude. This decision was also supported by initial simulations showing increased stiffness and ultimate force levels. A comparison of the validation simulations based on Ariza et al. (2015) carried out with and without the scaled material is supplied in Appendix A.9. The blue curves are the results without scaling the cortical bone for head, neck and GT. The effect of this down-scaling is shown in the orange curves, where the overall force plateau is about 2kN lower. It is readily evident that by reducing the stiffness of the cortical bone in selected areas, the approach to the target curves is better achieved.

Modeling representative average trabecular bone proved to be difficult, since we found no reliable way of creating a realistic density distribution map for the trabecular bone of the proximal femur. The set density of 0.27 g/cm³ might be an applicable mean value, but the real density of trabecular bone in the proximal femur is certainly not homogeneous and the material shows different behavior depending on the anatomical site (Bauer et al., 2006; Cummings et al., 1993; Eckstein et al., 2002; Goldstein, 1987; Keaveny et al., 1997; Martens et al., 1983; Morgan et al., 2003). The influence of different densities for the trabecular bone were studied using one load-case from Ariza et al. (2015) as an example and are shown in Appendix A.10. The density was halved (0.12 g/cm³), doubled (0.56 g/cm³) and the trabecular bone removed from the femur. An influence on the overall stiffness and even the MPS values in the cortical bone was noted. We believe that further work on this matter, especially implementing site-dependent density and corresponding property-relationships, would further increase the validity of the model.

5.3 Validation results

The decision to base our simulation model on the data published by Ariza et al. (2015) had several reasons:

- The same set of specimen was also used by Gilchrist et al. (2014) and Enns-Bray et al. (2018), who published additional data on the matter
- the loading is dynamic, a better approximation for car-to-pedestrian accidents,
- individual force-time, displacement-time and force-displacement curves are published in Ariza (2014)
- the boundary conditions are clearly stated
- Enns-Bray et al. (2018) had good success replicating this setup with subject specific FE-models

Using the cortical material gathered from experimental data for the whole femur showed a drastic increase in stiffness when tested in the sideways fall configuration. The mean force at the time of fracture in this simulation (5779 N) is almost twofold of the one published in Ariza et al. (2015) (2492 N). It has to be noted however, that 12 out of 15 specimens used by Ariza et al. (2015) suffered from reduced bone mineral density, which was found to influence bone strength, fracture loads and the femoral stiffness negatively (see chapter 2.2.3) (Beason et al., 2003; Bouxsein et al., 1995; Bouxsein et al., 1999; Cheng et al., 1997; Courtney et al., 1994; Cummings et al., 1993; Dragomir-Daescu et al., 2011; Eckstein et al., 2002; Eckstein et al., 2004; Fleps et al., 2020; Greenspan et al., 1994; Nevitt et al., 1994; Osterhoff et al., 2016; Rezaei & Dragomir-Daescu, 2015; Ross et al., 1990).

Implementing the scaled cortical bone properties for GT, neck and head brought the simulated mean fracture force down to 4021 N, which is comparable to other experiments carried out with similar setups, where ultimate forces between 3-5 kN are reported. (see Table 2-4).

The modified SWF setup we used for additional testing has been implemented, among others, by Askarinejad et al. (2019), Cheng et al. (1997), Cheng et al. (1998), Dall'Ara et al. (2013), Courtney et al. (1994), Dragomir-Daescu et al. (2011), Grassi et al. (2012), Grassi, Fleps et al. (2020), Kolta et al. (2012), Op Den Buijs and Dragomir-Daescu (2011), Pinilla et al. (1996), Rezaei et al. (2019) and Zani et al. (2015) with various slight modifications, different loading rates and even divergent boundary conditions.
The datasets we selected for comparison in this configuration were chosen based on how detailed the specimen and results descriptions were, which level of osteoporosis was reported and whether the tested individuals were identifiable as female or not.
The developed female femur model is slightly stiffer when tested in the side-ways fall configuration than comparable samples published in literature (Dall'Ara et al., 2013; Dragomir-Daescu et al., 2011). The result from pure three-point bending does not lead to the same conclusion of increased stiffness, as the simulated contact force at 12.5 mm displacement is 30 % lower than the force supplied by Yamada (1970). However, the curve by Yamada (1970) does not specifically represent a female and is widely used for the validation of femur models from 50th percentile male models (Iwamoto et al., 2000; Schuster et al., 2000; Untaroiu et al., 2005).

5.4 Injury risk curve

The created injury risk curve is currently solely based on simulations representing subjects where injury occurred. Together with the high age of the tested specimen (mean age 75.3 years), this inevitably introduces biased estimation of a risk curve of a 50th percentile female proximal femur (Praxl, 2011). An implementation of an age-factor was attempted to account for the high age, but failed due to the small number of samples included. Although Dragomir-Daescu et al. supplied more samples (T2-4, T6, V2, V6) fitting the selection criteria detailed in section 3.4, they could not be included since their reported fracture load is higher than the maximum force in our simulation.
The chosen Weibull density function is also proposed by general statistical analysis (Petitjean & Trosseille, 2011) and proved to result in a plausible injury risk curve for hip fractures based on several hundred femoral neck forces (Kleiven, 2020). However, it is challenging to apply the risk curved developed directly for HBM simulations, as it is based on experimental strains. In our study, a specific model-dependent curve was derived. To the knowledge of the authors no other openly available human body model includes a specific injury risk curve for the proximal femur. Given the novelty of the work, further improvements are needed, and, thanks to the open-source principle of the project possible for anyone.

6 CONCLUSION

A representative femur model of a 50th percentile female was developed using available data for geometry and material properties. Material properties were assumed to be homogenous for all of the trabecular bone and scaled for particular regions of the cortical bone. The model was validated specifically for the proximal region, since this area was found to be at high risk in car-to-pedestrian and car-to-bicycle accidents. Validation was also carried out for the shaft using a conventional three-point bending setup. The developed femur model includes injury risk curves based on the cortical maximum principal strain (100th and 99th percentile) created explicitly based on simulations of proximal femur fractures in a side-ways fall setup. The current versions of the IRCs however are based on limited data, mostly from elderly specimen. For the future, it would be very valuable to have more detailed data from younger female cadavers available, to further improve the validation work and to increase the robustness of the injury risk curve. The model can now be used within the full HBM to study the injury risk in vulnerable road user accidents and investigate the reasons for sex-specific differences, which have been observed when analyzing real-world accidents.

7 REFERENCES

Abrams, M. Z., & Bass, C. R. (2020). Female vs. Male Relative Fatality Risk in Fatal Crashes. In International Research Council on the Biomechanics of Injury (Chair), *IRCOBI Conference*.

Aldman, B., Kajzer, J., Bunketorp, O., & Eppinger, R. (1985). An experimental study of a modified compliant bumper. In *International Technical Conference on the Enhanced Safety of Vehicles,* Oxford, England.

Alms, M. (1961). Fracture Mechanics. *The Journal of Bone and Joint Surgery*, 162–166. https://doi.org/10.1302/0301-620X.43B1.162

Ariza, O. R. (2014). *A novel approach to finite element analysis of hip fractures due to sideways falls* [Master's Thesis]. University of British Columbia, Vancouver.

Ariza, O. R., Gilchrist, S. M., Widmer, R. P., Guy, P., Ferguson, S. J., Cripton, P. A., & Helgason, B. (2015). Comparison of explicit finite element and mechanical simulation of the proximal femur during dynamic drop-tower testing. *Journal of Biomechanics*, *48*(2), 224–232. https://doi.org/10.1016/j.jbiomech.2014.11.042

Ashman, R. B., & Rho, J.-Y. (1988). Elastic modulus of trabecular bone material. *Journal of Biomechanics*, *21*(3), 177–181. https://doi.org/10.1016/0021-9290(88)90167-4

Askarinejad, S., Johnson, J. E., Rahbar, N., & Troy, K. L. (2019). Effects of loading rate on the of mechanical behavior of the femur in falling condition. *Journal of the Mechanical Behavior of Biomedical Materials*, *96*, 269–278. https://doi.org/10.1016/j.jmbbm.2019.04.038

Atkinson, P. J. (1998). *A stress-based damage criterion to predict articular joint injury from subfracture insult* [Dissertation]. Michigan State University. https://doi.org/10.25335/M5TM7244X

Backman, S. (1957). The proximal end of the femur: Investigations with special reference to the etiology of femoral neck fractures; anatomical studies; roentgen projections; theoretical stress calculations; experimental production of fractures. *Acta Radiologica. Supplementum*(146), 1–166.

Bailey, A. J., Sims, T. J., Ebbesen, E. N., Mansell, J. P., Thomsen, J. S., & Mosekilde, L. (1999). Age-related changes in the biochemical properties of human cancellous bone collagen: Relationship to bone strength. *Calcified Tissue International*, *65*(3), 203–210. https://doi.org/10.1007/s002239900683

Bauer, J. S., Kohlmann, S., Eckstein, F., Mueller, D., Lochmüller, E.-M., & Link, T. M. (2006). Structural Analysis of Trabecular Bone of the Proximal Femur Using Multislice Computed Tomography: A

Comparison with Dual X-Ray Absorptiometry for Predicting Biomechanical Strength In Vitro. *Calcified Tissue International*, *78*(2), 78–89. https://doi.org/10.1007/s00223-005-0070-3

Baum, T., Carballido-Gamio, J., Huber, M. B., Müller, D., Monetti, R., Räth, C., Eckstein, F., Lochmüller, E.-M., Majumdar, S., Rummeny, E. J., Link, T. M., & Bauer, J. S. (2010). Automated 3D trabecular bone structure analysis of the proximal femur—Prediction of biomechanical strength by CT and DXA. *Osteoporosis International*, *21*(9), 1553–1564. https://doi.org/10.1007/s00198-009-1090-z

Bayraktar, H. H., Morgan, E. F., Niebur, G. L., Morris, G. E., Wong, E. K., & Keaveny, T. M. (2004). Comparison of the elastic and yield properties of human femoral trabecular and cortical bone tissue. *Journal of Biomechanics*, *37*(1), 27–35. https://doi.org/10.1016/S0021-9290(03)00257-4

Beason, D. P., Dakin, G. J., Lopez, R. R., Alonso, J. E., Bandak, F. A., & Eberhardt, A. W. (2003). Bone mineral density correlates with fracture load in experimental side impacts of the pelvis. *Journal of Biomechanics*, *36*(2), 219–227. https://doi.org/10.1016/S0021-9290(02)00330-5

Bedewi, P. G. (1998). *The biomechanics of human lower extremity injury in the automotive crash environment* (9826808) [Dissertation]. The George Washington University.

Beillas, P., Begeman, P. C., Yang, K. H., King, A. I., Arnoux, P. J., Kang, H. S., Kayvantash, K., Brunet, C., Cavallero, C., & Prasad, P. (2001). Lower Limb: Advanced FE Model and New Experimental Data. *Stapp Car Crash Journal*, *45*, 469–494.

Beillas, P., Lavaste, F.\a., Nicolopoulos, D., Kayventash, K., Yang, K. H., & Robin, S.\a. (1999). Foot and Ankle Finite Element Modeling Using Ct-Scan Data. In *SAE Technical Paper Series.* SAE International, 400 Commonwealth Drive, Warrendale, PA, United States. https://doi.org/10.4271/99SC11

Bermond, F., Ramet, M., Bouquet, R., & Cesari, D. (1994). A finite element model of the pedestrian leg in lateral impact. In *14th International Technical Conference on the Enhanced Safety of Vehicles,* Munich, Germany. http://wbldb.lievers.net/10086128.html

Bessho, M., Ohnishi, I., Matsuyama, J., Matsumoto, T., Imai, K., & Nakamura, K. (2007). Prediction of strength and strain of the proximal femur by a CT-based finite element method. *Journal of Biomechanics*, *40*(8), 1745–1753. https://doi.org/10.1016/j.jbiomech.2006.08.003

Bini, F., Marinozzi, A., Marinozzi, F., & Patanè, F. (2002). Microtensile measurements of single trabeculae stiffness in human femur. *Journal of Biomechanics*, *35*(11), 1515–1519. https://doi.org/10.1016/S0021-9290(02)00182-3

Boehm, H. F., Horng, A., Notohamiprodjo, M., Eckstein, F., Burklein, D., Panteleon, A., Lutz, J., & Reiser, M. (2008). Prediction of the fracture load of whole proximal femur specimens by

topological analysis of the mineral distribution in DXA-scan images. *Bone*, *43*(5), 826–831. https://doi.org/10.1016/j.bone.2008.07.244

Boonen, S., Autier, P., Barette, M., Vanderschueren, D., Lips, P., & Haentjens, P. (2004). Functional outcome and quality of life following hip fracture in elderly women: A prospective controlled study. *Osteoporosis International*, *15*(2), 87–94. https://doi.org/10.1007/s00198-003-1515-z

Bose, D., Segui-Gomez, M., & Crandall, J. R. (2011). Vulnerability of Female Drivers Involved in Motor Vehicle Crashes: An Analysis of US Population at Risk. *American Journal of Public Health*, *101*(12), 2368–2373. https://doi.org/10.2105/AJPH.2011.300275

Bouxsein, M. L. (2001). Biomechanics of Age-Related Fractures. In R. Marcus, D. Feldman, & J. L. Kelsey (Eds.), *Osteoporosis* (2nd ed., pp. 509–531). Academic Press. https://doi.org/10.1016/B978-012470862-4/50020-9

Bouxsein, M. L., Coan, B.S., & Lee, S.C. (1999). Prediction of the strength of the elderly proximal femur by bone mineral density and quantitative ultrasound measurements of the heel and tibia. *Bone*, *25*(1), 49–54. https://doi.org/10.1016/S8756-3282(99)00093-9

Bouxsein, M. L., Courtney, A. C., & Hayes, W. C. (1995). Ultrasound and densitometry of the calcaneus correlate with the failure loads of cadaveric femurs. *Calcified Tissue International*, *56*(2), 99–103. https://doi.org/10.1007/BF00296338

Brown, T. D., & Vrahas, M. S. (1984). The apparent elastic modulus of the juxtarticular subchondral bone of the femoral head. *Journal of Orthopaedic Research*, *2*(1), 32–38. https://doi.org/10.1002/jor.1100020106

Brown, T. D., & Ferguson, A. B. (1980). Mechanical Property Distributions in the Cancellous Bone of the Human Proximal Femur. *Acta Orthopaedica Scandinavica*, *51*(1-6), 429–437. https://doi.org/10.3109/17453678008990819

Bunketorp, O. (1983). *Pedestrian Leg Protection In Car Accidents. An Experimental And Clinical Study.*

Burstein, A. H., Currey, J. D., Frankel, V. H., & Reilly, D. T. (1972). The ultimate properties of bone tissue: The effects of yielding. *Journal of Biomechanics*, *5*(1), 35–44. https://doi.org/10.1016/0021-9290(72)90017-6

Burstein, A. H., Reilly, D. T., & Martens, M. (1976). Aging of bone tissue: Mechanical properties. *The Journal of Bone and Joint Surgery. American Volume*, *58*(1), 82–86.

Carlsson, A., Chang, F., Lemmen, P., Kullgren, A., Schmitt, K.-U., Linder, A., & Svensson, M. (2012). EVARID - A 50th Percentile Female Rear Impact Finite Element Dummy Model. In International Research Council on the Biomechanics of Injury (Chair), *IRCOBI Conference,* Dublin, Ireland.

Carr, J. C., Fright, R., & Beatson, R. K. (1997). Surface Interpolation with Radial Basis Functions for Medical Imaging. *IEEE Transactions on Medical Imaging*, *16*(1), 96–107. https://doi.org/10.1109/42.552059

Carter, D. R., & Hayes, W. C. (1977). The compressive behavior of bone as a two-phase porous structure. *The Journal of Bone and Joint Surgery. American Volume*, *59*(7), 954–962.

Chandran, V., Maquer, G., Gerig, T., Zysset, P. K., & Reyes, M. (2019). Supervised learning for bone shape and cortical thickness estimation from CT images for finite element analysis. *Medical Image Analysis*, *52*, 42–55. https://doi.org/10.1016/j.media.2018.11.001

Cheng, X. G., Lowet, G., Boonen, S., Nicholson, P. H. F., Brys, P., Nijs, J., & Dequeker, J. (1997). Assessment of the strength of proximal femur in vitro: Relationship to femoral bone mineral density and femoral geometry. *Bone*, *20*(3), 213–218. https://doi.org/10.1016/S8756-3282(96)00383-3

Cheng, X. G., Lowet, G., Boonen, S., Nicholson, P. H. F., van der Perre, G., & Dequeker, J. (1998). Prediction of vertebral and femoral strength in vitro by bone mineral density measured at different skeletal sites. *Journal of Bone and Mineral Research*, *13*(9), 1439–1443. https://doi.org/10.1359/jbmr.1998.13.9.1439

Ciarelli, M. J., Goldstein, S. A., Kuhn, J. L., Cody, D. D., & Brown, M. B. (1991). Evaluation of orthogonal mechanical properties and density of human trabecular bone from the major metaphyseal regions with materials testing and computed tomography. *Journal of Orthopaedic Research*, *9*(5), 674–682. https://doi.org/10.1002/jor.1100090507

Ciarelli, T. E., Fyhrie, D. P., Schaffler, M. B., & Goldstein, S. A. (2000). Variations in three-dimensional cancellous bone architecture of the proximal femur in female hip fractures and in controls. *Journal of Bone and Mineral Research*, *15*(1), 32–40. https://doi.org/10.1359/jbmr.2000.15.1.32

Clauss, W., & Clauss, C. (2018). Halte- und Bewegungsapparat. In W. Clauss & C. Clauss (Eds.), *Lehrbuch. Humanbiologie kompakt* (2nd ed., pp. 63–94). Springer Spektrum. https://doi.org/10.1007/978-3-662-55850-8_3

Cody, D. D., Gross, G. J., J. Hou, F., Spencer, H. J., Goldstein, S. A., & Fyhrie, D. P. (1999). Femoral strength is better predicted by finite element models than QCT and DXA. *Journal of Biomechanics*, *32*(10), 1013–1020. https://doi.org/10.1016/S0021-9290(99)00099-8

Courtney, A. C., Wachtel, E. F., Myers, E. R., & Hayes, W. C. (1994). Effects of loading rate on strength of the proximal femur. *Calcified Tissue International*, *55*(1), 53–58. https://doi.org/10.1007/BF00310169

Cowin, S. C. (1989). *Bone mechanics* (1. ed., 2. printing). CRC Press.

Crandall, J. R., Bose, D., Forman, J. L., Untaroiu, C. D., Arregui-Dalmases, C., Shaw, C. G., & Kerrigan, J. R. (2011). Human surrogates for injury biomechanics research. *Clinical Anatomy (New York, N.Y.)*, *24*(3), 362–371. https://doi.org/10.1002/ca.21152

Cristofolini, L., & Viceconti, M. (2000). Mechanical validation of whole bone composite tibia models. *Journal of Biomechanics*, *33*(3), 279–288. https://doi.org/10.1016/S0021-9290(99)00186-4

Cristofolini, L., Viceconti, M., Cappello, A., & Toni, A. (1996). Mechanical validation of whole bone composite femur models. *Journal of Biomechanics*, *29*(4), 525–535. https://doi.org/10.1016/0021-9290(95)00084-4

Cummings, S. R., Browner, W., Black, D. M., Nevitt, M. C., Genant, H. K., Cauley, J., Ensrud, K., Scott, J., & Vogt, T. M. (1993). Bone density at various sites for prediction of hip fractures. *The Lancet*, *341*(8837), 72–75. https://doi.org/10.1016/0140-6736(93)92555-8

Cuppone, M., Seedhom, B. B., Berry, E., & Ostell, A. E. (2004). The Longitudinal Young's Modulus of Cortical Bone in the Midshaft of Human Femur and its Correlation with CT Scanning Data. *Calcified Tissue International*, *74*(3), 302–309. https://doi.org/10.1007/s00223-002-2123-1

Currey, J. D., & Butler, G. (1975). The mechanical properties of bone tissue in children. *The Journal of Bone and Joint Surgery. American Volume*, *57*(6), 810–814.

Currey, J. D. (2004). Tensile yield in compact bone is determined by strain, post-yield behaviour by mineral content. *Journal of Biomechanics*, *37*(4), 549–556. https://doi.org/10.1016/j.jbiomech.2003.08.008

Currey, J. D., Foreman, J., Laketić, I., Mitchell, J., Pegg, D. E., & Reilly, G. C. (1997). Effects of ionizing radiation on the mechanical properties of human bone. *Journal of Orthopaedic Research*, *15*(1), 111–117. https://doi.org/10.1002/jor.1100150116

Dagan, D., Be'ery, M., & Gefen, A. (2004). Single-trabecula building block for large-scale finite element models of cancellous bone. *Medical and Biological Engineering and Computing*, *42*(4), 549–556. https://doi.org/10.1007/BF02350998

Dall'Ara, E., Luisier, B., Schmidt, R., Kainberger, F., Zysset, P. K., & Pahr, D. (2013). A nonlinear QCT-based finite element model validation study for the human femur tested in two configurations in vitro. *Bone*, *52*(1), 27–38. https://doi.org/10.1016/j.bone.2012.09.006

Dall'Ara, E., Öhman, C., Baleani, M., & Viceconti, M. (2011). Reduced tissue hardness of trabecular bone is associated with severe osteoarthritis. *Journal of Biomechanics*, *44*(8), 1593–1598. https://doi.org/10.1016/j.jbiomech.2010.12.022

de Bakker, P. M., Manske, S. L., Ebacher, V., Oxland, T. R., Cripton, P. A., & Guy, P. (2009). During sideways falls proximal femur fractures initiate in the superolateral cortex: Evidence from high-

speed video of simulated fractures. *Journal of Biomechanics*, *42*(12), 1917–1925. https://doi.org/10.1016/j.jbiomech.2009.05.001

Denisiuk, M., & Afsari, A. (2021). *Femoral Shaft Fractures*. https://www.ncbi.nlm.nih.gov/books/NBK556057/

Ding, M. (2000). Age variations in the properties of human tibial trabecular bone and cartilage. *Acta Orthopaedica Scandinavica*, *71*(sup292), i-45. https://doi.org/10.1080/17453674.2000.11744841

Ding, M., Dalstra, M., Danielsen, C. C., Kabel, J., Hvid, I., & Linde, F. (1997). Age variations in the properties of human tibial trabecular bone. *The Journal of Bone and Joint Surgery. British Volume*, *79*(6), 995–1002. https://doi.org/10.1302/0301-620x.79b6.7538

Dokko, Y., Ito, O., & Ohashi, K. (2009). Development of Human Lower Limb and Pelvis FE Models for Adult and the Elderly. In *SAE Technical Paper Series.* SAE International, 400 Commonwealth Drive, Warrendale, PA, United States. https://doi.org/10.4271/2009-01-0396

Dragomir-Daescu, D., Op Den Buijs, J., McEligot, S., Dai, Y., Entwistle, R. C., Salas, C., Melton, L. J., Bennet, K. E., Khosla, S., & Amin, S. (2011). Robust QCT/FEA models of proximal femur stiffness and fracture load during a sideways fall on the hip. *Annals of Biomedical Engineering*, *39*(2), 742–755. https://doi.org/10.1007/s10439-010-0196-y

Du, W., Zhang, J., & Hu, J. (2018). A Method to Determine Cortical Bone Thickness of Human Femur and Tibia Using Clinical CT Scans. In International Research Council on the Biomechanics of Injury (Chair), *IRCOBI Conference,* Athens, Greece.

Eckstein, F., Lochmüller, E.-M., Lill, C. A., Kuhn, V., Schneider, E., Delling, G., & Müller, R. (2002). Bone strength at clinically relevant sites displays substantial heterogeneity and is best predicted from site-specific bone densitometry. *Journal of Bone and Mineral Research*, *17*(1), 162–171. https://doi.org/10.1359/jbmr.2002.17.1.162

Eckstein, F., Wunderer, C., Boehm, H. F., Kuhn, V., Priemel, M., Link, T. M., & Lochmüller, E.-M. (2004). Reproducibility and side differences of mechanical tests for determining the structural strength of the proximal femur. *Journal of Bone and Mineral Research*, *19*(3), 379–385. https://doi.org/10.1359/JBMR.0301247

Ehler, E., & Lösche, H. (1970). Biegeversuche am menschlichen Femur. *Beitr. Orthop*, *17*(5), 857–867.

Enns-Bray, W. S., Bahaloo, H., Fleps, I., Ariza, O. R., Gilchrist, S. M., Widmer, R., Guy, P., Pálsson, H., Ferguson, S. J., Cripton, P. A., & Helgason, B. (2018). Material mapping strategy to improve the predicted response of the proximal femur to a sideways fall impact. *Journal of the Mechanical Behavior of Biomedical Materials*, *78*, 196–205. https://doi.org/10.1016/j.jmbbm.2017.10.033

Evans, F. G. (Ed.). (1961). *Biomechanical studies of the musculo-skeletal system.*

Evans, F. G. (1973). *Mechanical properties of bone*. Thomas. https://archive.org/details/mechanicalproper0000evan

Evans, F. G., & Lebow, M. (1951). Regional differences in some of the physical properties of the human femur. *Journal of Applied Physiology*, *3*(9), 563–572. https://doi.org/10.1152/jappl.1951.3.9.563

Fleps, I., Bahaloo, H., Zysset, P. K., Ferguson, S. J., Pálsson, H., & Helgason, B. (2020). Empirical relationships between bone density and ultimate strength: A literature review. *Journal of the Mechanical Behavior of Biomedical Materials*, *110*, 103866. https://doi.org/10.1016/j.jmbbm.2020.103866

Fleps, I., Guy, P., Ferguson, S. J., Cripton, P. A., & Helgason, B. (2019). Explicit Finite Element Models Accurately Predict Subject-Specific and Velocity-Dependent Kinetics of Sideways Fall Impact. *Journal of Bone and Mineral Research*, *34*(10), 1837–1850. https://doi.org/10.1002/jbmr.3804

Ford, C. M., Keaveny, T. M., & Hayes, W. C. (1996). The effect of impact direction on the structural capacity of the proximal femur during falls. *Journal of Bone and Mineral Research*, *11*(3), 377–383. https://doi.org/10.1002/jbmr.5650110311

Forman, J. L., del Pozo de Dios, Eduardo, Symeonidis, I., Duart, J., Kerrigan, J. R., Salzar, R. S., Balasubramanian, S., Segui-Gomez, M., & Kent, R. W. (2012). Fracture Tolerance Related to Skeletal Development and Aging Throughout Life: 3-Point Bending of Human Femurs. In International Research Council on the Biomechanics of Injury (Chair), *IRCOBI Conference,* Dublin, Ireland.

Frysz, M., Gregory, J. S., Aspden, R. M., Paternoster, L., & Tobias, J. H. (2020). Sex differences in proximal femur shape: Findings from a population-based study in adolescents. *Scientific Reports*, *10*(1), 4612. https://doi.org/10.1038/s41598-020-61653-4

Fung, Y.-C. (1993). *Biomechanics: Mechanical Properties of Living Tissues* (Second edition). Springer New York.

Funk, J. R., Kerrigan, J. R., & Crandall, J. R. (2004). Dynamic bending tolerance and elastic-plastic material properties of the human femur. *Annual Proceedings / Association for the Advancement of Automotive Medicine*, *48*, 215–233.

Gayzik, F. S., Moreno, D. P., Danelson, K. A., McNally, C., Klinich, K. D., & Stitzel, J. D. (2012). External landmark, body surface, and volume data of a mid-sized male in seated and standing postures. *Annals of Biomedical Engineering*, *40*(9), 2019–2032. https://doi.org/10.1007/s10439-012-0546-z

Gayzik, F. S., Moreno, D. P., Geer, C. P., Wuertzer, S. D., Martin, R. S., & Stitzel, J. D. (2011). Development of a full body CAD dataset for computational modeling: A multi-modality approach.

Annals of Biomedical Engineering, *39*(10), 2568–2583. https://doi.org/10.1007/s10439-011-0359-5

Gibson, L. J. (1985). The mechanical behaviour of cancellous bone. *Journal of Biomechanics*, *18*(5), 317–328. https://doi.org/10.1016/0021-9290(85)90287-8

Gilchrist, S. M. (2014). *Comparison of proximal femur deformations, failures and fractures in quasi-static and inertially-driven simulations of a sideways fall from standing : An experimental study utilizing novel fall simulation, digital image correlation, and development of digital volume correlation techniques* [Dissertation]. University of British Columbia, Vancouver. https://doi.org/10.14288/1.0166885

Gilchrist, S. M., Guy, P., & Cripton, P. A. (2013). Development of an inertia-driven model of sideways fall for detailed study of femur fracture mechanics. *Journal of Biomechanical Engineering*, *135*(12), 121001. https://doi.org/10.1115/1.4025390

Gilchrist, S. M., Nishiyama, K. K., de Bakker, P. M., Guy, P., Boyd, S. K., Oxland, T. R., & Cripton, P. A. (2014). Proximal femur elastic behaviour is the same in impact and constant displacement rate fall simulation. *Journal of Biomechanics*, *47*(15), 3744–3749. https://doi.org/10.1016/j.jbiomech.2014.06.040

Goldstein, S. A. (1987). The mechanical properties of trabecular bone: Dependence on anatomic location and function. *Journal of Biomechanics*, *20*(11-12), 1055–1061. https://doi.org/10.1016/0021-9290(87)90023-6

Grassi, L., Fleps, I., Sahlstedt, H., Väänänen, S. P., Ferguson, S. J., Isaksson, H., & Helgason, B. (2020). Validation of 3D finite element models from simulated DXA images for biofidelic simulations of sideways fall impact to the hip. *Bone*, *142.* https://doi.org/10.1016/j.bone.2020.115678

Grassi, L., Kok, J., Gustafsson, A., Zheng, Y., Väänänen, S. P., Jurvelin, J. S., & Isaksson, H. (2020). Elucidating failure mechanisms in human femurs during a fall to the side using bilateral digital image correlation. *Journal of Biomechanics*, *106.* https://doi.org/10.1016/j.jbiomech.2020.109826

Grassi, L., Schileo, E., Taddei, F., Zani, L., Juszczyk, M. M., Cristofolini, L., & Viceconti, M. (2012). Accuracy of finite element predictions in sideways load configurations for the proximal human femur. *Journal of Biomechanics*, *45*(2), 394–399. https://doi.org/10.1016/j.jbiomech.2011.10.019

Grassi, L., Väänänen, S. P., Ristinmaa, M., Jurvelin, J. S., & Isaksson, H. (2016). How accurately can subject-specific finite element models predict strains and strength of human femora? Investigation using full-field measurements. *Journal of Biomechanics*, *49*(5), 802–806. https://doi.org/10.1016/j.jbiomech.2016.02.032

Grassi, L., Väänänen, S. P., Ristinmaa, M., Jurvelin, J. S., & Isaksson, H. (2017). Prediction of femoral strength using 3D finite element models reconstructed from DXA images: Validation against experiments. *Biomechanics and Modeling in Mechanobiology*, *16*(3), 989–1000. https://doi.org/10.1007/s10237-016-0866-2

Greenspan, S. L., Myers, E. R., Kiel, D. P., Parker, R. A., Hayes, W. C., & Resnick, N. M. (1998). Fall Direction, Bone Mineral Density, and Function: Risk Factors for Hip Fracture in Frail Nursing Home Elderly. *The American Journal of Medicine*, *104*(6), 539–545. https://doi.org/10.1016/S0002-9343(98)00115-6

Greenspan, S. L., Myers, E. R., Maitland, L. A., Resnick, N. M., & Hayes, W. C. (1994). Fall Severity and Bone Mineral Density as Risk Factors for Hip Fracture in Ambulatory Elderly. *JAMA*, *271*(2), 128–133. https://doi.org/10.1001/jama.1994.03510260060029

Güneş, M. (2009). *Verification and Validation of Simulation Models.* Freie Universität Berlin. Modeling and Performance Analysis with Simulation, Berlin.

Gustafsson, A., Tognini, M., Bengtsson, F., Gasser, T. C., Isaksson, H., & Grassi, L. (2021). Subject-specific FE models of the human femur predict fracture path and bone strength under single-leg-stance loading. *Journal of the Mechanical Behavior of Biomedical Materials*, *113*, 104118. https://doi.org/10.1016/j.jmbbm.2020.104118

Hansen, S., Jensen, J.-E. B., Ahrberg, F., Hauge, E. M., & Brixen, K. (2011). The Combination of Structural Parameters and Areal Bone Mineral Density Improves Relation to Proximal Femur Strength: An In Vitro Study with High-Resolution Peripheral Quantitative Computed Tomography. *Calcified Tissue International*, *89*(4), 335–346. https://doi.org/10.1007/s00223-011-9523-z

Hansen, U., Zioupos, P., Simpson, R., Currey, J. D., & Hynd, D. (2008). The effect of strain rate on the mechanical properties of human cortical bone. *Journal of Biomechanical Engineering*, *130*(1), 11011. https://doi.org/10.1115/1.2838032

Harris, M. D., Anderson, A. E., Henak, C. R., Ellis, B. J., Peters, C. L., & Weiss, J. A. (2011). Finite element prediction of cartilage contact stresses in normal human hips. *Journal of Orthopaedic Research*, *30*(7), 1133–1139. https://doi.org/10.1002/jor.22040

Helgason, B., Gilchrist, S. M., Ariza, O. R., Chak, J. D., Zheng, G., Widmer, R. P., Ferguson, S. J., Guy, P., & Cripton, P. A. (2014). Development of a balanced experimental-computational approach to understanding the mechanics of proximal femur fractures. *Medical Engineering & Physics*, *36*(6), 793–799. https://doi.org/10.1016/j.medengphy.2014.02.019

Helgason, B., Gilchrist, S. M., Ariza, O. R., Vogt, P. J., Enns-Bray, W. S., Widmer, R. P., Fitze, T., Pálsson, H., Pauchard, Y., Guy, P., Ferguson, S. J., & Cripton, P. A. (2016). The influence of the modulus-

density relationship and the material mapping method on the simulated mechanical response of the proximal femur in side-ways fall loading configuration. *Medical Engineering & Physics*, *38*(7), 679–689. https://doi.org/10.1016/j.medengphy.2016.03.006

Helgason, B., Perilli, E., Schileo, E., Taddei, F., Brynjólfsson, S., & Viceconti, M. (2008). Mathematical relationships between bone density and mechanical properties: A literature review. *Clinical Biomechanics (Bristol, Avon)*, *23*(2), 135–146. https://doi.org/10.1016/j.clinbiomech.2007.08.024

Hirsch, C., & Evans, F. G. (1965). Studies on Some Physical Properties of Infant Compact Bone. *Acta Orthopaedica Scandinavica*, *35*, 300–313. https://doi.org/10.3109/17453676508989361

Hoffler, C. E., Guo, X. E., Zysset, P. K., & Goldstein, S. A. (2005). An application of nanoindentation technique to measure bone tissue Lamellae properties. *Journal of Biomechanical Engineering*, *127*(7), 1046–1053. https://doi.org/10.1115/1.2073671

Hoffler, C. E., Moore, K. E., Kozloff, K., Zysset, P. K., & Goldstein, S. A. (2000). Age, gender, and bone lamellae elastic moduli. *Journal of Orthopaedic Research*, *18*(3), 432–437. https://doi.org/10.1002/jor.1100180315

Hu, J., Fanta, A., Neal, M., Reed, M. P., & Wang, J.-T. (2016). Vehicle Crash Simulations with Morphed GHBMC Human Models of Different Stature, BMI, and Age. In *4th International Digital Human Modeling Conference*.

Hu, J., Zhang, K., Fanta, A., Jones, M., Reed, M. P., Neal, M., Wang, J.-T., Lin, C.-H., & Cao, L. (2017). Stature and body shape effects on driver injury risks in frontal crashes: a parametric human modelling study. In International Research Council on the Biomechanics of Injury (Chair), *IRCOBI Conference,* Antwerp, Belgium.

Hu, J., Zhang, K., Reed, M. P., Wang, J.-T., Neal, M., & Lin, C.-H. (2019). Frontal crash simulations using parametric human models representing a diverse population. *Traffic Injury Prevention*, *20*(sup1), S97-S105. https://doi.org/10.1080/15389588.2019.1581926

Huang, J., Long, Y., Yan, Y., & Hu, L. (2018). Development and Validation of an Age-Specific Lower Extremity Finite Element Model for Simulating Pedestrian Accidents. *Applied Bionics and Biomechanics*, *2018*(5), 5906987. https://doi.org/10.1155/2018/5906987

Huang, S. N., Yang, J. K., & Eklund, F. (2007). *Analysis of car-pedestrian impact scenarios for the evaluation of a pedestrian sensor system based on the accident data from Sweden*. https://bast.opus.hbz-nrw.de/opus45-bast/frontdoor/index/index/docId/396

Humbert, L., Martelli, Y., Fonolla, R., Steghofer, M., Di Gregorio, S., Malouf, J., Romera, J., & Barquero, L. M. D. R. (2017). 3d-DXA: Assessing the Femoral Shape, the Trabecular

Macrostructure and the Cortex in 3D from DXA images. *IEEE Transactions on Medical Imaging*, *36*(1), 27–39. https://doi.org/10.1109/TMI.2016.2593346

Hunter, R. L., Briley, K., & Agnew, A. M. (2019). Sex Differences in Human Tibia Cortical Bone Morphometrics from Computed Tomography (CT). In International Research Council on the Biomechanics of Injury (Chair), *IRCOBI Conference,* Florence, Italy.

Insurance Institute for Highway Safety. (2021). *Fatality Facts 2018 - Gender*. https://www.iihs.org/topics/fatality-statistics/detail/gender

Ivarsson, B. J., Genovese, D., Crandall, J. R., Bolton, J. R., Untaroiu, C. D., & Bose, D. (2009). The tolerance of the femoral shaft in combined axial compression and bending loading. *Stapp Car Crash Journal*, *53*, 251–290.

Iwamoto, M., Kisanuki, Y., Watanabe, I., Furusu, K., Miki, K., & Hasegawa, M. (2002). Development of a Finite Element Model of the Total Human Body Model for Safety (THUMS) and Application to Injury Reconstruction. In International Research Council on the Biomechanics of Injury (Chair), *IRCOBI Conference,* Munich, Germany.

Iwamoto, M., Tamura, A., Furusu, K., Kato, C., Miki, K., Hasegawa, J., & Yang, K. H. (2000). Development of a Finite Element Model of the Human Lower Extremity for Analyses of Automotive Crash Injuries. In *SAE Technical Paper Series.* SAE International, 400 Commonwealth Drive, Warrendale, PA, United States. https://doi.org/10.4271/2000-01-0621

Jazinizadeh, F., Mohammadi, H., & Quenneville, C. E. (2020). Comparing the fracture limits of the proximal femur under impact and quasi-static conditions in simulation of a sideways fall. *Journal of the Mechanical Behavior of Biomedical Materials*, *103.* https://doi.org/10.1016/j.jmbbm.2019.103593

Jirousek, O. (2012). Nanoindentation of Human Trabecular Bone – Tissue Mechanical Properties Compared to Standard Engineering Test Methods. In L. Zhang (Ed.), *Application of Nanoindentation Technique in Martensitic Structures.* IntechOpen. https://doi.org/10.5772/50152

Johannesdottir, F., Thrall, E., Muller, J. A., Keaveny, T. M., Kopperdahl, D. L., & Bouxsein, M. L. (2017). Comparison of non-invasive assessments of strength of the proximal femur. *Bone*, *105*, 93–102. https://doi.org/10.1016/j.bone.2017.07.023

Kahane, C. J. (2013). *Injury Vulnerability and Effectiveness of Occupant Protection Technologies for Older Occupants and Women* (DOT HS 811 766). National Highway Traffic Safety Administration.

Kajzer, J., Cavallero, C., Bonnoit, J., Morjane, A., & Ghanouchi, S. (1993). Response of the knee joint in lateral impact: effect of bending moment. In International Research Council on the Biomechanics of Injury (Chair), *IRCOBI Conference*.

Kajzer, J., Cavallero, C., Ghanouchi, S., Bonnoit, J., & Ghorbel, A. (1990). Response of the knee joint in lateral impact: effect of shearing loads. In International Research Council on the Biomechanics of Injury (Chair), *IRCOBI Conference*.

Kajzer, J., Schroeder, G., Ishikawa, H., Matsui, Y., & Bosch, U. (1997). Shearing and Bending Effects at the Knee Joint at High Speed Lateral Loading. In *SAE Technical Paper Series.* SAE International, 400 Commonwealth Drive, Warrendale, PA, United States. https://doi.org/10.4271/973326

Kannus, P., Leiponen, P., Parkkari, J., Palvanen, M., & Järvinen, M. (2006). A sideways fall and hip fracture. *Bone*, *39*(2), 383–384. https://doi.org/10.1016/j.bone.2006.01.148

Karakaş, H. M., & Harma, A. (2008). Femoral shaft bowing with age: A digital radiological study of Anatolian Caucasian adults. *Diagnostic and Interventional Radiology (Ankara, Turkey)*, *14*(1), 29–32.

Keaveny, T. M., & Hayes, W. C. (1993). A 20-year perspective on the mechanical properties of trabecular bone. *Journal of Biomechanical Engineering*, *115*(4B), 534–542. https://doi.org/10.1115/1.2895536

Keaveny, T. M., Pinilla, T. P., Crawford, R. P., Kopperdahl, D. L., & Lou, A. (1997). Systematic and random errors in compression testing of trabecular bone. *Journal of Orthopaedic Research*, *15*(1), 101–110. https://doi.org/10.1002/jor.1100150115

Keller, T. S. (1994). Predicting the compressive mechanical behavior of bone. *Journal of Biomechanics*, *27*(9), 1159–1168. https://doi.org/10.1016/0021-9290(94)90056-6

Keller, T. S., Mao, Z., & Spengler, D. M. (1990). Young's modulus, bending strength, and tissue physical properties of human compact bone. *Journal of Orthopaedic Research*, *8*(4), 592–603. https://doi.org/10.1002/jor.1100080416

Kelly, N., & McGarry, J. P. (2012). Experimental and numerical characterisation of the elasto-plastic properties of bovine trabecular bone and a trabecular bone analogue. *Journal of the Mechanical Behavior of Biomedical Materials*, *9*, 184–197. https://doi.org/10.1016/j.jmbbm.2011.11.013

Kennedy, E. A., Hurst, W. J., Stitzel, J. D., Cormier, J. M., Hansen, G. A., Smith, E. P., & Duma, S. M. (2004). Lateral and posterior dynamic bending of the mid-shaft femur: Fracture risk curves for the adult population. *Stapp Car Crash Journal*, *48*, 27–51.

Kent, R. W., & Funk, J. R. (2004). Data Censoring and Parametric Distribution Assignment in the Development of Injury Risk Functions from Biochemical Data. In *SAE Technical Paper Series.* SAE International, 400 Commonwealth Drive, Warrendale, PA, United States. https://doi.org/10.4271/2004-01-0317

Kerrigan, J. R., Bhalla, K. S., Madeley, N. J., Funk, J. R., Bose, D., & Crandall, J. R. (2003). *Experiments for Establishing Pedestrian-Impact Lower Limb Injury Criteria* (SAE Technical Paper 2003-01-0895). https://doi.org/10.4271/2003-01-0895

Kerrigan, J. R., Drinkwater, D. C., Kam, C. Y., Murphy, D. B., Ivarsson, B. J., Crandall, J. R., & Patrie, J. (2004). Tolerance of the human leg and thigh in dynamic latero-medial bending. *International Journal of Crashworthiness*, *9*(6), 607–623. https://doi.org/10.1533/ijcr.2004.0315

Keyak, J. H. (2000). Relationships between femoral fracture loads for two load configurations. *Journal of Biomechanics*, *33*(4), 499–502. https://doi.org/10.1016/S0021-9290(99)00202-X

Keyak, J. H., Lee, I. Y., & Skinner, H. B. (1994). Correlations between orthogonal mechanical properties and density of trabecular bone: Use of different densitometric measures. *Journal of Biomedical Materials Research*, *28*(11), 1329–1336. https://doi.org/10.1002/jbm.820281111

Keyak, J. H., Meagher, J. M., Skinner, H. B., & Mote, C. D. (1990). Automated three-dimensional finite element modelling of bone: a new method. *Journal of Biomedical Engineering*(12), 389–397. https://doi.org/10.1016/0141-5425(90)90022-F

Keyak, J. H., & Rossi, S. A. (2000). Prediction of femoral fracture load using finite element models: an examination of stress- and strain-based failure theories. *Journal of Biomechanics*, *33*(33 // 2), 209–214. https://doi.org/10.1016/S0021-9290(99)00152-9

Keyak, J. H., Rossi, S. A., Jones, K. A., Les, C. M., & Skinner, H. B. (2001). Prediction of fracture location in the proximal femur using finite element models. *Medical Engineering & Physics*, *23*(9), 657–664. https://doi.org/10.1016/S1350-4533(01)00094-7

Keyak, J. H., Rossi, S. A., Jones, K. A., & Skinner, H. B. (1997). Prediction of femoral fracture load using automated finite element modeling. *Journal of Biomechanics*, *31*(2), 125–133. https://doi.org/10.1016/S0021-9290(97)00123-1

Khor, F., Cronin, D. S., Watson, B., Gierczycka, D., & Malcolm, S. (2018). Importance of asymmetry and anisotropy in predicting cortical bone response and fracture using human body model femur in three-point bending and axial rotation. *Journal of the Mechanical Behavior of Biomedical Materials*, *87*, 213–229. https://doi.org/10.1016/j.jmbbm.2018.07.033

Kikuchi, Y., Takahashi, Y., & Mori, F. (2006). Development of a Finite Element Model for a Pedestrian Pelvis and Lower Limb. In *SAE Technical Paper Series.* SAE International, 400 Commonwealth Drive, Warrendale, PA, United States. https://doi.org/10.4271/2006-01-0683

Kim, Y. S., Choi, H. H., Cho, Y. N., Park, Y. J., Lee, J. B., Yang, K. H., & King, A. I. (2005). Numerical Investigations of Interactions between the Knee-Thigh-Hip Complex with Vehicle Interior Structures. *Stapp Car Crash Journal*, *49*, 85–115.

Klein, K. F., Hu, J., Reed, M. P., Hoff, C. N., & Rupp, J. D. (2015). Development and Validation of Statistical Models of Femur Geometry for Use with Parametric Finite Element Models. *Annals of Biomedical Engineering*, *43*(10), 2503–2514. https://doi.org/10.1007/s10439-015-1307-6

Kleiven, S. (2020). Hip fracture risk functions for elderly men and women in sideways falls. *Journal of Biomechanics*, *105*, 109771. https://doi.org/10.1016/j.jbiomech.2020.109771

Klug, C., Feist, F., Schneider, B., Sinz, W., Ellway, J., & van Ratingen, M. (2019). Development Of A Certification Procedure For Numerical Pedestrian Models. *The 26th International Technical Conference and Exhibition on the Enhanced Safety of Vehicles (ESV)*.

Klug, C., Iraeus, J., John, J., Svenning, E., Kranjec, M., Svensson, M., Leo, C., Schubert, A., & Linder, A. (2020). Introduction of the VIVA+ Vulnerable Road User Models. In carhs.de (Ed.), *Human Modeling and Simulation in Automotive Engineering 2020.*

Ko, R. (1953). Tensile Tests on Cortical Bones of Human Extremity Long Bones. *Journal of Kyoto Prefectural University of Medicine*(53), 503–525.

Koivumäki, J. E. M., Thevenot, J., Pulkkinen, P., Kuhn, V., Link, T. M., Eckstein, F., & Jämsä, T. (2012). Cortical bone finite element models in the estimation of experimentally measured failure loads in the proximal femur. *Bone*, *51*(4), 737–740. https://doi.org/10.1016/j.bone.2012.06.026

Koivumäki, J. E. M., Thevenot, J., Pulkkinen, P., Kuhn, V., Link, T. M., Eckstein, F., & Jämsä, T. (2012). CT-based finite element models can be used to estimate experimentally measured failure loads in the proximal femur. *Bone*, *50*(4), 824–829. https://doi.org/10.1016/j.bone.2012.01.012

Kolta, S., Paratte, S., Amphoux, T., Persohn, S., Campana, S., Skalli, W., Paternotte, S., Argenson, J.-N., Bouler, J.-M., Gagey, O., & Roux, C. (2012). Bone texture analysis of human femurs using a new device (BMA™) improves failure load prediction. *Osteoporosis International*, *23*(4), 1311–1316. https://doi.org/10.1007/s00198-011-1674-2

Konda, S. R. (2018). Anatomy of the Proximal Femur. In K. A. Egol & P. Leucht (Eds.), *Proximal Femur Fractures: An Evidence-Based Approach to Evaluation and Management* (pp. 1–7). Springer International Publishing. https://doi.org/10.1007/978-3-319-64904-7_1

Kopperdahl, D. L., & Keaveny, T. M. (1998). Yield strain behavior of trabecular bone. *Journal of Biomechanics*, *31*(7), 601–608. https://doi.org/10.1016/S0021-9290(98)00057-8

Kuhn, J. L., Goldstein, S. A., Ciarelli, M. J., & Matthews, L. S. (1989). The limitations of canine trabecular bone as a model for human: A biomechanical study. *Journal of Biomechanics*, *22*(2), 95–107. https://doi.org/10.1016/0021-9290(89)90032-8

Kullgren, A., Stigson, H., & Krafft, M. (2013). Development of Whiplash Associated Disorders for Male and Female Car Occupants in Cars Launched Since the 80s in Different Impact Directions. In

International Research Council on the Biomechanics of Injury (Chair), *IRCOBI Conference,* Gothenburg, Sweden.

Lang, T. F., Keyak, J. H., Heitz, M. W., Augat, P., Lu, Y., Mathur, A., & Genant, H. K. (1997). Volumetric quantitative computed tomography of the proximal femur: Precision and relation to bone strength. *Bone*, *21*(1), 101–108. https://doi.org/10.1016/S8756-3282(97)00072-0

Lanner, D., Halldin, P., Iraeus, J., Holmqvist, K., Mroz, K., Pipkorn, B., Jakobsson, L., Backlund, M., Bolte, J. H., & Kleiven, S. (2010). Evaluation of finite element human body models in lateral padded pendulum impacts to the shoulder. *International Journal of Crashworthiness*, *15*(2), 125–142. https://doi.org/10.1080/13588260903048208

Larsson, K.-J., Pipkorn, B., Iraeus, J., Bolte, J. H., Agnew, A. M., Hu, J., Reed, M. P., & Sunnevang, C. (2019). Evaluation of the Benefits of Parametric Human Body ModelMorphingfor Prediction of Injury to Elderly Occupants in Side Impact. In International Research Council on the Biomechanics of Injury (Chair), *IRCOBI Conference,* Florence, Italy.

Le Corroller, T., Halgrin, J., Pithioux, M., Guenoun, D., Chabrand, P., & Champsaur, P. (2012). Combination of texture analysis and bone mineral density improves the prediction of fracture load in human femurs. *Osteoporosis International*, *23*(1), 163–169. https://doi.org/10.1007/s00198-011-1703-1

Leo, C., Klug, C., Ohlin, M., & Linder, A. (2019). Analysis of pedestrian injuries in pedestrian-car collisions with focus on age and gender. In International Research Council on the Biomechanics of Injury (Chair), *IRCOBI Conference,* Florence, Italy.

Li, X., Xu, Y., Lin, W., & Fan, Y. (2020). The comparison of bone mineral density of femoral head between non-hip fracture side and hip fracture side. *Scientific Reports*, *10*(1), 13015. https://doi.org/10.1038/s41598-020-70144-5

Li, Z., Zou, D., Liu, N., Zhong, L., Shao, Y., Wan, L., Huang, P., & Chen, Y. (2013). Finite element analysis of pedestrian lower limb fractures by direct force: The result of being run over or impact? *Forensic Science International*, *229*(1-3), 43–51. https://doi.org/10.1016/j.forsciint.2013.03.027

Lindahl, O., & Lindgren, A. G. (1967). Cortical bone in man. Ii. Variation in tensile strength with age and sex. *Acta Orthopaedica Scandinavica*, *38*(2), 141–147. https://doi.org/10.3109/17453676708989628

Linde, F. (1994). Elastic and viscoelastic properties of trabecular bone by a compression testing approach. *Danish Medical Bulletin*, *41*(2), 119–138.

Linder, A., & Svensson, M. (2019). Road safety: the average male as a norm in vehicle occupant crash safety assessment. *Interdisciplinary Science Reviews*, *44*(2), 140–153. https://doi.org/10.1080/03080188.2019.1603870

Livermore Software Technology Corporation (Ed.). (2018). LS-Dyna Keyword User's Manual [Special issue]. Livermore, California.

Lochmüller, E.-M., Groll, O., Kuhn, V., & Eckstein, F. (2002). Mechanical strength of the proximal femur as predicted from geometric and densitometric bone properties at the lower limb versus the distal radius. *Bone*, *30*(1), 207–216. https://doi.org/10.1016/S8756-3282(01)00621-4

Lotz, J. C., Cheal, E. J., & Hayes, W. C. (1991a). Fracture prediction for the proximal femur using finite element models: Part II--Nonlinear analysis. *Journal of Biomechanical Engineering*, *113*(4), 361–365. https://doi.org/10.1115/1.2895413

Lotz, J. C., Cheal, E. J., & Hayes, W. C. (1991b). Fracture prediction for the proximal femur using finite element models: Part I--Linear analysis. *Journal of Biomechanical Engineering*, *113*(4), 353–360. https://doi.org/10.1115/1.2895412

Lotz, J. C., Gerhart, T. N., & Hayes, W. C. (1990). Mechanical properties of trabecular bone from the proximal femur: A quantitative CT study. *Journal of Computer Assisted Tomography*, *14*(1), 107–114. https://doi.org/10.1097/00004728-199001000-00020

Lotz, J. C., Gerhart, T. N., & Hayes, W. C. (1991). Mechanical properties of metaphyseal bone in the proximal femur. *Journal of Biomechanics*, *24*(5), 317–329. https://doi.org/10.1016/0021-9290(91)90350-V

Lotz, J. C., & Hayes, W. C. (1990). The use of quantitative computed tomography to estimate risk of fracture of the hip from falls. *The Journal of Bone and Joint Surgery. American Volume*, *72*(5), 689–700.

Manske, S. L., Liu-Ambrose, T., de Bakker, P. M., Liu, D., Kontulainen, S., Guy, P., Oxland, T. R., & McKay, H. A. (2006). Femoral neck cortical geometry measured with magnetic resonance imaging is associated with proximal femur strength. *Osteoporosis International*, *17*(10), 1539–1545. https://doi.org/10.1007/s00198-006-0162-6

Marques, E. A., Carballido-Gamio, J., Gudnason, V., Sigurdsson, G., Sigurdsson, S., Aspelund, T., Siggeirsdottir, K., Launer, L., Eiriksdottir, G., Lang, T., & Harris, T. B. (2018). Sex differences in the spatial distribution of bone in relation to incident hip fracture: Findings from the AGES-Reykjavik study. *Bone*, *114*, 72–80. https://doi.org/10.1016/j.bone.2018.05.016

Martens, M., van Audekercke, R., Delport, P., Meester, P. de, & Mulier, J. C. (1983). The mechanical characteristics of cancellous bone at the upper femoral region. *Journal of Biomechanics*, *16*(12), 971–983. https://doi.org/10.1016/0021-9290(83)90098-2

Martens, M., van Audekercke, R., Meester, P. de, & Mulier, J. C. (1986). Mechanical behaviour of femoral bones in bending loading. *Journal of Biomechanics*, *19*(6), 443–454. https://doi.org/10.1016/0021-9290(86)90021-7

Mather, B. S. (1967). The symmetry of the mechanical properties of the human femur. *Journal of Surgical Research*, *7*(5), 222–225. https://doi.org/10.1016/0022-4804(67)90055-8

Mather, B. S. (1968). Variation with age and sex in strength of the femur. *Medical and Biological Engineering*, *6*(2), 129–132. https://doi.org/10.1007/BF02474265

McCalden, R. W., McGeough, J. A., Barker, M. B., & Court-Brown, C. M. (1993). Age-related changes in the tensile properties of cortical bone. The relative importance of changes in porosity, mineralization, and microstructure. *The Journal of Bone and Joint Surgery. American Volume*, *75*(8), 1193–1205. https://doi.org/10.2106/00004623-199308000-00009

McElhaney, J. H. (1966). Dynamic response of bone and muscle tissue. *Journal of Applied Physiology*, *21*(4), 1231–1236. https://doi.org/10.1152/jappl.1966.21.4.1231

Mente, P. L., & Lewis, J. L. (1994). Elastic modulus of calcified cartilage is an order of magnitude less than that of subchondral bone. *Journal of Orthopaedic Research*, *12*(5), 637–647. https://doi.org/10.1002/jor.1100120506

Milovanovic, P., Potocnik, J., Djonic, D., Nikolic, S., Zivkovic, V., Djuric, M., & Rakocevic, Z. (2012). Age-related deterioration in trabecular bone mechanical properties at material level: Nanoindentation study of the femoral neck in women by using AFM. *Experimental Gerontology*, *47*(2), 154–159. https://doi.org/10.1016/j.exger.2011.11.011

Milovanovic, P., Potocnik, J., Stoiljkovic, M., Djonic, D., Nikolic, S., Neskovic, O., Djuric, M., & Rakocevic, Z. (2011). Nanostructure and mineral composition of trabecular bone in the lateral femoral neck: Implications for bone fragility in elderly women. *Acta Biomaterialia*, *7*(9), 3446–3451. https://doi.org/10.1016/j.actbio.2011.05.028

Mirzaali, M. J., Schwiedrzik, J., Thaiwichai, S., Best, J. P., Michler, J., Zysset, P. K., & Wolfram, U. (2016). Mechanical properties of cortical bone and their relationships with age, gender, composition and microindentation properties in the elderly. *Bone*, *93*, 196–211. https://doi.org/10.1016/j.bone.2015.11.018

Mirzaei, M., Keshavarzian, M., & Naeini, V. (2014). Analysis of strength and failure pattern of human proximal femur using quantitative computed tomography (QCT)-based finite element method. *Bone*, *64*, 108–114. https://doi.org/10.1016/j.bone.2014.04.007

Miura, M., Nakamura, J., Matsuura, Y., Wako, Y., Suzuki, T., Hagiwara, S., Orita, S., Inage, K., Kawarai, Y., Sugano, M., Nawata, K., & Ohtori, S. (2017). Prediction of fracture load and stiffness of the proximal femur by CT-based specimen specific finite element analysis: Cadaveric validation study. *BMC Musculoskeletal Disorders*, *18*(1), 1–8. https://doi.org/10.1186/s12891-017-1898-1

Morgan, E. F., Bayraktar, H. H., & Keaveny, T. M. (2003). Trabecular bone modulus–density relationships depend on anatomic site. *Journal of Biomechanics*, *36*(7), 897–904. https://doi.org/10.1016/S0021-9290(03)00071-X

Morgan, E. F., & Keaveny, T. M. (2001). Dependence of yield strain of human trabecular bone on anatomic site. *Journal of Biomechanics*, *34*(5), 569–577. https://doi.org/10.1016/S0021-9290(01)00011-2

Morgan, E. F., Unnikrisnan, G. U., & Hussein, A. I. (2018). Bone Mechanical Properties in Healthy and Diseased States. *Annual Review of Biomedical Engineering*, *20*, 119–143. https://doi.org/10.1146/annurev-bioeng-062117-121139

Mosekilde, L., Mosekilde, L., & Danielsen, C. C. (1987). Biomechanical competence of vertebral trabecular bone in relation to ash density and age in normal individuals. *Bone*, *8*(2), 79–85. https://doi.org/10.1016/8756-3282(87)90074-3

Motoshima, T. (1960). Studies on the Strength for Bending of Human Long Extremity Bones. *Journal of Kyoto Prefectural University of Medicine*(68), 1377–1397.

Nalla, R. K., Kinney, J. H., & Ritchie, R. O. (2003). Mechanistic fracture criteria for the failure of human cortical bone. *Nature Materials*, *2*(3), 164–168. https://doi.org/10.1038/nmat832

Nasiri Sarvi, M., & Luo, Y. (2017). Sideways fall-induced impact force and its effect on hip fracture risk: A review. *Osteoporosis International*, *28*(10), 2759–2780. https://doi.org/10.1007/s00198-017-4138-5

National Library of Medicine (Ed.). *Visible Human Project*. https://www.nlm.nih.gov/research/visible/visible_human.html

Nevitt, M. C., Johnell, O., Black, D. M., Ensrud, K., Genant, H. K., & Cummings, S. R. (1994). Bone mineral density predicts non-spine fractures in very elderly women. Study of Osteoporotic Fractures Research Group. *Osteoporosis International*, *4*(6), 325–331. https://doi.org/10.1007/BF01622192

Niebur, G. L., Feldstein, M. J., Yuen, J. C., Chen, T. J., & Keaveny, T. M. (2000). High-resolution finite element models with tissue strength asymmetry accurately predict failure of trabecular bone. *Journal of Biomechanics*, *33*(12), 1575–1583. https://doi.org/10.1016/S0021-9290(00)00149-4

Nishiyama, K. K., Gilchrist, S. M., Guy, P., Cripton, P. A., & Boyd, S. K. (2013). Proximal femur bone strength estimated by a computationally fast finite element analysis in a sideways fall configuration. *Journal of Biomechanics*, *46*(7), 1231–1236. https://doi.org/10.1016/j.jbiomech.2013.02.025

Nyquist, G. W. (1986). Injury Tolerance Characteristics of the Adult Human Lower Extremities Under Static and Dynamic Loading. In *SAE Technical Paper Series.* SAE International, 400 Commonwealth Drive, Warrendale, PA, United States. https://doi.org/10.4271/861925

Op Den Buijs, J., & Dragomir-Daescu, D. (2011). Validated finite element models of the proximal femur using two-dimensional projected geometry and bone density. *Computer Methods and Programs in Biomedicine*, *104*(2), 168–174. https://doi.org/10.1016/j.cmpb.2010.11.008

Osterhoff, G., Morgan, E. F., Shefelbine, S. J., Karim, L., McNamara, L. M., & Augat, P. (2016). Bone mechanical properties and changes with osteoporosis. *Injury*, *47*, S11-S20. https://doi.org/10.1016/S0020-1383(16)47003-8

Östh, J., Mendoza-Vazquez, M., Sato, F., Svensson, M. Y., Linder, A., & Brolin, K. (2017). A female head-neck model for rear impact simulations. *Journal of Biomechanics*, *51*, 49–56. https://doi.org/10.1016/j.jbiomech.2016.11.066

Ott, S. M. (2018). Cortical or Trabecular Bone: What's the Difference? *American Journal of Nephrology*, *47*(6), 373–375. https://doi.org/10.1159/000489672

Palanca, M., Perilli, E., & Martelli, S. (2020). Body Anthropometry and Bone Strength Conjointly Determine the Risk of Hip Fracture in a Sideways Fall. *Annals of Biomedical Engineering.* Advance online publication. https://doi.org/10.1007/s10439-020-02682-y

Parfitt, A. M. (1984). Age-related structural changes in trabecular and cortical bone: Cellular mechanisms and biomechanical consequences. *Calcified Tissue International*, *36 Suppl 1*, S123-8. https://doi.org/10.1007/BF02406145

Parfitt, A. M. (2002). Misconceptions (2): turnover is always higher in cancellous than in cortical bone. *Bone*, *30*(6), 807–809. https://doi.org/10.1016/S8756-3282(02)00735-4

Park, G., Kim, T., Crandall, J. R., Svendsen, A., Saunders, N., & Markusic, C. (2014). Evaluation of Biofidelity of Side Impact Computational Surrogates (ES-2re, WorldSID, GHBMC). In *SAE Technical Paper Series.* SAE International, 400 Commonwealth Drive, Warrendale, PA, United States. https://doi.org/10.4271/2014-01-0541

Park, G., Kim, T., Forman, J. L., Panzer, M. B., & Crandall, J. R. (2016). Prediction of the Structural Response of the Femoral Shaft under Dynamic Bending Loading using Geometric Subject-Specific Finite Element Models. *Ohio State University Injury Biomechanics Symposium*.

Park, G., Kim, T., Forman, J. L., Panzer, M. B., & Crandall, J. R. (2017). Prediction of the structural response of the femoral shaft under dynamic loading using subject-specific finite element models. *Computer Methods in Biomechanics and Biomedical Engineering*, *20*(11), 1151–1166. https://doi.org/10.1080/10255842.2017.1340459

Park, S., Chae, S.-W., Park, J., Han, S.-H., Hong, J., & Kim, Y. E. (2013). Finite element modeling to estimate the apparent material properties of trabecular bone. *International Journal of Precision Engineering and Manufacturing*, *14*(8), 1479–1485. https://doi.org/10.1007/s12541-013-0199-3

Patton, D. M., Bigelow, E. M. R., Schlecht, S. H., Kohn, D. H., Bredbenner, T. L., & Jepsen, K. J. (2019). The relationship between whole bone stiffness and strength is age and sex dependent. *Journal of Biomechanics*, *83*, 125–133. https://doi.org/10.1016/j.jbiomech.2018.11.030

Pawlikowski, M., Skalski, K., Bańczerowski, J., Makuch, A., & Jankowski, K. (2017). Stress–strain characteristic of human trabecular bone based on depth sensing indentation measurements. *Biocybernetics and Biomedical Engineering*, *37*(2), 272–280. https://doi.org/10.1016/j.bbe.2017.01.002

Peres, J., Auer, S., & Praxl, N. (2016). Development and comparison of different injury risk functions predicting pelvic fractures in side impact for a Human Body Model. In International Research Council on the Biomechanics of Injury (Chair), *IRCOBI Conference,* Seoul, South Korea.

Petitjean, A., & Trosseille, X. (2011). Statistical Simulations to Evaluate the Methods of the Construction of Injury Risk Curves. In *SAE Technical Paper Series.* SAE International, 400 Commonwealth Drive, Warrendale, PA, United States. https://doi.org/10.4271/2011-22-0015

Petitjean, A., Trosseille, X., Petit, P., Irwin, A., Hassan, J., & Praxl, N. (2009). Injury Risk Curves for the WorldSID 50th Male Dummy. In *SAE Technical Paper Series.* SAE International, 400 Commonwealth Drive, Warrendale, PA, United States. https://doi.org/10.4271/2009-22-0016

Pinilla, T. P., Boardman, K. C., Bouxsein, M.L., Myers, E. R., & Hayes, W. C. (1996). Impact direction from a fall influences the failure load of the proximal femur as much as age-related bone loss. *Calcified Tissue International*, *58*(4), 231–235. https://doi.org/10.1007/BF02508641

Praxl, N. (2011). How reliable are injury risk curves? *22nd International Technical Conference on the Enhanced Safety of Vehicles (ESV)*, Article 11-0089.

Preutenborbeck, M. (2018). *Image Based Fracture Prediction Diagnostic Tool for Avascular Necrosis of the Femoral Head* [Dissertation]. University of Leeds.

Project Virtual. https://projectvirtual.eu/

Pulkkinen, P., Eckstein, F., Lochmüller, E.-M., Kuhn, V., & Jämsä, T. (2006). Association of geometric factors and failure load level with the distribution of cervical vs. Trochanteric hip fractures. *Journal of Bone and Mineral Research*, *21*(6), 895–901. https://doi.org/10.1359/jbmr.060305

Pulkkinen, P., Jämsä, T., Lochmüller, E.-M., Kuhn, V., Nieminen, M. T., & Eckstein, F. (2008). Experimental hip fracture load can be predicted from plain radiography by combined analysis of trabecular bone structure and bone geometry. *Osteoporosis International*, *19*(4), 547–558. https://doi.org/10.1007/s00198-007-0479-9

Rajapakse, C. S., Farid, A. R., Kargilis, D. C., Jones, B. C., Lee, J. S., Johncola, A. J., Batzdorf, A. S., Shetye, S. S., Hast, M. W., & Chang, G. (2020). Mri-based assessment of proximal femur strength compared to mechanical testing. *Bone*, *133*, 115227. https://doi.org/10.1016/j.bone.2020.115227

Ramme, A. J., Vira, S., Hotca, A., Miller, R., Welbeck, A., Honig, S., Egol, K. A., Rajapakse, C. S., & Chang, G. (2019). A Novel MRI Tool for Evaluating Cortical Bone Thickness of the Proximal Femur. *Bulletin of the Hospital for Joint Disease (2013)*, *77*(2), 115–121.

Reilly, D. T., & Burstein, A. H. (1975). The elastic and ultimate properties of compact bone tissue. *Journal of Biomechanics*, *8*(6), 393–405. https://doi.org/10.1016/0021-9290(75)90075-5

Reilly, D. T., Burstein, A. H., & Frankel, V. H. (1974). The elastic modulus for bone. *Journal of Biomechanics*, *7*(3), 271–275. https://doi.org/10.1016/0021-9290(74)90018-9

Rezaei, A., Carlson, K. D., Giambini, H., Javid, S., & Dragomir-Daescu, D. (2019). Optimizing Accuracy of Proximal Femur Elastic Modulus Equations. *Annals of Biomedical Engineering*, *47*(6), 1391–1399. https://doi.org/10.1007/s10439-019-02238-9

Rezaei, A., & Dragomir-Daescu, D. (2015). Femoral Strength Changes Faster With Age Than BMD in Both Women and Men: A Biomechanical Study. *Journal of Bone and Mineral Research*, *30*(12), 2200–2206. https://doi.org/10.1002/jbmr.2572

Rho, J.-Y., Kuhn-Spearing, L., & Zioupos, P. (1998). Mechanical properties and the hierarchical structure of bone. *Medical Engineering & Physics*, *20*(2), 92–102. https://doi.org/10.1016/S1350-4533(98)00007-1

Riggs, B. L., Wahner, H. W., Dunn, W. L., Mazess, R. B., Offord, K. P., & Melton, L. J. (1981). Differential changes in bone mineral density of the appendicular and axial skeleton with aging: Relationship to spinal osteoporosis. *The Journal of Clinical Investigation*, *67*(2), 328–335. https://doi.org/10.1172/JCI110039

Riggs, B. L., Wahner, H. W., Seeman, E., Offord, K. P., Dunn, W. L., Mazess, R. B., Johnson, K. A., & Melton, L. J. (1982). Changes in bone mineral density of the proximal femur and spine with aging.

Differences between the postmenopausal and senile osteoporosis syndromes. *The Journal of Clinical Investigation*, *70*(4), 716–723. https://doi.org/10.1172/jci110667

Roberts, B. J., Thrall, E., Muller, J. A., & Bouxsein, M. L. (2010). Comparison of hip fracture risk prediction by femoral aBMD to experimentally measured factor of risk. *Bone*, *46*(3), 742–746. https://doi.org/10.1016/j.bone.2009.10.020

Ross, P. D., Davis, J. W., Vogel, J. M., & Wasnich, R. D. (1990). A critical review of bone mass and the risk of fractures in osteoporosis. *Calcified Tissue International*, *46*(3), 149–161. https://doi.org/10.1007/BF02555036

Ruff, C. B., & Hayes, W. C. (1988). Sex differences in age-related remodeling of the femur and tibia. *Journal of Orthopaedic Research*, 886–896.

Saha, S., & Hayes, W. C. (1976). Tensile impact properties of human compact bone. *Journal of Biomechanics*, *9*(4), 243–251. https://doi.org/10.1016/0021-9290(76)90010-5

Sarkalkan, N., Waarsing, J. H., Bos, P. K., Weinans, H., & Zadpoor, A. A. (2014). Statistical shape and appearance models for fast and automated estimation of proximal femur fracture load using 2D finite element models. *Journal of Biomechanics*, *47*(12), 3107–3114. https://doi.org/10.1016/j.jbiomech.2014.06.027

Sato, F., Odani, M., Miyazaki, Y., Yamazaki, K., Östh, J., & Svensson, M. (2017). Effects of whole spine alignment patterns on neck responses in rear end impact. *Traffic Injury Prevention*, *18*(2), 199–206. https://doi.org/10.1080/15389588.2016.1227072

Schileo, E., Pitocchi, J., Falcinelli, C., & Taddei, F. (2020). Cortical bone mapping improves finite element strain prediction accuracy at the proximal femur. *Bone*, *136*, 115348. https://doi.org/10.1016/j.bone.2020.115348

Schileo, E., Taddei, F., Cristofolini, L., & Viceconti, M. (2008). Subject-specific finite element models implementing a maximum principal strain criterion are able to estimate failure risk and fracture location on human femurs tested in vitro. *Journal of Biomechanics*, *41*(2), 356–367. https://doi.org/10.1016/j.jbiomech.2007.09.009

Schmitt, K.-U., Niederer, P. F., Cronin, D. S., Muser, M. H., & Walz, F. H. (2014). *Trauma-Biomechanik: Einführung in die Biomechanik von Verletzungen* (2. Aufl. 2014). *VDI-Buch*. Springer Vieweg. https://doi.org/10.1007/978-3-642-54281-7

Schoell, S. L., Weaver, A. A., Urban, J. E., Jones, D. A., Stitzel, J. D., Hwang, E., Reed, M. P., Rupp, J. D., & Hu, J. (2015). Development and Validation of an Older Occupant Finite Element Model of a Mid-Sized Male for Investigation of Age-related Injury Risk. *Stapp Car Crash Journal*, *59*, 359–383.

Schoenfeld, C. M., Lautenschlager, E. P., & Meyer, P. R. (1974). Mechanical properties of human cancellous bone in the femoral head. *Medical & Biological Engineering*, *12*(3), 313–317. https://doi.org/10.1007/BF02477797

Schuster, P. J., Chou, C. C., Prasad, P., & Jayaraman, G. (2000). Development and validation of a pedestrian lower limb non-linear 3-d finite element model. *Stapp Car Crash Journal*, *44*, 315–334. https://doi.org/10.4271/2000-01-SC21

Sedlin, E. D., & Hirsch, C. (1966). Factors affecting the determination of the physical properties of femoral cortical bone. *Acta Orthopaedica Scandinavica*, *37*(1), 29–48. https://doi.org/10.3109/17453676608989401

Shahar, R., Zaslansky, P., Barak, M., Friesem, A. A., Currey, J. D., & Weiner, S. (2007). Anisotropic Poisson's ratio and compression modulus of cortical bone determined by speckle interferometry. *Journal of Biomechanics*, *40*(2), 252–264. https://doi.org/10.1016/j.jbiomech.2006.01.021

Skalak, R., & Chien, S. (Eds.). (1987). *Handbook of bioengineering*. McGraw-Hill.

Snedeker, J. G., Walz, F. H., & Muser, M. H. (2003). Assessment of pelvis and upper leg injury risk in car-pedestrian collisions: Comparison of accident statistics, impactor tests and a human body finite element model. *Stapp Car Crash Journal*(47), Article 2003-22-019, 437–457.

Strømsøe, K., Høiseth, A., Alho, A., & Kok, W. L. (1995). Bending strength of the femur in relation to non-invasive bone mineral assessment. *Journal of Biomechanics*, *28*(7), 857–861. https://doi.org/10.1016/0021-9290(95)95274-9

Takahashi, Y., Kikuchi, Y., Konosu, A., & Ishikawa, H. (2000). Development and validation of the finite element model for the human lower limb of pedestrians. *Stapp Car Crash Journal*, *44*, 335–355.

Takahashi, Y., Kikuchi, Y., Mori, F., & Konosu, A. (2003). Advanced FE Lower Limb Model for Pedestrians. In National Highway Traffic Safety Administration (Chair), *Proceedings of 18th International Technical Conference on the Enhanced Safety of Vehicles,* Nagoya, Japan.

Taylor, D. (2003). Fracture mechanics: How does bone break? *Nature Materials*, *2*(3), 133–134. https://doi.org/10.1038/nmat843

Toniolo, I., Salmaso, C., Bruno, G., Stefani, A. de, Stefanini, C., Gracco, A. L. T., & Carniel, E. L. (2020). Anisotropic computational modelling of bony structures from CT data: An almost automatic procedure. *Computer Methods and Programs in Biomedicine*, *189*, 105319. https://doi.org/10.1016/j.cmpb.2020.105319

Trabelsi, N., Yosibash, Z., Wutte, C., Augat, P., & Eberle, S. (2011). Patient-specific finite element analysis of the human femur--a double-blinded biomechanical validation. *Journal of Biomechanics*, *44*(9), 1666–1672. https://doi.org/10.1016/j.jbiomech.2011.03.024

Treece, G., Poole, K. E. S., & Gee, A. (2012). Imaging the femoral cortex: Thickness, density and mass from clinical CT. *Medical Image Analysis*, *16*(5), 952–965. https://doi.org/10.1016/j.media.2012.02.008

Untaroiu, C. D. (2005). *Development and validation of a finite element model of human lower limb: Including detailed geometry, physical material properties, and component validations for pedestrian injuries* (3161280) [Dissertation]. University of Virginia, Ann Arbor.

Untaroiu, C. D. (2010). A numerical investigation of mid-femoral injury tolerance in axial compression and bending loading. *International Journal of Crashworthiness*, *15*(1), 83–92. https://doi.org/10.1080/13588260903047671

Untaroiu, C. D., Darvish, K., Crandall, J. R., Deng, B., & Wang, J.-T. (2005). A finite element model of the lower limb for simulating pedestrian impacts. *Stapp Car Crash Journal*, *49*, 157–181. https://doi.org/10.4271/2005-22-0008

Untaroiu, C. D., Genovese, D., Ivarsson, B. J., & Crandall, J. R. (2008). A Finite Element Analysis of Mid-Shaft Femoral Tolerance under Combined Axial-Bending Loading. In *10th International LS-DYNA Users Conference*.

Untaroiu, C. D., Kerrigan, J. R., & Crandall, J. R. (2006). Material Identification using Successive Response Surface Methodology, with Application to a Human Femur Subjected to Three-Point Bending Loading. *SAE Transactions*, *115*, 26–35.

Untaroiu, C. D., Yue, N., & Shin, J. (2013). A finite element model of the lower limb for simulating automotive impacts. *Annals of Biomedical Engineering*, *41*(3), 513–526. https://doi.org/10.1007/s10439-012-0687-0

Väänänen, S. P., Grassi, L., Flivik, G., Jurvelin, J. S., & Isaksson, H. (2015). Generation of 3D shape, density, cortical thickness and finite element mesh of proximal femur from a DXA image. *Medical Image Analysis*, *24*(1), 125–134. https://doi.org/10.1016/j.media.2015.06.001

Väänänen, S. P., Grassi, L., Venäläinen, M. S., Matikka, H., Zheng, Y., Jurvelin, J. S., & Isaksson, H. (2019). Automated segmentation of cortical and trabecular bone to generate finite element models for femoral bone mechanics. *Medical Engineering & Physics*, *70*, 19–28. https://doi.org/10.1016/j.medengphy.2019.06.015

Väänänen, S. P., Jurvelin, J. S., & Isaksson, H. (2012). Estimation of 3D shape, internal density and mechanics of proximal femur by combining bone mineral density images with shape and density templates. *Biomechanics and Modeling in Mechanobiology*, *11*(6), 791–800. https://doi.org/10.1007/s10237-011-0352-9

van den Kroonenberg, A. J., Hayes, W. C., & McMahon, T. A. (1996). Hip impact velocities and body configurations for voluntary falls from standing height. *Journal of Biomechanics*, *29*(6), 807–811. https://doi.org/10.1016/0021-9290(95)00134-4

van Rooij, L., van Hoof, J., Barbir, A., van der Made, R., Slaats, P.M.A., McCann, M. J., Ridella, S. A., Rupp, J. D., & TNO Wegtransportmiddelen (2004). A finite element lower extremity and pelvis model for predicting bone injuries due to knee bolster loading. In SAE International (Chair), *Proceedings of the SAE Digital Human Modelling Symposium 2004,* Oakland, California.

Varga, P., Schwiedrzik, J., Zysset, P. K., Fliri-Hofmann, L., Widmer, D., Gueorguiev, B., Blauth, M., & Windolf, M. (2016). Nonlinear quasi-static finite element simulations predict in vitro strength of human proximal femora assessed in a dynamic sideways fall setup. *Journal of the Mechanical Behavior of Biomedical Materials*, *57*, 116–127. https://doi.org/10.1016/j.jmbbm.2015.11.026

Dynasaur (Version 1.3.7) [Computer software]. (2021). https://gitlab.com/VSI-TUGraz/Dynasaur

Verhulp, E., van Rietbergen, B., Müller, R., & Huiskes, R. (2008). Indirect determination of trabecular bone effective tissue failure properties using micro-finite element simulations. *Journal of Biomechanics*, *41*(7), 1479–1485. https://doi.org/10.1016/j.jbiomech.2008.02.032

Viano, D. C. (1986). Biomechanics of Bone and Tissue: A Review of Material Properties and Failure Characteristics. In *SAE Technical Paper Series.* SAE International, 400 Commonwealth Drive, Warrendale, PA, United States. https://doi.org/10.4271/861923

Villette, C. C., & Phillips, A. T. M. (2018). Rate and age-dependent damage elasticity formulation for efficient hip fracture simulations. *Medical Engineering & Physics*, *61*, 1–12. https://doi.org/10.1016/j.medengphy.2018.07.016

Vulović, A. Z., & Filipovic, N. (2020). The biomechanics of lower human extremities. In N. Filipovic (Ed.), *Computational Modeling in Bioengineering and Bioinformatics* (pp. 179–210). Academic Press, an imprint of Elsevier. https://doi.org/10.1016/B978-0-12-819583-3.00006-0

Wall, J. C., Chatterji, S. K., & Jeffery, J. W. (1979). Age-related changes in the density and tensile strength of human femoral cortical bone. *Calcified Tissue International*, *27*(2). https://doi.org/10.1007/BF02441170

Wang, X., & Puram, S. (2004). The Toughness of Cortical Bone and Its Relationship with Age. *Annals of Biomedical Engineering*, *32*(1), 123–135. https://doi.org/10.1023/B:ABME.0000007797.92559.5e

Wang, X., Shen, X., Li, X., & Mauli Agrawal, C. (2002). Age-related changes in the collagen network and toughness of bone. *Bone*, *31*(1), 1–7. https://doi.org/10.1016/S8756-3282(01)00697-4

Weber, C. O. (1859). *Chirurgische Erfahrungen und Untersuchungen: nebst Zahlreichen Beobachtungen aus der chirurgischen Klinik und dem evangelischen Krankenhause zu Bonn*. Georg Reimer.

Whitmarsh, T., Otake, Y., Uemura, K., Takao, M., Sugano, M., & Sato, Y. (2018). A cross-sectional study on the age-related cortical and trabecular bone changes at the femoral head in elderly female hip fracture patients. *Scientific Reports*, *9*(1), 1–8. https://doi.org/10.1038/s41598-018-36299-y

Wolfram, U., Wilke, H.-J., & Zysset, P. K. (2010). Rehydration of vertebral trabecular bone: Influences on its anisotropy, its stiffness and the indentation work with a view to age, gender and vertebral level. *Bone*, *46*(2), 348–354. https://doi.org/10.1016/j.bone.2009.09.035

World Health Organization. (2018). *Global status report on road safety 2018*. World Health Organization.

Yamada, H. (1970). *Strength of biological materials*. The Williams & Wilkins Company.

Yang, J., Wittek, A., & Kajzer, J. (1996). Finite element model of the human lower extremity skeleton system in a lateral impact. In International Research Council on the Biomechanics of Injury (Chair), *IRCOBI Conference*.

Yang, K. H. (2017a). Introduction. In *Basic Finite Element Method As Applied to Injury Biomechanics* (pp. 3–49). Academic Pr. https://doi.org/10.1016/B978-0-12-809831-8.00001-5

Yang, K. H. (2017b). Material Laws and Properties. In *Basic Finite Element Method As Applied to Injury Biomechanics* (pp. 231–256). Academic Pr. https://doi.org/10.1016/B978-0-12-809831-8.00005-2

Yang, K. H. (2017c). Meshing, Element Types, and Element Shape Functions. In *Basic Finite Element Method As Applied to Injury Biomechanics* (pp. 51–109). Academic Pr. https://doi.org/10.1016/B978-0-12-809831-8.00002-7

Yang, L., Burton, A. C., Bradburn, M., Nielson, C. M., Orwoll, E. S., & Eastell, R. (2012). Distribution of bone density in the proximal femur and its association with hip fracture risk in older men: The MrOS Study. *Journal of Bone and Mineral Research*, *27*(11), 2314–2324. https://doi.org/10.1002/jbmr.1693

Zani, L., Erani, P., Grassi, L., Taddei, F., & Cristofolini, L. (2015). Strain distribution in the proximal Human femur during in vitro simulated sideways fall. *Journal of Biomechanics*, *48*(10), 2130–2143. https://doi.org/10.1016/j.jbiomech.2015.02.022

Zhang, K., Cao, L., Fanta, A., Reed, M. P., Neal, M., Wang, J.-T., Lin, C.-H., & Hu, J. (2017). An automated method to morph finite element whole-body human models with a wide range of

stature and body shape for both men and women. *Journal of Biomechanics*, *60*, 253–260. https://doi.org/10.1016/j.jbiomech.2017.06.015

Zuckerman, J. D. (1996). Hip fracture. *The New England Journal of Medicine*, *334*(23), 1519–1525. https://doi.org/10.1056/NEJM199606063342307

A APPENDIX

A.1 FEM lower extremity models – summary table

Table A.1-I: summary of selected lower extremity finite element models,
SRS = strain rate sensitivity, * = epiphyses, § = shaft, ° tension, #compression, & based on GHMBC

Study	Discretization		Constitutive Models		Young's modulus [GPa]		Yield Stress [GPa]		Material data		Femur validation	
	Cortical	Trabecular	Cortical	Trabecular	Cortical	Trabecular	Cortical	Trabecular	Cortical	Trabecular	Shaft	Proximal
Bermond et al., 1994	Shell	-	Viscoelastic	-	17.6	-	0.12	-	Skalak & Chien, 1987; Viano, 1986	-	-	-
Yang et al., 1996	Solid		isotropic, linear viscoelastic		16.5	1.65	-	-	Cowin, 1989; Evans, 1973; Fung, 1993; Yamada, 1970		-	-
Iwamoto et al., 2000	Shell	Solid	Isotropic elastic-plastic		14	0.735	-	-	Yamada, 1970		Yamada, 1970	-
Schuster et al., 2000	Shell	Solid	transversely isotropic, non-linear composite (asymmetric)		17	0.3	0.1°, 0.145#	0.001°, 0.0019#	Cowin, 1989; Viano, 1986	Carter & Hayes, 1977; Evans, 1961	Ehler & Lösche, 1970; Mather, 1967, 1968; Nyquist, 1986; Strømsøe et al., 1995; Yamada, 1970	-
Beillas et al., 2001	Shell	Solid	isotropic elastic-plastic		5-17.5	0.075-0.45	0.08-0.12	0.01	Atkinson, 1998; Beillas et al., 1999; Burstein et al., 1972; Lotz, Gerhart et al., 1991; Mente & Lewis, 1994; Reilly & Burstein, 1975	Goldstein, 1987; Linde, 1994	-	-
Takahashi et al., 2003	Shell* + Solid§	Solid	Non-linear isotropic elastic-plastic (SRS)		14.3	0.295-0.792	0.114	0.0037-0.0091	> 30 sources reviewed in Takahashi et al. (2000)		Kerrigan et al., 2003	
van Rooij et al., 2004	Shell	-	Linear isotropic elastic-plastic		14	-	0.175	-	Burstein et al., 1976; Evans & Lebow, 1951; Sedlin & Hirsch, 1966; Yamada, 1970	-	-	-
Untaroiu et al., 2005	Shell* + Solid§	Solid	isotropic elastic-plastic (SRS)	isotropic elastic-plastic	13.5	0.298-0.9	0.115	0.0093-0.0056	Currey et al., 1997; Keller et al., 1990	Kuhn et al., 1989; Martens et al., 1983	Ehler & Lösche, 1970; Funk et al., 2004; Mather, 1968; Strømsøe et al., 1995; Yamada, 1970	
Dokko et al., 2009	Shell* + Solid§	Solid	isotropic elastic-plastic (SRS)		Age-function		Age-function		> 30 sources reviewed in Takahashi et al. (2000)		Kerrigan et al., 2003; Motoshima, 1960	Keyak et al., 1997
Li et al., 2013	Solid	-	isotropic elastic-plastic (SRS)	-	14.6	-	0.133	-	Kim et al., 2005; Schileo et al., 2008	-	Funk et al., 2004; Untaroiu, 2010	
Untaroiu et al., 2013	Shell* + Solid§	Solid	isotropic elastic-plastic		2, 6, 13.5	0.2, 0.4, 0.7	0.017, 0.051, 0.115		Brown & Vrahas, 1984; Keller et al., 1990; Lotz, Gerhart et al., 1991; Untaroiu et al., 2005; Untaroiu, 2005	Evans, 1961; Martens et al., 1983	Funk et al., 2004; Ivarsson et al., 2009	Keyak et al., 1997; Keyak et al., 2001
Huang et al., 2018&	Solid	Solid	isotropic elastic-plastic (SRS)	Dynamic elastoplastic	16.2 + 13.9	0.752 + 0.816	0.1 + 0.094	0.013 + 0.01	Currey & Butler, 1975; Mather, 1967; McCalden et al., 1993; Reilly et al., 1974	Ding et al., 1997	Kerrigan et al., 2003	

A.2 Cortical bone - average force and strain curves

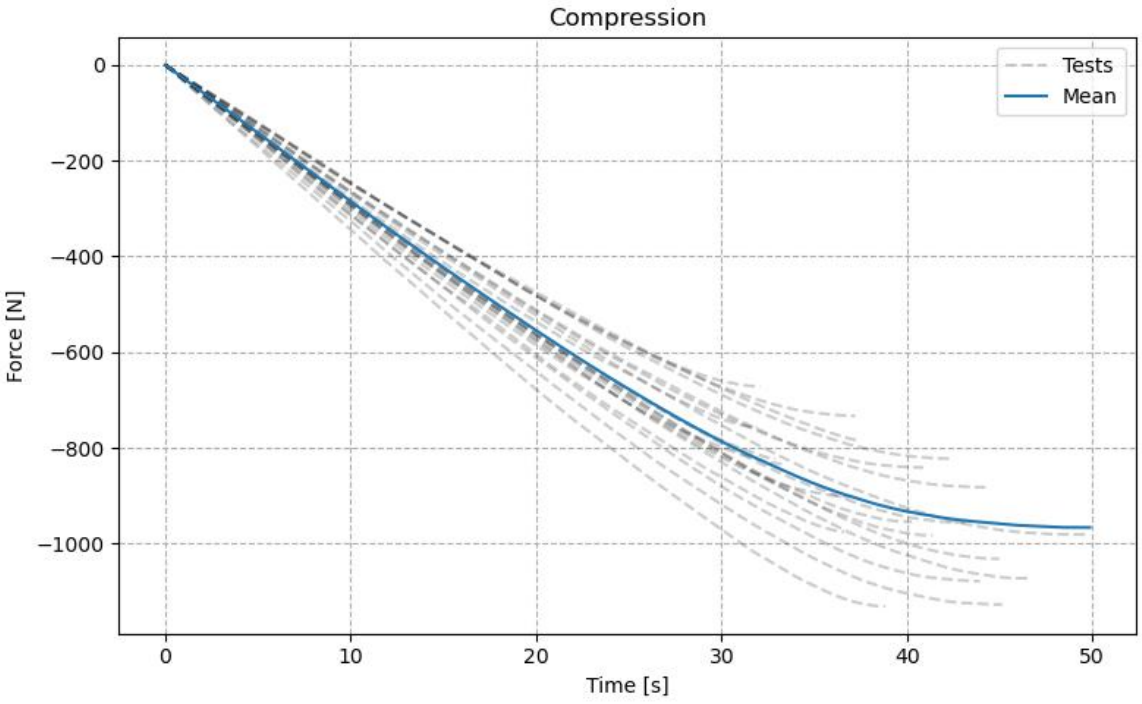

Figure A.2-1: Mean force over time in compression

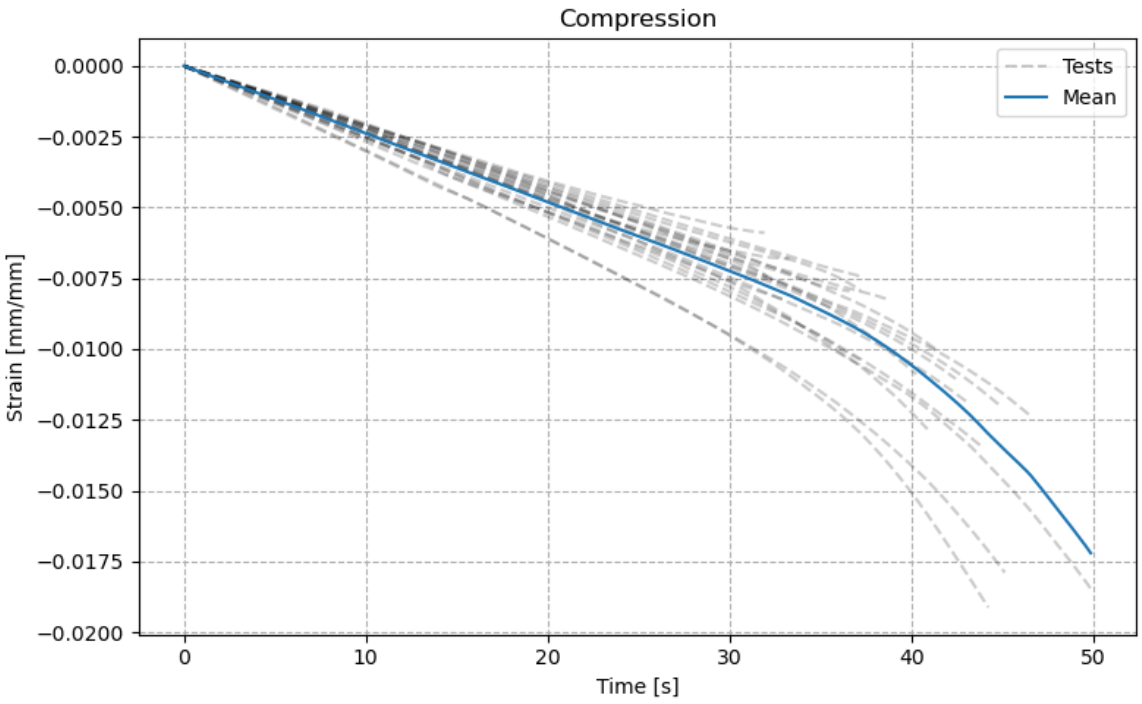

Figure A.2-2: Mean strain over time in compression

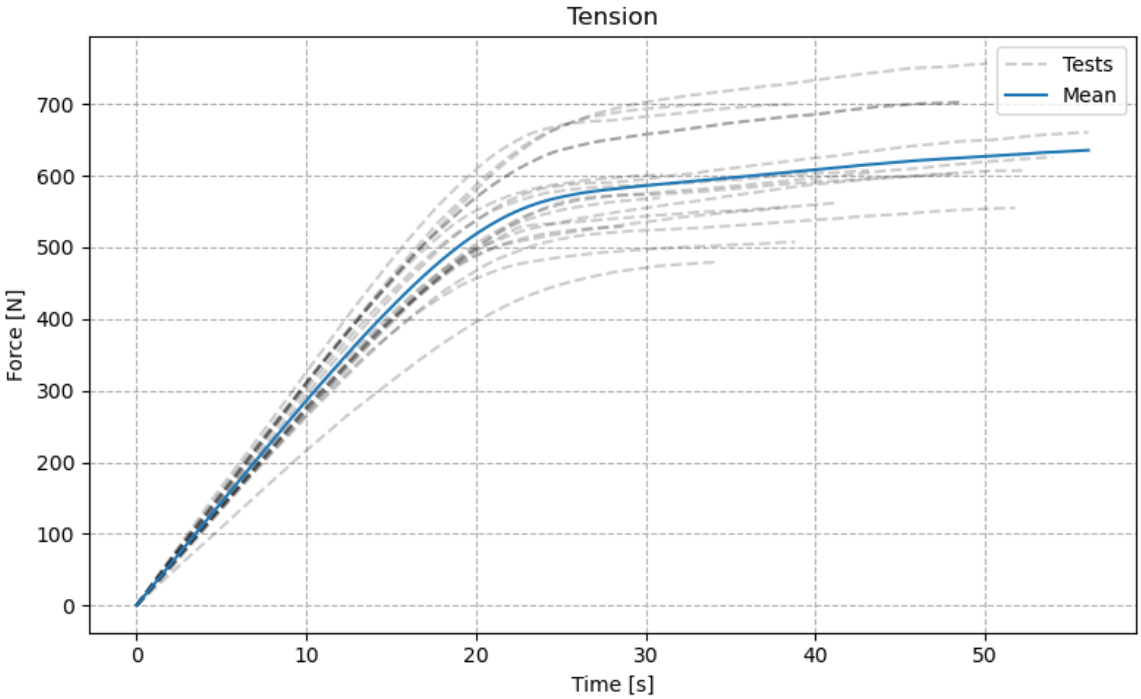

Figure A.2-3: Mean force over time in tension

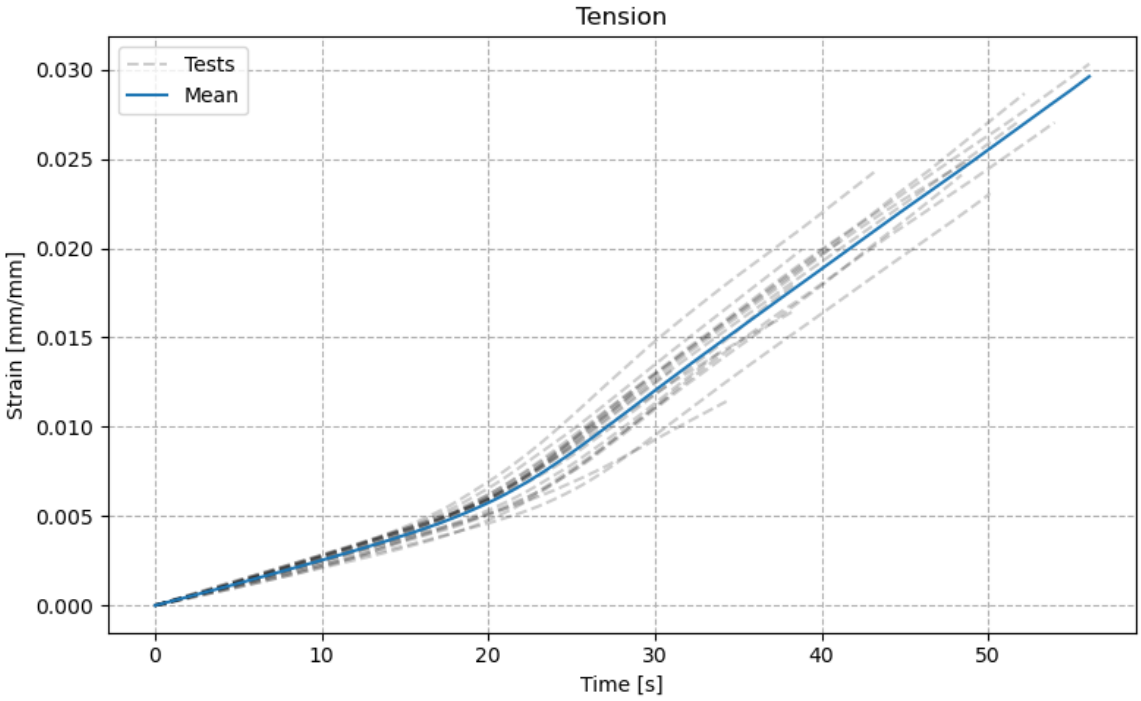

Figure A.2-4: Mean strain over time in tension

A.3 Landmarks used to morph proximal femur meshes

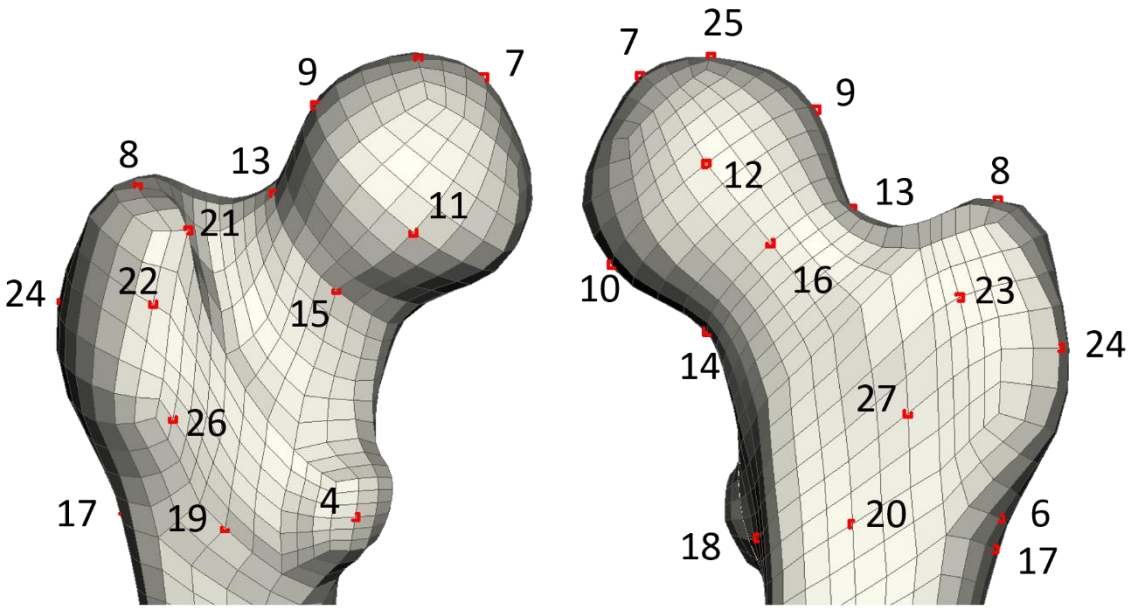

Figure A.3-1: landmarks used for morphing the sample CT-scan meshes to the target geometry, numbering and positions based on Väänänen et al. (2012)

A.4 Simulation setups – masses

Table A.4-I: masses side-ways fall setup

Part	*Mass [kg]*
Rigid plate	10.24
GT PMMA pad	0.022
Cut Femur	0.179
Head PMMA pad	0.021

Table A.4-II: masses three-point bending setup

Part	*Mass [kg]*
Potting Housing	2.276
Potting	0.770
Impactor	0.035
Femur	0.267

A.5 Cortical bone material – additional figures

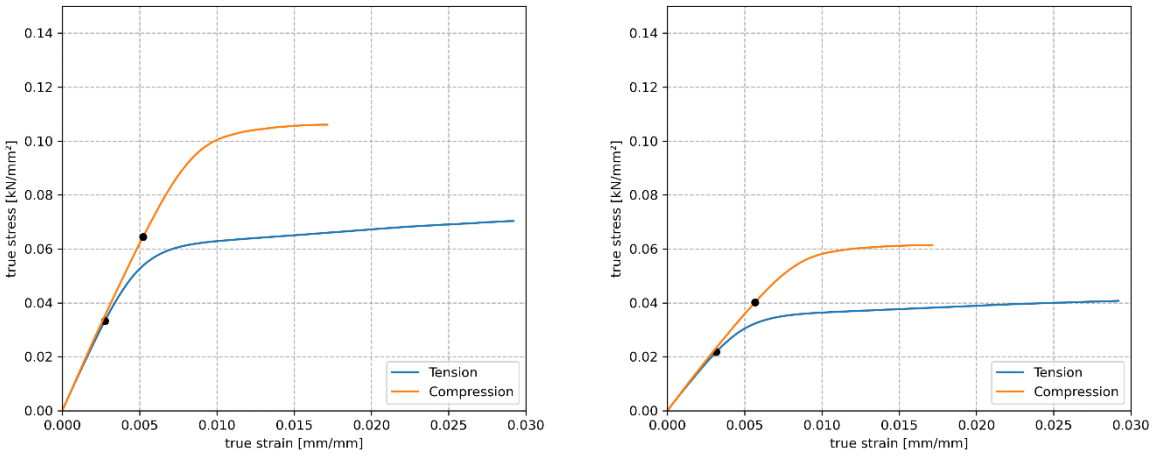

Figure A.5-1: Cortical bone true stress-strain curves in tension and compression, (a) is scaled by factor 0.76, (b) by 0.44

A.6 Validation – proximal femur – additional figures

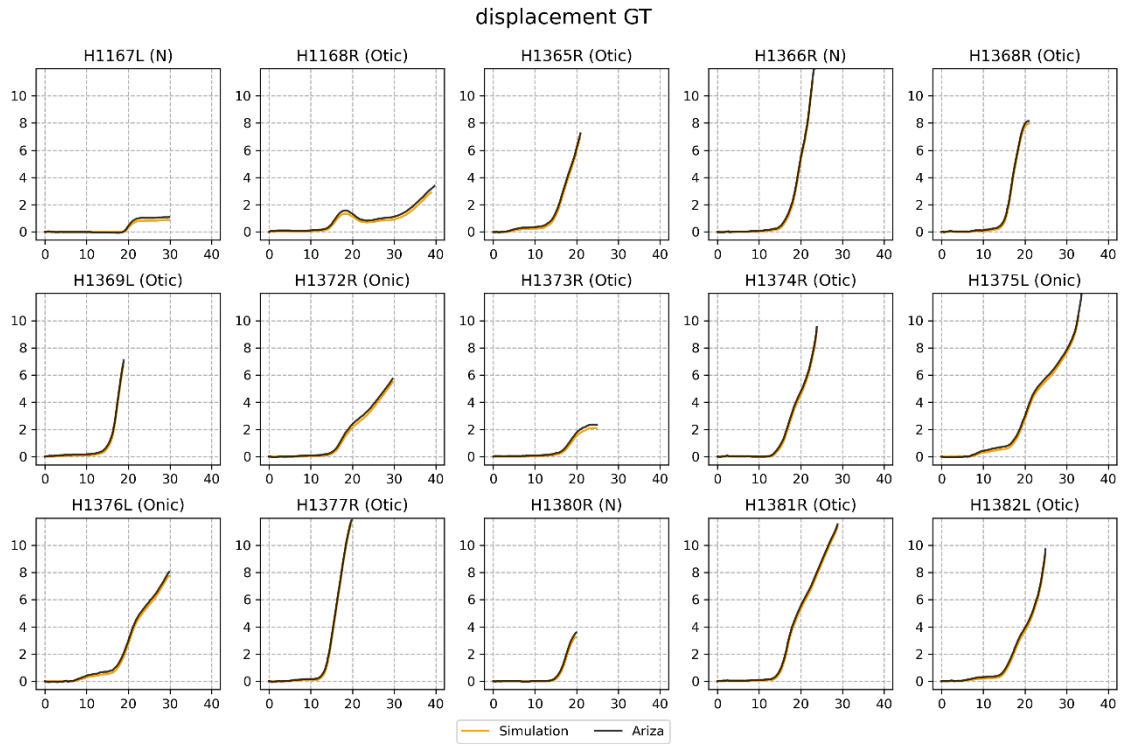

Figure A.6-1: displacement curves from sideway falls from Ariza (2014) (black) compared to our simulation with modified cortical bone (orange)

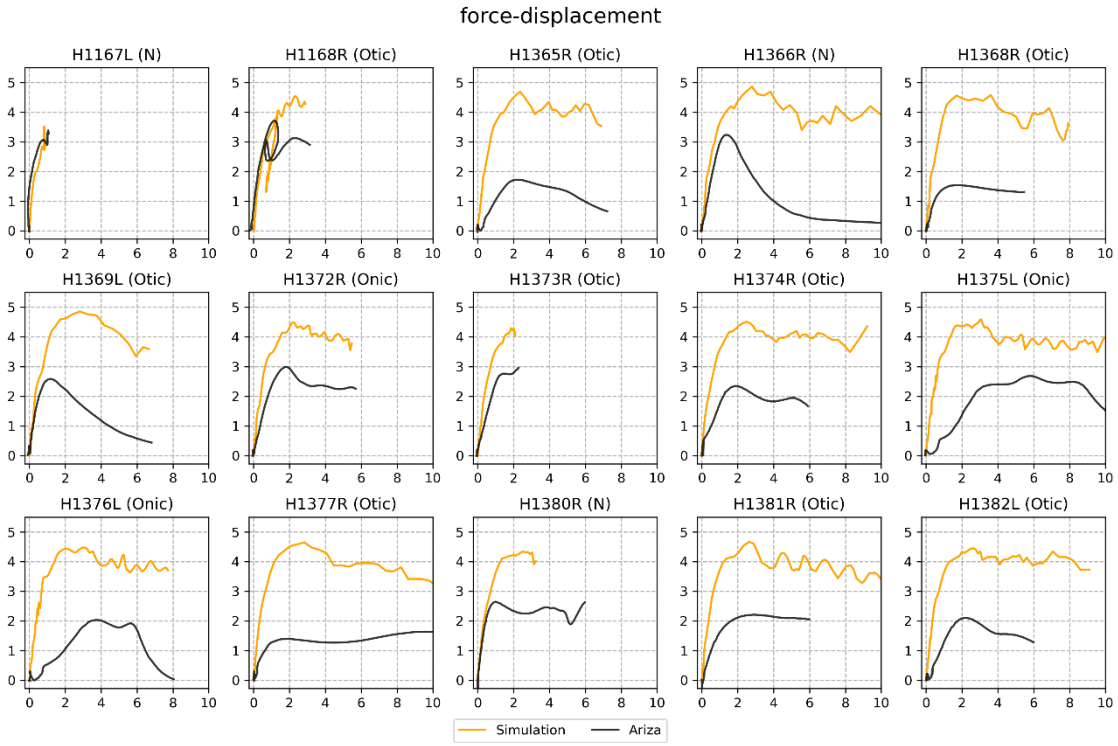

Figure A.6-2: force-displacement curves from sideway falls from Ariza (2014) (black) compared to our simulation with modified cortical bone (orange)

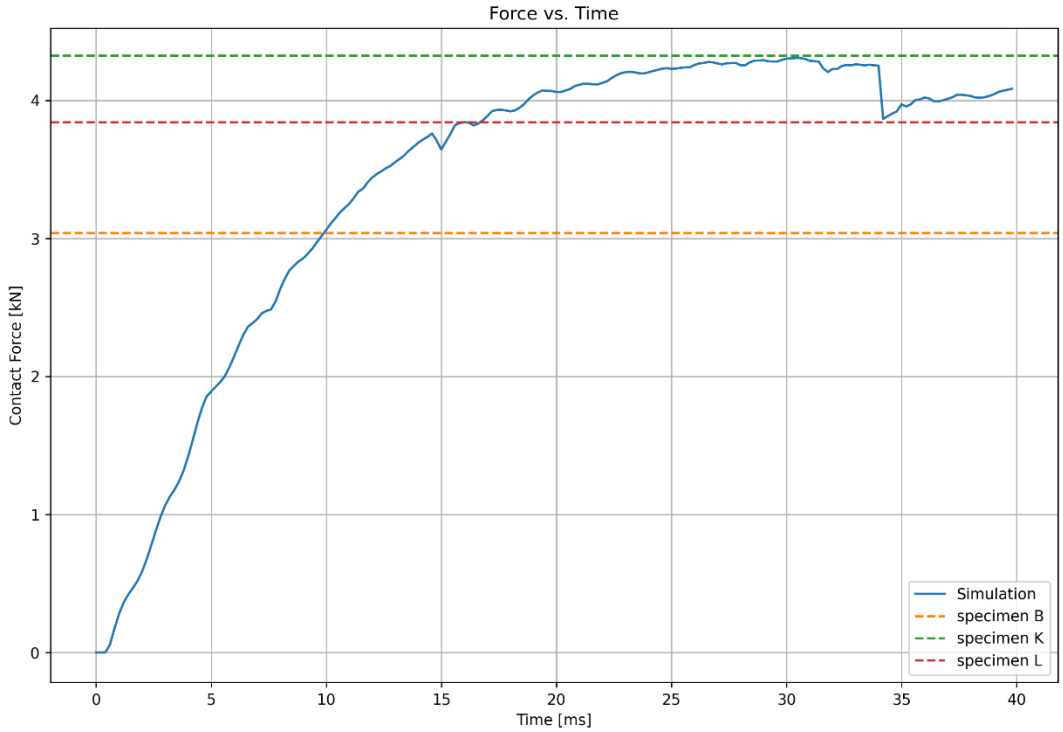

Figure A.6-3: force curve in the sideways fall configuration with a constant displacement of 100 mm/s at the GT, selected fracture forces from specimen B, K, L supplied in de Bakker et al. (2009) are marked

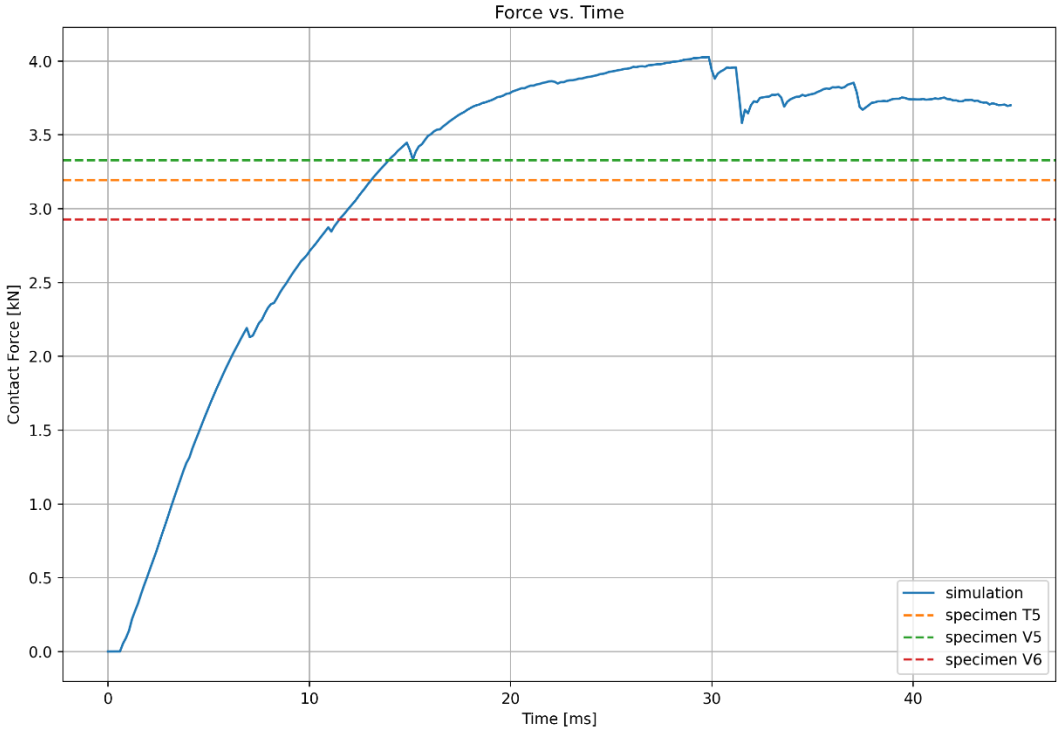

Figure A.6-4: force curve in the flipped sideways fall configuration with a constant displacement of 100 mm/s at the head, selected fracture forces from Dragomir-Daescu et al. (2011) are marked

A.7 Injury risk curves – additional figures

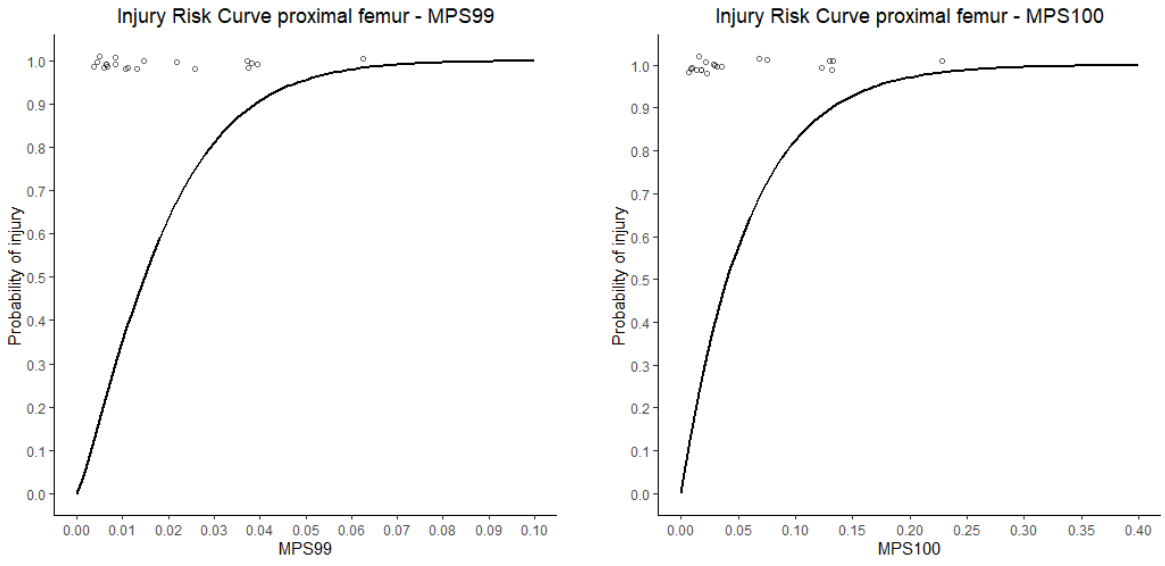

a b

Figure A.7-1: injury risk curves based on MPS99 (a) and MPS100 (b) including the data points for fracture

A.8 Element formulation – comparison

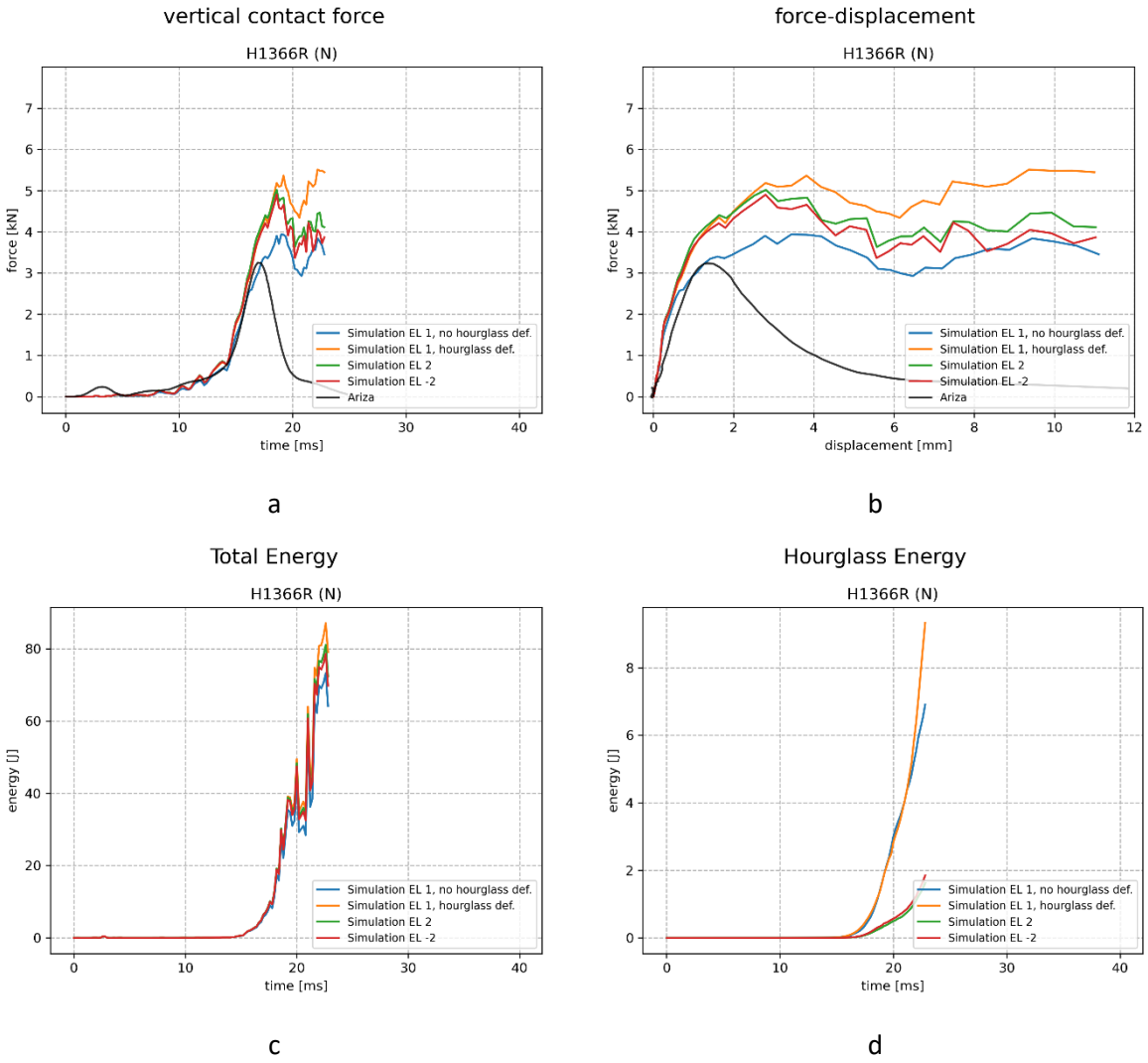

Figure A.8-1: influence of element formulation on force (a), force-displacement (b), total (c) and hourglass energy (d) for a selected specimen from Ariza et al. (2015)

A.9 Scaled cortical bone material - comparison

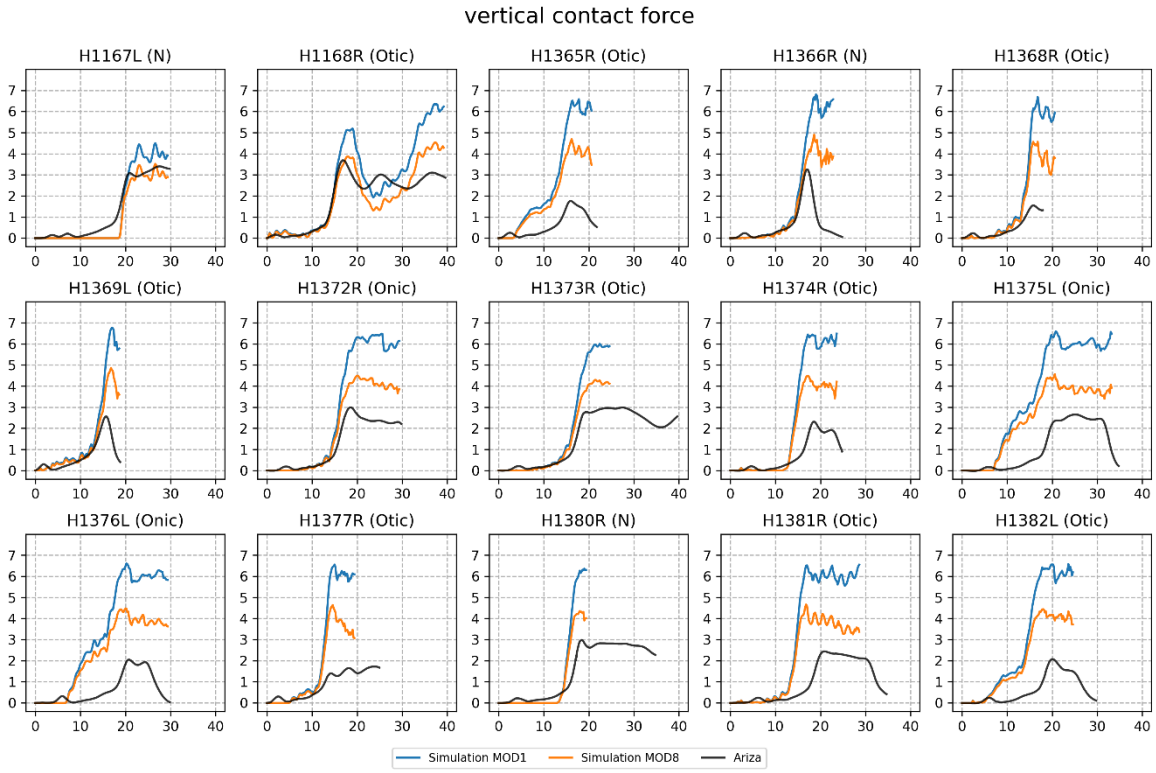

Figure A.9-1: forces in side-ways fall, simulation with scaled cortical bone properties (orange) vs. original (blue) and data from Ariza (2014)

A.10 Influence of trabecular bone density

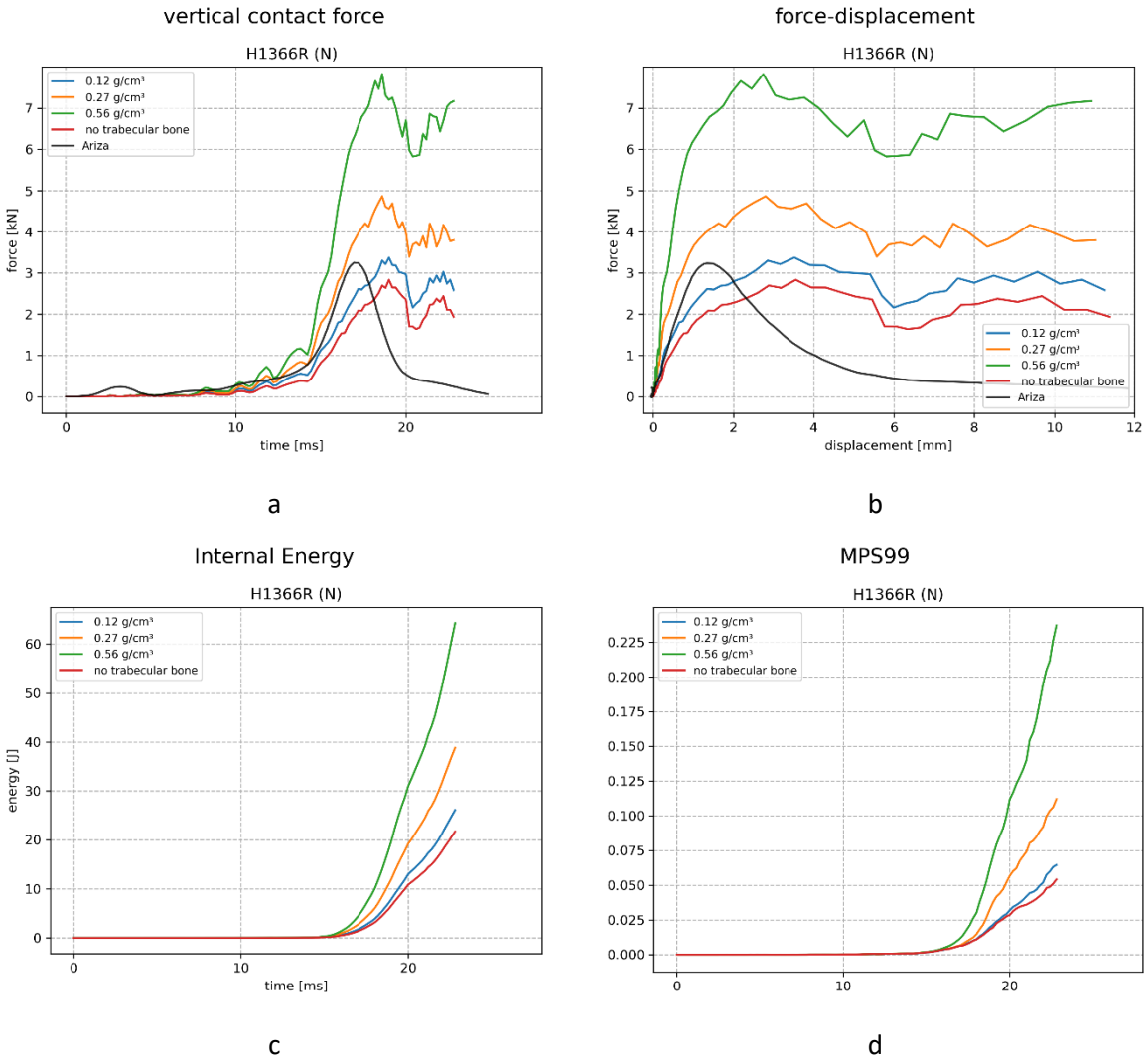

Figure A.10-1: influence of trabecular bone density on force (a), force-displacement (b), internal (c) and cortical MPS99 (d) for a selected specimen from Ariza et al. (2015)